Characterizing the Plasma Exhaust Plume from a Sheared-Flow Stabilized Z-Pinch

Collin Parsons

A thesis
submitted in partial fulfillment of the
requirements for the degree of

Master of Science

in Aeronautics and Astronautics

University of Washington

2020

Committee:

Uri Shumlak

Brian Nelson

Program Authorized to Offer Degree:
Aeronautics and Astronautics

University of Washington

Abstract

Characterizing the Plasma Exhaust Plume from a Sheared-Flow Stabilized Z-Pinch

Collin Parsons

Chair of the Supervisory Committee:
Uri Shumlak
Aeronautics and Astronautics

A plasma Z-pinch has often been overlooked as a method for magnetic confinement fusion due to instabilities. Using sheared-flow to stabilize the Z-pinch extends its life to where it is a plausible solution for fusion and an attractive possibility for fusion-based space propulsion. To investigate this, the plasma plume of the Fusion Z-Pinch Experiment (FuZE) at the University of Washington is characterized using ion Doppler spectroscopy and quadruple Langmuir probe measurements. During pulses, signals characteristic of discharge arcs driven by quadruple probe bias capacitors are observed on probe tips at a probability proportional to the bias voltage. Quadruple probe measurements show average electron temperatures of 14.4 ± 7.8 eV that are approximately constant over the plasma and peak densities of $9.5 \times 10^{20} \pm 3.4 \times 10^{20}$ m^{-3} that fall off nearly linearly as radius increases, suggesting a collimated plasma plume. EMI noise in quadruple probe voltage measurements prevents more accurate determinations of parameters. Spectroscopy reveals plasma velocities of 86.2 ± 2.8 km/s, while significant EMI noise and suspected unreliability preclude velocity measurements from the Mach probe. A hypothetical space thruster built with these parameters would have a specific impulse of 8790 ± 290 s and a Thrust of 1420 ± 260 N, performance significantly better than current-day electromagnetic thrusters.

TABLE OF CONTENTS

LIST OF FIGURES

LIST OF TABLES

NOMENCLATURE

θ	Angle of incidence of spectroscopy chord $[rad]$
λ	Wavelength of light $[m]$
c	Speed of light, $2.998e8$ $[m/s]$
e	Charge of an electron, $1.602e{-}19$ $[C]$
F_T	Rocket thrust force $[N]$
$FWHM$	Full-width half-max of a Gaussian curve [nm]
g_0	Gravitational acceleration at sea level, 9.81 $[m/s]$
I_1	Current on positively biased double probe tip in triple probe array $[A]$
I_2	Current on floating probe tip in triple probe array $[A]$
I_3	Current on negatively biased double probe tip in triple probe array $[A]$
I_{esat}	Electron saturation current $[A]$
I_{isat}	Ion saturation current $[A]$
I_{sp}	Specific impulse $[s]$
J	Current density $[A/m^2]$
k_B	Boltzmann constant, $8.617e{-}5$ $[eV/K]$
K	Mach probe calibration constant
$\dot{m}$	Mass flow rate $[kg/s]$
m_i	Ion mass $[kg]$
M_i	Ion Mach number
n_e	Electron number density $[m^{-3}]$
Q_{exp}	Charge expended in a discharge $[C]$
R	Ratio of upstream to downstream ion saturation current

S	Electrode surface area [m^2]
T_e	Electron temperature [K, eV]
T_i	Ion temperature [K, eV]
v_e	Rocket exhaust velocity [m/s]
v_{flow}	Plasma flow speed [m/s]
v_s	Speed of sound [m/s]
V_1	Potential on positively biased double probe tip in triple probe array [V]
V_2	Potential on floating probe tip in triple probe array [V]
V_3	Potential on negatively biased double probe tip in triple probe array [V]
V_{d2}	Difference in potential between floating probe tip and double probe tip of a Langmuir triple probe [V]
V_{d3}	Bias voltage on double probe & Mach probe tips of a quadruple probe [V]
V_f	Langmuir probe floating potential [V]
V_p	Plasma potential [V]

ACKNOWLEDGMENTS

This thesis would not have been possible without help from the faculty at the University of Washington and employees, researchers, and fellow graduate students at the FuZE laboratory.

I would first like to thank my thesis adviser, Professor Uri Shumlak, whose suggestions, constructive criticism, and guidance were instrumental to my research. Thank you for consistently pushing me forward to new paths and ideas. Your advice and support have been essential to my success at the UW.

I am grateful to Dr. Anton Stepanov, who was my first introduction to plasmas through teaching the AA 405 course, inspired me to join the FuZE project, and provided advice on my thesis and diagnostics throughout. Your assistance in helping me understand plasmas was fundamental to my time here. Thank you for guiding my research and helping me discover ways to expand and advance my work.

I would also like to thank Dr. Brian Nelson for teaching me the ways of the electrical engineer. Your help in getting my diagnostics set up properly and in diagnosing the inevitable noise and errors that came my way was invaluable.

I am thankful to the other researchers and graduate students in the FuZE lab for always being willing and ready to provide support when I needed it, from helping me run the experiment to diagnosing MATLAB bugs with me and everywhere in between.

Finally, I would like to thank the institutions that gave me this opportunity — the US Air Force, for giving me my start in the engineering career field, and the UW Aeronautics and Astronautics department for sponsoring my degree.

Chapter 1

INTRODUCTION

The scientific community has pursued sustained magnetic confinement of plasmas as a viable method for achieving nuclear fusion since the 1950s. In the early decades of fusion research, magnetic confinement fusion concepts were limited to tokamaks, stellerators, magnetic mirrors, and Z-pinches. Since then, approaches to magnetic confinement fusion through the use of spheromaks, spherical tori, and field-reversed configurations have been introduced. Present-day implementations of these concepts include the National Spherical Torus Experiment-Upgrade (NSTX-U) at Princeton University, the Joint European Torus (JET) in the UK, and the upcoming International Thermonuclear Experimental Reactor (ITER) in France.

Of the feasible magnetic confinement concepts, the Z-pinch has the most simple construction and geometry. Z-pinches use a cylindrical plasma column subjected to an axial current; this current generates an azimuthal magnetic field, which causes plasma to pinch in on itself through Lorentz forces. The greater the current applied, the stronger the azimuthal magnetic fields will be, and hotter and denser resulting pinch plasmas will become. Pure plasma pinches require no external magnetic fields, eliminating the need for expensive coils. Although the geometry is straightforward and the design is more simple and cost-effective to construct than alternative magnetic confinement fusion devices, the Z-pinch has been largely rejected as a practical solution to magnetic confinement fusion because of its native instabilities. The “sausage” (m=0) and “kink” (m=1) instabilities arise quickly in static Z-pinch plasmas, destroying the stable pinch before plasma temperatures and densities can grow large enough to produce sustained nuclear fusion.

However, recent research and experimentation has shown that sheared-flows to stabilize the pinch can produce pinches that are stable for thousands of times longer than the expected time scale of instability growth [26, 28]. If the pinch can be successfully stabilized, then pinch current can increase without destabilizing the pinch. Greater pinch currents produce increased plasma densities and temperatures, closing the gap to sustained fusion.

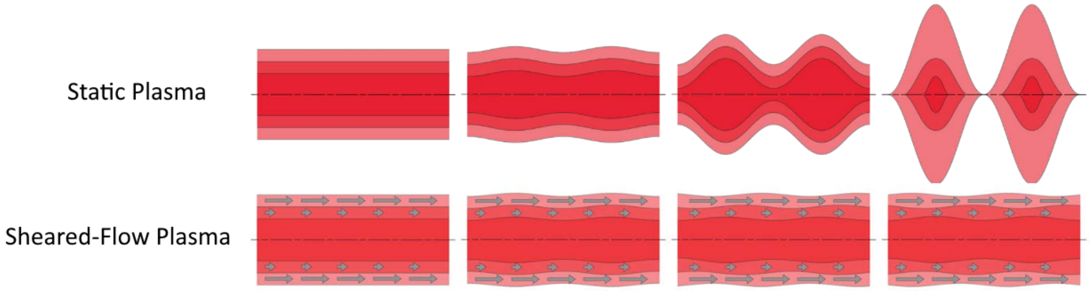

Figure 1.1: Research has shown that a sheared-flow Z-pinch maintains plasma stability for 700 times longer than the expected time of instability growth. Reprinted from *Roadmap to a Compact Fusion Device based on the Sheared Flow Stabilized Z-Pinch*, ARPA-E Fusion Workshop 2019 Slides by Uri Shumlak, slide 6; retrieved from https://arpa-e.energy.gov/sites/default/files/Shumlak_ arpae2019_ compressed.pdf

The primary goal for achieving sustained nuclear fusion is for high-capacity, clean power generation. If the break-even point of nuclear fusion is surpassed and more energy is released from the reaction than used to create it, the excess energy can be captured, stored, and released as electrical power. However, direct power generation is not the only use for nuclear fusion — fusion-based space propulsion systems have the potential to drastically increase engine fuel efficiency and power output over traditional chemical or electromagnetic space propulsion systems [3, 19, 27]. Nuclear fusion reactions create extra energy that provides power generation for the engine and the spacecraft, and in certain configurations the hot plasma from fusion exhaust can be used directly as propellant.

The Z-pinch is an especially attractive scheme for fusion space propulsion because of its linear configuration, high plasma densities, and light weight from simpler construction. A sheared-flow Z-pinch improves this concept by stabilizing the classical Z-pinch instability modes, extending the pulse time and enhancing plasma parameters.

Converting a standard Z-pinch concept to an engine would essentially just remove the end wall and physical cathode in favor of a “virtual cathode”, removing any barriers to downstream plasma flow and letting plasma exhaust out to provide thrust. Through this configuration, estimates of thruster performance include specific impulses near 10^6 seconds and thrusts in the hundreds of kilonewtons [27]. Considering these estimates and the energy density of fusion reactions, a sheared-flow stabilized Z-pinch based thruster could theoretically propel spacecraft to Mars in a matter of weeks rather than months, or to the outer planets of the solar system or even interstellar space.

1.1 The Fusion Z-Pinch Experiment (FuZE)

A standard pure Z-pinch injects an amount of gas into a vacuum chamber, and runs a current through it between a defined anode and cathode to create a pinch. With static plasma, the basic structure of a pinch will still form, but will develop instabilities far faster than a sheared-flow stabilized Z-pinch.

The sheared-flow stabilized Z-pinch was first examined at the University of Washington (UW) with the flow Z-pinch experiment, ZaP. Experimentation with ZaP revealed that flow can be stabilized in the way theory predicts, by stabilizing the m = 0 and m = 1 MHD instability modes with sheared axial plasma flow [26]. The Fusion Z-Pinch (FuZE) experiment expands the scale of ZaP, increasing pinch currents from 275 kA to upwards of 400 kA and increasing pinch ion temperatures from 250 eV to above keV. FuZE has shown a plasma quiescent period of 16 μs, 5000 times longer than the quiescent period for static Z-pinches.

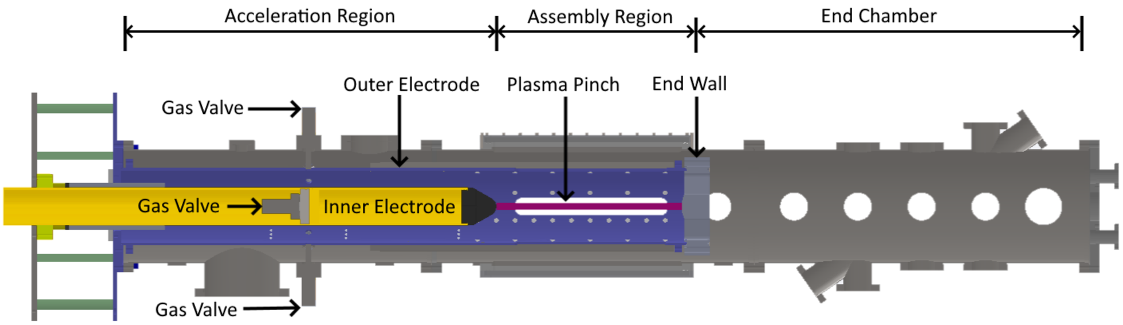

Figure 1.2: Side view of FuZE. Plasma is accelerated in the acceleration region, forms into a sheared-flow stabilized Z-pinch in, and passes through the end wall downstream into the end chamber.

To create a sheared-flow stabilized Z-pinch, FuZE first injects neutral gas between two electrodes. A current, provided by a capacitor bank with thyristor switches, is run from the outer electrode into the inner electrode, and just as a railgun propels a projectile, the $J \times B$ force created by the current and the resulting magnetic field accelerate the plasma in the axial Z direction as the current loop expands down the outer and inner electrodes. The inner edge of the current loop cannot travel further downstream than the nosecone at the end of the inner electrode; the outer corner of the current loop continues to travel downstream until the end wall. At this point the current loops which have formed on opposite halves of FuZE merge at the center of the end wall, which acts as an anode for the Z-pinch with the inner electrode nosecone acting as a cathode. This plasma coalesces into a pinch between the anode and cathode in the assembly region, while a deflagration front in the accelerator continually supplies plasma to accelerate into and sustain the pinch.

Plasma that has been accelerated and has passed through the assembly region travels downstream through the spoked end wall and into the "end chamber." At this point, little is known about the plasma. Experimental work on FuZE thus far has focused on the acceleration and assembly regions, examining phenomena like plasma

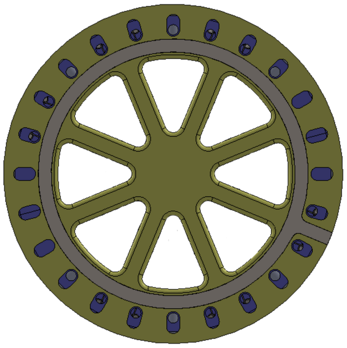

Figure 1.3: Spoked end wall of FuZE. Plasma that has been accelerated in the acceleration region and traveled through the assembly region passes through this end wall into the end chamber downstream. The end chamber and spoked gaps in the end wall are present to prevent plasma from piling up at the upstream side of the end wall.

breakdown, gas fill profiles, plasma parameters inside the pinch, and of course pinch stability. In 2019, a laser interferometry chord was directed through the windows immediately after the end wall, reading plasma densities in the 10^{21} range. This data has yet to be published, but confirms that plasma does exit the end wall.

One possibility is that plasma could exit the end wall and travel directly downstream in a collimated flow at a similar speed to that with which it exited the acceleration region. However, the end wall provides an initial obstacle to this flow, so there may be a notable decrease in velocity or divergence of the plasma plume. Pressure differentials of gases expanding into a vacuum will likely also cause some plume divergence. Additionally, high pinch currents create large magnetic fields in the assembly region, and magnetized plasma follows magnetic field lines. Because the current travels from the outer electrode through the end wall and into to the pinch, strong magnetic fields do not continue into the end chamber. Thus, plasma traveling freely into the end chamber must be demagnetized, and the nature of this demagnetization is as of yet unknown.

1.2 Objectives and Approach

The goal of this thesis is to determine essential plasma parameters and behavior of downstream flow through the end wall. These measurements will contribute to understanding of plasma detachment from magnetic fields, plasma plume divergence, and potential performance of a sheared-flow stabilized Z-pinch-based space propulsion system.

Two diagnostics will be used to pursue this goal. The first is a quadruple Langmuir probe, designed and built by a previous student, which was present in the FuZE lab at the time I arrived but not in use. Quadruple Langmuir probes take measurements using four conducting electrodes immersed directly in the plasma, from which electron temperatures and densities and ion flow velocities can be measured. This particular quadruple probe also has the ability to extend and retract into and out of the plasma flow, to enable a 1-dimensional profile in measurements. The second diagnostic used is ion Doppler spectroscopy. A spectroscopy telescope will be positioned near the Langmuir probe, observing the plasma and recorded the light the plasma emits. From the spectra of this light we can calculate plasma velocity using Doppler shifts as a secondary measurement of velocity to the Mach probe electrodes on the quadruple Langmuir probe.

Measurements are taken according to the characteristics of the diagnostics used. Langmuir probes are time resolved, taking data over the course of the experiment, while the spectroscope is a single shot time-integrated acquisition requiring a trigger at a specific time during the pulse. The Langmuir probe can be positioned at any point between its zero point and its maximum extension. With the Langmuir probe positioned radially on the experiment, this extension ability will be exploited to gather a radial profile of plasma measurements along its extension path. Meanwhile, spectroscopy, although focused at a point in the plasma, gathers line integrated measurements and cannot be adjusted to view specific points in 3D space, so its measurements are of the plasma as a whole along its entire viewing chord.

The general approach to taking measurements starts with initial setup and testing of the diagnostics. Only the floating probe electrode of the quadruple probe has been used before, so initial setup requires connection of the other four probe tips and proper data digitization of all of their measurements. Spectroscopes have been used on FuZE before, although at different locations in the experiment, so setup of spectroscopy is less unknown than the Langmuir probe. However, setup still requires hooking up the telescope and fiber and ensuring that the data is properly acquired and stored.

The second element of this investigation involves actually taking the measurements. The Langmuir probe will measure a radial profile of the plasma and the entire data record can be stored. The reliability of the probe is not known nor is the repeatability of data shot-to-shot, so enough measurements will be taken to ensure that outliers are recognized and results have statistical significance. Spectroscopy, being line-integrated and measured at a single point in time, will be measured at the time plasma is most visible to get a higher amplitude signal from which to calculate velocities. The time of this measurement can be inferred from the time at which Langmuir probe signals are present. FuZE settings for these measurements should be settings widely used on the experiment so that the data traces are recognizable and logical and can be easily tied to plasma signal.

Once measurements are taken, data analysis will include calculations of plasma electron temperature, density, and velocity. We can determine the amount of divergence of the plasma plume using the radial profile of Langmuir probe measurements, and Doppler shift velocity measurements provide an extra and possibly more reliable check on the Langmuir probe velocity measurements. Langmuir probes are notoriously finicky, so the analysis of data will likely include an amount of data smoothing and noise screening.

Once the data is analyzed, conclusions can be drawn. The difference in plasma parameters between the plume and the assembly region allows us to make judgments on what happens in between; notably, how the plasma escapes from the end wall. Ideally, this investigation will conclude with a statement on whether or not the FuZE plasma plume characteristics are favorable for space propulsion applications.

To summarize, I am approaching this investigation through the following process:

1. Integrate the quadruple Langmuir probe with the FuZE end chamber and ensure reliable and accurate data collection.
2. Integrate the spectroscopy telescope to the FuZE end chamber and ensure reliable and accurate data collection.
3. Perform a radial scan of plasma measurements with the Langmuir probe.
4. Take Doppler shift spectroscopy measurements on the same pulses as the Langmuir probe measurements enable comparison of the two diagnostics' measurements.
5. Analyze Langmuir probe data and spectroscopy data to calculate electron temperature, density, and ion flow velocity, as well as the divergence of the plasma plume.

Chapter 2

THEORY

This thesis attempts to determine plasma properties in the end chamber of the experiment which had not yet been extensively measured by existing diagnostics. The basic plasma properties measured in this thesis are electron temperature, electron number density, and plasma flow velocity, measured with a quadruple Langmuir probe and ion Doppler spectroscopy. This chapter will detail the basic principles of these two diagnostics and methods used to calculate plasma parameters from the data they provide.

2.1 Langmuir Probes

One of the earliest plasma diagnostics used is the Langmuir probe, named after physicist Irving Langmuir. These probes consist of a conductive probe tip or tips inserted into a plasma in order to directly measure particle fluxes [16]. They can range from single-tip probes measuring a single voltage to more complex multi-tipped probes used to measure more than one parameter, as is the case in the FuZE experiment.

In all experimental methods using Langmuir probes, the ultimate goal of the probe is to determine a characteristic curve [5]. This characteristic curve can then be used to determine plasma parameters. The popular characteristic curve to analyze from a Langmuir probe is the I-V curve, from which floating potential, plasma potential, and ion saturation current can be determined [21, 24]. These measurements can then be used to calculate plasma parameters. A typical I-V curve for a Langmuir probe in a plasma [7] is shown in figure 2.1.

In all cases, these probes measure flux of charged particles from the plasma di-

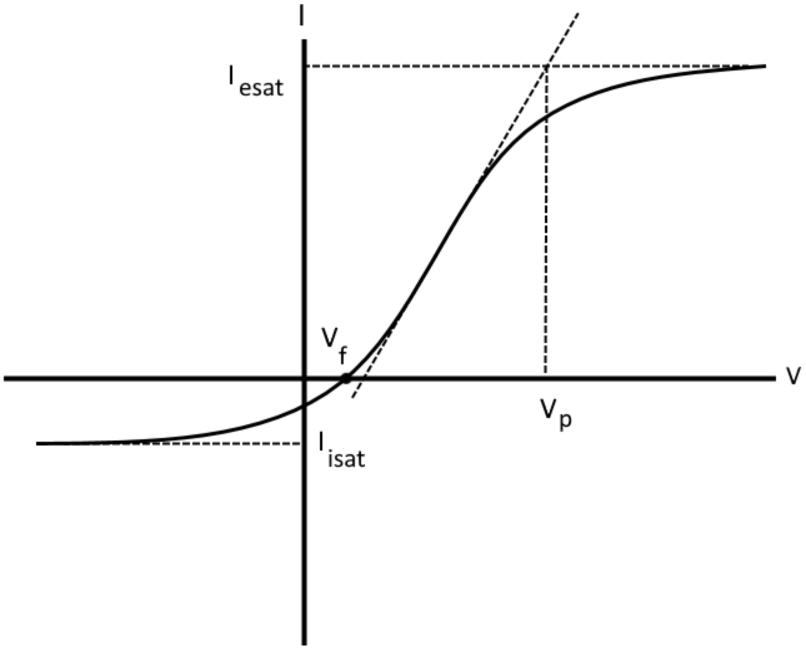

Figure 2.1: General I-V curve for a plasma, showing floating and plasma potential, and electron and ion saturation currents. If the voltage on the Langmuir probe is sufficiently negative, the probe will collect as many ions as the plasma allows at the ion saturation current, shown as I_{isat}. If the probe is biased sufficiently positive, it will collect electron saturation current at I_{esat}.

rectly into the probe tip. As such, these are considered intrusive as they will perturb the plasma around the probe. This complicates the measurement of some parameters in that the perturbation must be taken into effect to make judgments about properties of the plasma far from the probe. This perturbation is also necessary for some measurements, such as ion saturation current, where charging the probe tip to a significantly negative voltage will repel electrons from the probe tip and attract ions at a rate not exceeding the plasma ion saturation current. The following sections will identify the common types of Langmuir probes used in plasma experiments, the parameters that these Langmuir probes can measure, and how the measurements are made.

2.1.1 Single Langmuir Probes

Possibly one of the simplest configurations for a Langmuir probe is the floating probe. A floating probe consists simply of a single, conductive, non-biased electrode inserted into a plasma. The electrode floats to the voltage where there is no net current from the plasma, marked by the point V_f in figure 2.1. Note that this is lower than the overall plasma potential V_p. While the plasma may be electrically neutral, free electrons have less mass and will be moving faster, reaching the probe tip faster than ions, thus charging the probe negatively and producing a "sheath" around the probe. This sheath reduces the flow of electrons and increases that of ions until the electron and ion flux is equal, "floating" the probe to a negative potential relative to the plasma: the floating voltage, V_f [21]. This floating voltage is easily seen in an I-V curve such as figure 2.1 as the point where the current equals zero.

Note that this I-V curve is more powerful than just showing floating potential; it also shows plasma potential, ion and electron saturation currents, and can be used to calculate electron temperature. Riccardi, et al. describe how the characteristic I-V curve such as in figure 2.1 can be found using a fast-sweep Langmuir probe [24], a probe with a single tip that is biased to a swept voltage using a DC power supply. By using a single probe tip and sweeping the voltage bias across a range of expected values, the characteristic curve is traced, and from this the electron temperature can be determined via methods developed in Chen's 1965 paper [5].

2.1.2 Double Langmuir Probes

One drawback to single Langmuir probes is that if the plasma potential is varying significantly, a single Langmuir probe that measures relative to a fixed potential may not be sufficient. In this case, a double probe may be used to float the entire system, eliminating the issue of varying potential [31].

In a double probe scheme, a bias is set between two symmetric probe tips, oriented perpendicular to the plasma flow from one another as not to shadow one probe tip. A simple diagram of a double probe is shown in figure 2.2. This bias is then swept through a range of voltages to trace out an I-V curve similar to that of the single Langmuir probe.

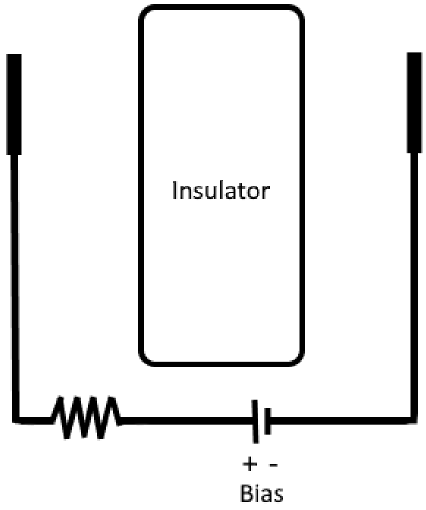

Figure 2.2: Electrical diagram of a Langmuir double probe, with two biased probe tips separated by an insulator. The insulator is present to prevent arcing directly between the two biased probe tips.

2.1.3 Triple Langmuir Probes

Single and double Langmuir probes are both effective schemes for measurement of a static plasma. However, if plasma parameters are varying rapidly, taking individual measurements or sweeping the biased voltage to trace out an I-V curve using one of these probes does not give the time resolution necessary for accurate measurements. Triple Langmuir probes do not require voltage sweeps, and thus will be more accurate for rapidly varying plasmas such as those found in pulsed plasma experiments like FuZE.

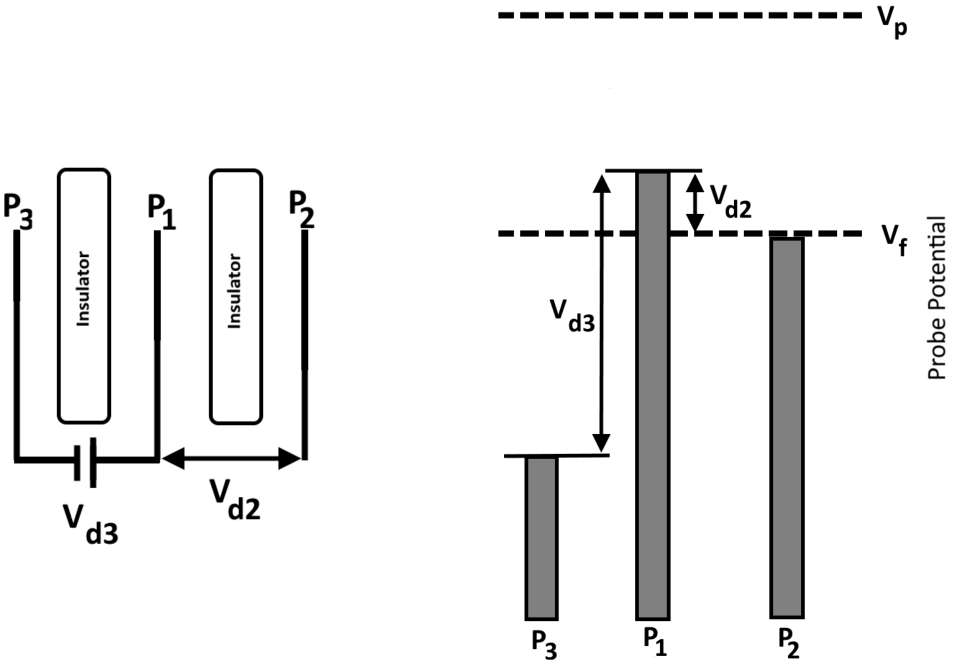

(a) Electrical diagram of a triple Langmuir probe in voltage mode. Electrode P_2 acts as a floating probe, and elecrodes P_1 and P_3 act together as a double probe separate from P_2, biased to potential V_{d3}.

(b) Potentials on electrodes for a Langmuir triple probe. Electrode P_2 is electrically separate from the others, while electrodes P_1 and P_3 are electrically connected and a bias is applied between them.

Figure 2.3: Electrical and potential diagrams of a triple Langmuir probe.

Triple Langmuir probes can be used in both current and voltage modes, depending on the construction and experiment [8, 33]. With three identical electrodes in voltage mode shown in figure 2.3, the single probe P_2 is allowed to float with the plasma to a potential V_f, lower than the plasma potential V_p due to the formation of a sheath around the electrode. A static bias voltage V_{d3} is applied between the two double probe electrodes P_1 and P_3, causing one to float to a voltage above the floating potential and the other to float below the floating potential. Current continuity ensures that neither probe tip will collect current greater than the other, which if the bias voltage

V_{d3} is sufficiently large, will be the ion saturation current [23].

It has been shown that triple probes in voltage mode are susceptible to measurement noise in experiments that emit notable EMI noise during operation [33]. Thus, many experimenters choose to use triple probes in current mode, where all electrodes are biased to a reference voltage. Three current balance equations, one for each electrode, are then solved for the electron temperature T_e, density n_e, and plasma potential V_p, which will be discussed in the following sections. However, for this experiment the plasma probe electronics were constructed in voltage mode, so this was the mode used for measurement.

2.1.4 Quadruple Langmuir Probes

Quadruple Langmuir probes have four electrodes: a floating probe, double probe, and Mach probe. These tips can be arranged in a variety of ways, but they must be insulated from each other to prevent electrical arcing. Some experiments have used flat plate probes, and some have used a spherically symmetric probe, reading differential voltage across the sphere. For this discussion, we will focus on a quadruple probe using identical electrodes arranged in a circle, with an insulator separating them.

The floating probe and the double probe are analyzed together as a triple probe, able to determine electron temperature and density of the plasma. The triple probe tips are on the upstream side of the insulator (the top of Figure 2.4), exposed to direct plasma flow from the end wall. Thus, they will measure parameters of the moving plasma.

For a moving plasma, temperature readings can be falsely amplified by velocity, and so a Mach probe is used to determine how much flow the probe tips are seeing. The Mach probe tip is a single probe tip on the downstream side of the insulator (seen on the bottom of Figure 2.4) and so plasma collection on the probe tip should be exposed only to a quasi-stationary plasma ("quasi" because flowing plasma is still only millimeters away, and fluid mechanics may still cause small eddies in the plasma

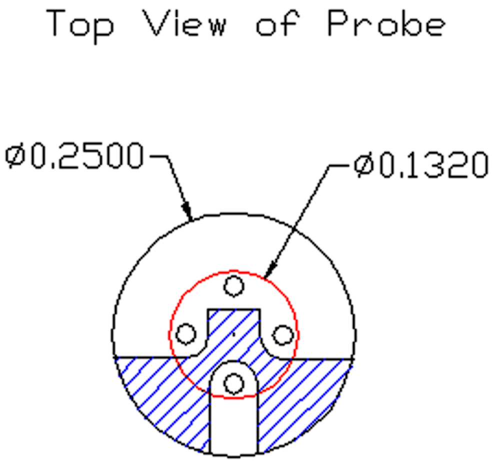

Figure 2.4: Drawing of quadruple Langmuir probe tip, where the top three circles in the array are triple probe electrodes, and the bottom circle is the Mach probe electrode. The four electrodes are separated by an insulator to mitigate arcing, shown with blue stripes.

in the shadow of the probe).

When using the probe in voltage mode, quadruple probe theory incorporates all of triple probe theory but with one extra probe tip; nothing changes about the first three. The fourth electrode is added to measure flow velocity, and is positioned behind the probe tip insulator to measure the plasma that is not in the direct flow.

In voltage mode configuration, a quadruple probe is also subjected to a bias like the double probe. Also like the double probe, the purpose of this bias is to force the Mach probe into ion saturation. By measuring the ion saturation current upstream with the biased double probe tip and downstream with the biased Mach probe tip, a ratio of ion saturation currents is measured, from which flow velocity can be extracted [1, 22]. The exact relationships between ion current ratios and Mach number are still undefined, and will be discussed further in section 2.1.7 on calculating flow velocity.

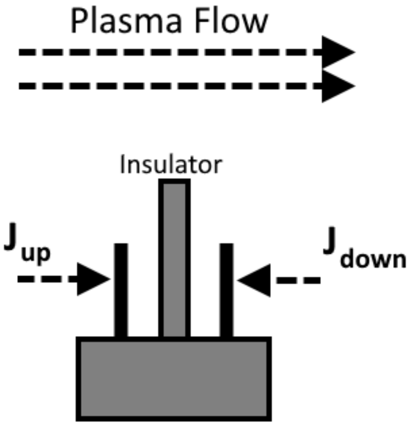

Figure 2.5: Diagram of an ion saturation current ratio type Mach probe. The upstream probe is fully exposed to plasma flow and the downstream probe is sheltered from the flow by a solid insulator.

2.1.5 Calculating Electron Temperature

Electron temperature is one of the most commonly measured plasma parameters because knowledge of electron temperature can be used to make judgments on overall plasma temperature and energy content. Additionally, calculations of density based on ion saturation current measurements require knowledge of temperature [23]. Measuring electron temperature with a Langmuir probe is typically done by using a single biased Langmuir probe and sweeping the voltage or by using a triple probe.

Using a single swept-voltage Langmuir probe, an I-V curve is traced. Assuming that the electron distribution function (EDF) is Maxwellian, the electron temperature can be found as

$$k_B T_e = e \frac{dV}{d(\ln(I_e))} \tag{2.1}$$

where, if the change of the ion component of the current in the transition region (the central linear part of the I-V curve) is slow, its influence can be neglected and the derivative of total current as measured by the probe is approximately equal to the derivative of electron current in equation 2.1 [7]. Using a single swept-voltage Langmuir probe for measurement of electron temperature is robust in that it uses only one probe tip and accurate in that it traces out the entire relevant I-V curve; however, a single probe may be subject to inaccuracies from large variations in plasma potential. As mentioned in section 2.1.2, a double probe fixes this issue. Per Welzel, Dunger, Kupfer, and Richter [31], using a swept double probe the plasma electron temperature may be found with

$$k_B T_e = e \frac{I_{fl}}{2 \frac{dI}{dV}_{fl} - \frac{dI}{dV}_{sat}} \tag{2.2}$$

where $\frac{dI}{dV}_{fl}$ and $\frac{dI}{dV}_{sat}$ are the slopes of the I-V curve at floating potential and ion saturation potential, respectively, and I_{fl} is the ion current on the probe at the floating potential. According to Welzel, et al., an estimate of this is at the intersection of $\frac{dI}{dV}_{sat}$ and the vertical axis.

These methods are reasonable for static plasmas, but for fast pulsed plasmas a triple Langmuir probe provides greater temporal resolution. Triple probe theory was established by Chen in 1965 [5] and voltage mode detailed in Qayyum [23], Burton [2], and Chen [4]. Current equations are written for each probe tip:

$$-I_1 = SJ_+(V_1) + SJ_- \exp\left(\frac{-eV_1}{k_B T_e}\right) \tag{2.3}$$

$$0 = SJ_+(V_2) + SJ_- \exp\left(\frac{-eV_2}{k_B T_e}\right) \tag{2.4}$$

$$I_1 = SJ_+(V_3) + SJ_- \exp\left(\frac{-eV_3}{k_B T_e}\right) \tag{2.5}$$

where J_+ and J_- are the ion current density and electron current density, respectively, and S is the collection area of the electrode. Solving these equations for electron temperature shows that

$$2 \exp\left(-\frac{eV_{d2}}{k_B T_e}\right) = 1 + \exp\left(-\frac{eV_{d3}}{k_B T_e}\right) \tag{2.6}$$

where V_{d2} is the difference in potential between the floating probe and the positively floating biased double probe tip, as shown in figure 2.3.

These calculations rely on a few major assumptions. The first of which are probe theory assumptions [33], that:

1. The radius of the probe is much less than the mean free path of charged particle to neutral particle collisions. Thus, the probe is in the collisionless regime.
2. Debye length is much smaller than the radius of the probe, thus sheath is collisionless.
3. All probes have equal collection areas.
4. Current conservation applies for connected probes. In a voltage mode triple probe, this applies to the double probe electrodes. In current mode, this applies to all electrodes.

At this point, many sources make a further assumption: that the bias voltage between the double probe tips times the elementary charge is significantly larger than the plasma temperature k_BT. By making this assumption, the V_{d3} term in equation 2.6 drops out, and we can solve for electron temperature, yielding:

$$k_BT_e = \frac{eV_{d2}}{\ln(2)} \tag{2.7}$$

This is a linear equation for electron temperature, showing that if V_{d3} is much larger than k_BT_e, the measured potential difference between the floating probe electrode and the positively floating biased double probe electrode is directly proportional to temperature. Riccardi, et al. [24] quantify this assumption, saying that it can be made as long as long as $eV_{d3} > 3k_BT_e$.

This assumption is perfectly reasonable for cold plasmas with temperatures in the single digits eV. However, FuZE plasmas in the assembly region reach keV levels, so temperatures in the downstream plume may be much hotter than single digits eV.

This could pose a problem for the linearity assumption for this setup, where the bias voltage on the Langmuir double probe is set to 200 V.

Numerically solving equation 2.6 for different bias voltages reveals more about the linearity assumption necessary to get to equation 2.7. Figure 2.6a shows the region in which equation 2.6 numerically converges to a solution. Outside this region, the equation does not converge to a finite temperature. For the bias voltage setting of 200 V on this probe, the maximum difference in potential measured between the floating probe and the double probe tips is 96 V. Figure 2.6b shows the values for T_e given by both the numerical solution and by the linear solution for different bias voltages. At $V_{d3} = 200$ V, the numerical answer diverges from the linear answer at V_{d2} of around 40 V.

Pulses hereafter are determined to have "physical" or "nonphysical" temperatures based on a 10% threshold in the difference between the linear and nonlinear curves shown in figure 2.6b; this threshold occurs at 48 V for a 200 V double probe bias. Figure 2.7 shows how the difference between electron temperatures calculated numerically and analytically increases as the V_{d2} difference voltage increases, where $V_{d2} = 48$ V corresponds to an electron temperature (calculated numerically) of about 80 eV. Thus, to remain "physical" and have the linear solution for temperature be within 10% of the numerical solution (the solution that doesn't assume the bias voltage is much larger than the electron temperature), the bias voltage needs to be at least 2.5 times larger, $eV_{d3} > 2.5k_BT_e$. This multiplier is slightly lower than Riccardi's value of $3k_BT_e$; using the same analysis, that multiplier would limit temperatures to 66.7 eV to remain "physical." For this investigation, the smaller $2.5k_BT_e$ limit will be used due to the unknown nature of temperatures within FuZE's end chamber and the pre-constructed circuitry of the Langmuir quadruple probe. Additionally, temperature measurements hereafter will use the numerically calculated T_e from equation 2.6 rather than the more limited linear form of equation 2.7, although for low temperatures, these values will be nearly identical.

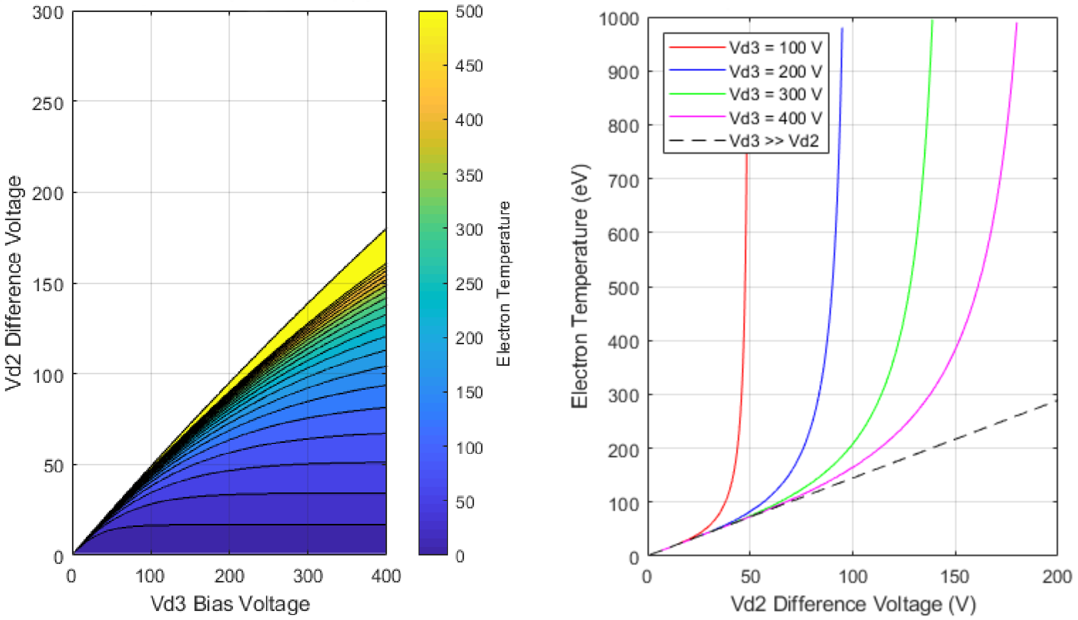

(a) Region of convergence of equation 2.6 for electron temperature T_e. As the V_{d3} bias voltage along the horizontal axis increases, equation 2.7 converges for higher V_{d2} difference voltages to higher temperatures.

(b) Curves showing values of T_e for different V_{d3} bias voltages. T_e scales linearly with the V_{d2} difference voltage per equation 2.7, shown on the horizontal axis.

Figure 2.6: Convergence plots for electron temperature equations 2.6 and 2.7.

2.1.6 Calculating Electron Number Density

The current off the Langmuir double probe tip I_3 is limited to the ion saturation current. Thus, the electron number density cannot be directly measured from a triple Langmuir probe. However, it can be indirectly calculated using the electron temperature and the ion saturation current, using assumptions about the ion sheath surrounding the probe tips.

The sheath formed around the probe has an internal electrostatic field, attracting ions towards the probe. Using the thin sheath approximation, the ion saturation current density is approximated by [2, 9, 23]:

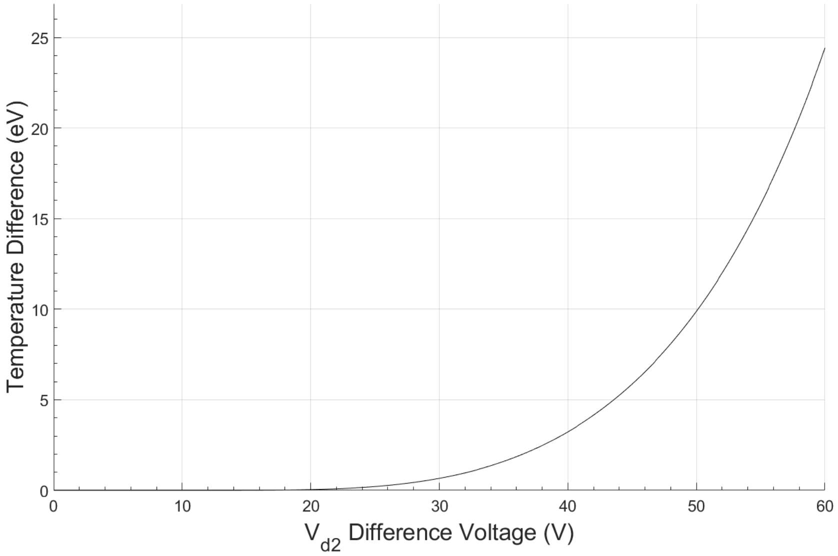

Figure 2.7: Difference between linear and numerical solutions for electron temperature for increasing values of the V_{d2} difference voltage, for a 200 V V_{d3} bias voltage. As the V_{d2} difference voltage increases, the difference in the numerical solution for temperature and the linear solution for temperature increases exponentially.

$$J_i = en_e \left[\frac{k_B(T_e + T_i)}{m_i}\right]^{1/2} \exp\left(-\frac{1}{2}\right) \tag{2.8}$$

Since the electron saturation current density is given by

$$J_e = n_e \left(\frac{k_B T_e}{2\pi m_e}\right) \tag{2.9}$$

then equations 2.9 and 2.8 can be combined with ion saturation current in the form

$$I_+ = I_3 \frac{\exp\left(-\frac{eV_{d2}}{k_B T_e}\right)}{1 - \exp\left(-\frac{eV_{d2}}{k_B T_e}\right)} \tag{2.10}$$

to yield the thin sheath electron density equation, assuming that $T_e \approx T_i$ [23]:

$$n_e = \frac{I_3}{\exp(-1/2) Se\sqrt{\frac{k_B T_e}{m_i}}} \frac{\exp\left(-\frac{eV_{d2}}{k_B T_e}\right)}{1 - \exp\left(-\frac{eV_{d2}}{k_B T_e}\right)} \tag{2.11}$$

where I_3 is the current through the double probe tip P_3 and S is the collection area of the electrode.

Some sources, such as Qayyum, et al. [23], stop here and calculate electron density using equation 2.11. However, S. Chen introduced corrections for the thin sheath assumption of electron density in his 1965 paper [5], further detailed in a 1971 paper [4], and are explained well in Eckman [9]. These corrections may be valuable for quadruple probes because each electrode has a different potential, and will have a slightly different sheath size.

However, for this analysis these corrections were not used. The complex equations required to perform the calculations could not be easily implemented without numerical data processing errors. Chen's and Sekiguchi's 1971 paper [4] states that even if the corrections are not used, density calculations will have an error to no more than three times the true value, meaning that the uncorrected density values will still be within the correct order of magnitude. It also states that temperature error will be no more than 40% higher than the uncorrected value, and that as the bias voltage on the double probes decreases, this error decreases.

2.1.7 Calculating Flow Velocity

The fourth probe tip of the quadruple probe measures the flow velocity, which can be inferred from the ratio of ion saturation currents upstream and downstream of the probe.

$$M_i = \frac{v_{flow}}{v_s} \tag{2.12}$$

$$v_s = \sqrt{\frac{k_B T_e}{m_i}} \tag{2.13}$$

How to calculate the Mach number from ion saturation current ratio is not universally agreed upon, and depends on the assumptions and plasma models being used. A convenient model for use with directional Langmuir probes, or "Mach" probes, comes from Hudis and Lidsky [12], and is based on a 1-D particle model of an unmagnetized plasma. It states that the ion flow at the outside of the plasma sheath around the probe is given by the Bohm criteria (flow velocity equals sound speed). To satisfy this criteria, an electric field forms inside the pre-sheath region, which is affected by the flow in a moving plasma through differing ion densities at sheath edge. According to this model, Mach number is

$$M_i = \frac{1}{2}\left(\frac{T_e}{T_i}\right)^{(1/2)} \frac{R-1}{R+1} \tag{2.14}$$

where R is the ratio of ion saturation currents, J_{up}/J_{down}. Ando [1] discusses how this equation, when we assume the difference between the upstream and downstream current densities is small, this reduces to the following exponential function:

$$M_i = \frac{1}{K}\ln(R) \tag{2.15}$$

where K is a calibration factor specific to the plasma and the experiment that is proportional to T_i/T_e.

Hutchinson [14] argues that this model is invalid, based on the assumption that flow that "wraps around" the probe and is then collected by the electrodes is not included in the one-dimensional model. He also describes how the calibration factor, shown as M_c in equation 2.15, is arbitrary and nonphysical. Shinohara [25] argues that Hutchinson's use of the Hudis & Lidsky model is inappropriate, and that while it is true that there is no existing reliable theory for unmagnetized Mach probes and it is difficult to estimate the correct value of the calibration constant K, the model can provide accurate values of flow velocity when K is found via calibration. Because no established alternative theory for Mach probes was found, established Mach probe theory as presented in this section will be used for this examination.

Peterson [22] also discusses how Hudis & Lidsky's model and a model by Hutchinson [13] that incorporates perpendicular viscosity both reduce to equation 2.15 above. For each of these papers, the constant K differs, and seems to range between 1.34 for a numerical simulation run by Hutchinson [15] to 2.5 for Ando's experimentation [1].

For use with FuZE, K will be determined using spectroscopy to calibrate. To do this, measurements of velocity are taken using spectroscopy with the Langmuir quadruple probe running simultaneously. The current from the double probe and the current from the Mach probe can be immediately compared to calculate R. Temperatures are calculated using equation 2.7, from which ion sound speed can be calculated. Inverting equation 2.15 to solve for K yields the calibration constant.

2.2 Emission Spectroscopy

As electrons in the atoms and molecules in a plasma are excited, the electrons rise to higher energy levels. Over time these excited electrons decay to lower energy levels, releasing light in the process. Emission spectroscopy is a versatile diagnostic that measures these light emissions to make judgments on plasma properties.

In contrast to Langmuir probes, spectroscopy is a non-intrusive diagnostic which will not interfere with the plasma, and thus no consideration is necessary to determine perturbations. In addition, a spectroscopy diagnostic can be set up outside the experiment, so no modification of the experiment itself is required; all that a spectroscopy diagnostic requires to run is visual access to the plasma being measured.

While plasmas can release radiation at wavelengths throughout the electromagnetic spectrum, the most common range for plasma spectroscopy is from infrared to ultraviolet, 195 nm to 1000 nm in wavelength. Below 195 nm, fused silica windows are no longer transparent and light emissions cannot be measured. Above 1000 nm, it becomes more difficult to subtract thermal noise from the spectrum [10].

Common measurements from plasma spectroscopy include temperature, density, and velocity of particles in a plasma, all of which can be calculated from the spectrum of light radiated by the plasma. The primary purpose of spectroscopy in this investigation is to determine plasma flow velocity, which is done by analyzing wavelength Doppler shift.

2.2.1 Calculating Flow Velocity

In the same way that the sound of a police car's siren shifts from higher to lower frequencies as the car moves towards and away from you, light is shifted in frequency and wavelength if the source of the light is moving relative to the observer. From this Doppler shift, we can determine the velocity of the source, in this case, the plasma.

The magnitude of the Doppler shift can be determined using emission spectroscopy per the following [18]:

$$v_{flow} = c\left(\frac{\Delta\lambda}{\lambda}\right)\frac{1}{cos(\theta)} \tag{2.16}$$

where c is the speed of light, $\Delta\lambda$ is the magnitude of the Doppler shift in wavelength, λ is the stationary emission wavelength of the element, and θ is the angle off-axis from which the spectroscopy diagnostic is facing.

Experimentally, the spectroscopy diagnostic will measure the light spectrum for the plasma as shifted in wavelength proportional to the velocity of the plasma. This spectrum is for the entire plasma, not just one element within it. Thus, it is essential for Doppler shift spectroscopy to determine the elements present in the spectrum and which peaks in the observed spectrum correspond to those elements.

If the makeup of the plasma is known, determining which elements are visible can be done by comparing the observed spectrum to known peaks of emission spectra for each element (these can be found from the NIST website). Inverting equation 2.16 for $\Delta\lambda$ with an estimate of the plasma velocity for v can yield a guess for how far red- or blue-shifted the observed wavelengths should be, further educating the decision on which elements are present. Once which element to focus observations on is determined, equation 2.16 can be used to calculate velocity.

2.3 Further Literature Review

The preceding sections have all drawn theory from literature in the plasmas field. This theory was presented in the context of establishing methods for measuring data and determining plasma parameters. This section will provide a more detailed literature review on how others have used Langmuir probes and Doppler shift spectroscopy, summarizing the contents of referenced works as they relate to this investigation.

The quadruple probe being used on FuZE is essentially a triple probe combined with a downstream Mach probe, so the first step in establishing probe theory for this investigation was to research triple probes and their application. Triple probe theory is well established and widely used in plasma experimentation, but single Langmuir probes are still a viable alternative for slow-changing plasmas. To this end, Riccardi, Longoni, Chiodini, and Fontanesi [24] compared single swept-voltage Langmuir probes to triple probes. They found that a 400 kHz fast-sweep Langmuir probe provided more reliable measurements of plasma parameters for plasmas in which fluctuation frequency is less than 50 kHz. However, for greater frequency fluctuations, only the triple probe is reliable.

This reliance on triple probes for quickly fluctuating plasma measurements is further detailed in Qayyum, et al. [23]. They use a triple probe with a voltage bias of 50 V to measure plasmas with temperatures of up to 2 eV, showing that triple probes can accurately map fast fluctuations in the plasma.

Chen and Sekiguchi [5] discuss limitations on triple probes and some sources of error in measurement. Primarily, they discuss how the ion saturation current, while assumed constant irrespective of probe potential, actually changes slightly as probe potential decreases even past the point of ion saturation. Corrections for temperature and density are introduced here and detailed further in a later paper [4]. They find that without these corrections, temperature can range up to 40% higher for the uncorrected value for temperatures and error in ion density up to 3 times the value of the ion density in magnitude, for bias voltage values of $10k_BT_e$. For lower bias voltage values, error decreases.

In Eckman's thesis [9] and an accompanying paper [8], a triple probe was used to analyze the plume of a pulsed plasma thruster (PPT), finding temperatures up to 4 eV and densities in the 10^{-21} m^{-3} range using Chen's corrections. Eckman also performed error analysis, showing that error in temperature was approximately 0.75 eV (±19%) due to scope error and error in density was ±60% due to assumptions in triple probe theory. FuZE plasmas are much hotter than 4 eV, though, so for this investigation, Chen's $-0.4k_BT_e$ and $\pm 3n_e$ are assumed for maximum theory error.

Burton, DelMedico, and Andrews [2] also investigated thruster plumes, but using quadruple probes, showing temperatures up to 8 eV with total estimated error of up to 37%. Triple probe theory in this paper is as is presented above, but they use a Mach probe that is angled 90 degrees to the flow rather than hidden behind an insulator. This changes the equations and assumptions used, so Burton's Mach probe theory is not used in this thesis. Neither is the Mach probe theory found in Zwahlen [33], which uses a quadruple probe in current mode, where all four probe tips are biased, as the probe used in this thesis is set up for voltage mode. However, the triple probe theory in these sources agrees with the others.

Ando, et al. [1] uses a multi-directional Mach probe for an unmagnetized plasma, for both subsonic and supersonic flow up to $M_i = 1.7$. Using Hudis & Lidksy's Mach probe model [12], they calculated the calibration constant in the Mach probe equation K to be 2.5, although they use the condition $T_i = 2T_e$, while for this investigation it is considered that $T_i = T_e$. This investigation also uses a quadruple probe where the Mach probe only measures velocity in the $\hat{z}$ direction, whereas Ando, et al. use a two-directional Mach probe with four tips, all collecting ion saturation current.

Choi, Woo, and Chung [6] use a quintuple probe similar to the way this investigation intends to use a quadruple probe, implementing it as a combined triple probe and Mach probe and using the applicable theory as outlined above. The difference between this investigation and Choi's is that their Mach probe uses two unique electrodes whereas this investigation's Mach probe uses the negatively biased double probe tip collecting ion saturation current as the upstream electrode. Using laser-induced fluorescence (LIF) to measure velocity of a background plasma, the calibration factor K was measured to be 1.66; this factor was then used for velocity measurements in an ion beam. The ion beam velocity measured by the calibrated Mach probe generally agreed with the velocity measured by LIF for beam energies up to 170 eV, velocities in the hundreds of meters per second. For higher supersonic velocities up to 3 km/s, it seems error between LIF results and Mach probe results increased to around 25%.

These experiments mentioned above measured temperatures less than 10 eV and velocities less than 3 km/s. Temperatures in FuZE pinch assembly region reach the keV range, so temperatures in the end chamber will possibly exceed 10 eV. Additionally, plasma velocity in FuZE reaches approximately 100 km/s, much faster than plasma in any of the experiments mentioned above. For these regimes, quadruple probe theory may not hold up.

Other experiments have used Langmuir probes in hotter plasmas. Matthews [20] reviewed and compiled literature on tokamak experiements like DIII-D and PDX, examining the use of electrical probes to diagnose tokamak edge plasmas where temperatures and velocities are higher than those in the experiments mentioned above. With regards to triple probes, Matthews emphasizes the importance of the assumption that plasma is considered uniform across the probe tips by mentioning mentioning magnetic field angles, non-saturation of ion currents, and sheath power transmission in the diverter areas of tokamaks. For FuZE, plasma is unmagnetized in the end chamber, and Debye length is still much less than the radius of the probe for expected values of plasma parameters, so probe theory should still apply. Matthews also considers Mach probes as methods of diagnosing tokamak plasma velocity, but cites irregularity in theory when examining effects of viscosity as I have above (the viscosity factor is included in the calibration constant K). He concludes that the great uncertainty in values of this constant at higher Mach numbers makes Mach probes “little more than flow direction meters,” and difficult to apply in tokamaks.

Langmuir probes’ uncertainty in theory and analysis stems from the intrusive nature of their collection and how it affects the plasma around the electrodes. Spectroscopy provides a non-intrusive alternative that may be more reliable for hot and fast plasmas.

Khachan and Collis [18] used Doppler shift spectroscopy of the hydrogen H_α line to measure ion energy distributions in discharges of inertial-electrostatic confinement devices. They observed the large central peak of static H_α arising from electron impact processes, as well as wider “wings” of Doppler-shifted H_α. By fitting Gaussian curves to these lines, they were able to precisely determine the kinetic energy of these other peaks, showing directional hydrogen ion beams in their device.

Groebner, Brooks, Burrell, and Rottler [11] used spectroscopy of the 468.6 nm helium-II line to measure plasma in the Doublet III tokamak. They used a neutral heating beam to excite helium inserted into the deuterium plasma, measuring Doppler shift to calculate velocity and line broadening to calculate temperature, showing velocities of 8.8 ± 0.3 km/s and temperatures of 1145 ± 42 eV. They cite three main sources of error: impurity interference, cold plasma interference, and difficulty in determining the charge transfer component of line broadening at low signal levels. However, the interference of lower temperature and velocity plasma in the spectroscopy measurement will require further discussion, included in later sections.

Chapter 3

DATA ACQUISITION

Using the analysis methods mentioned section 2, a quadruple probe and a spectroscopy telescope have been installed on FuZE and used to measure plasma parameters in the end chamber of the experiment. The following sections will go into detail on how these diagnostics are installed onto FuZE and how the data are measured. Some circuitry diagrams and pictures are included; more pictures of the experimental setup can be found in appendix A.

3.1 Langmuir Probe Setup

This quadruple Langmuir probe was constructed by a student named Emmett Lalish a few years prior to my arrival at the lab. The probe box was intact and present, but needed a few minor repairs before it could be integrated with the probe. This circuitry box contains voltage dividers, buffers, and switches used to safely direct signals from the plasma at the probe tips out to a data logging device.

The first effort after getting the probe was to verify its function. When received, there was little documentation accompanying it. Only a single circuit diagram without any labels or numerical values was found, so I needed to evaluate the electronics box manually to determine its properties.

It was only after manually redrawing the circuit diagram based on the physical circuitry that an archived hard copy of a circuit diagram with numerical values was discovered. This verified that the correct circuitry was in place, with the exception of the DC bias on the double probe being swapped between probe tips. To our relief, it confirmed my physical inspection of the device in showing that voltage dividers and

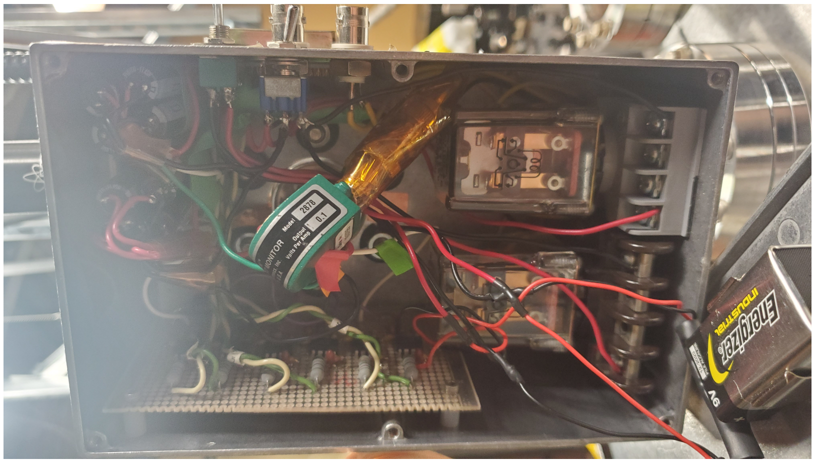

Figure 3.1: Internal wiring of Langmuir probe electronics box. Controlling circuitry board is on the bottom, with inputs from AC/DC power and DB25 output on the top. Transparent boxes to the right are relays used to turn the bias on the probe on & off.

buffers were installed on each input to prevent voltage spikes from the plasma from propagating directly to the attached oscilloscope. It also specified which power inputs were required for the probe, and which output pins corresponded to each quadruple probe electrode. These were also manually verified by examining circuit paths within the box.

The floating probe tip on the right side of figure 3.2 floats with the plasma, and is kept electrically isolated from the rest of the probe (except through machine ground). The voltage on this tip is subject to a voltage divider and a buffer before being read by the attached MDO-3014 oscilloscope with 1 MΩ impedance. The double probe uses a 200 V negative bias on one tip to force collection of the ion saturation current for sufficiently cold plasmas (see 2.1.5 for more discussion on this), supplied by an external high voltage power supply. 120 V AC power for the relays is fed from a standard wall power socket.

Additionally, the setup of this quadruple probe was done to ensure true differential measurements between DB 25 tips by avoiding contamination of grounds or setting

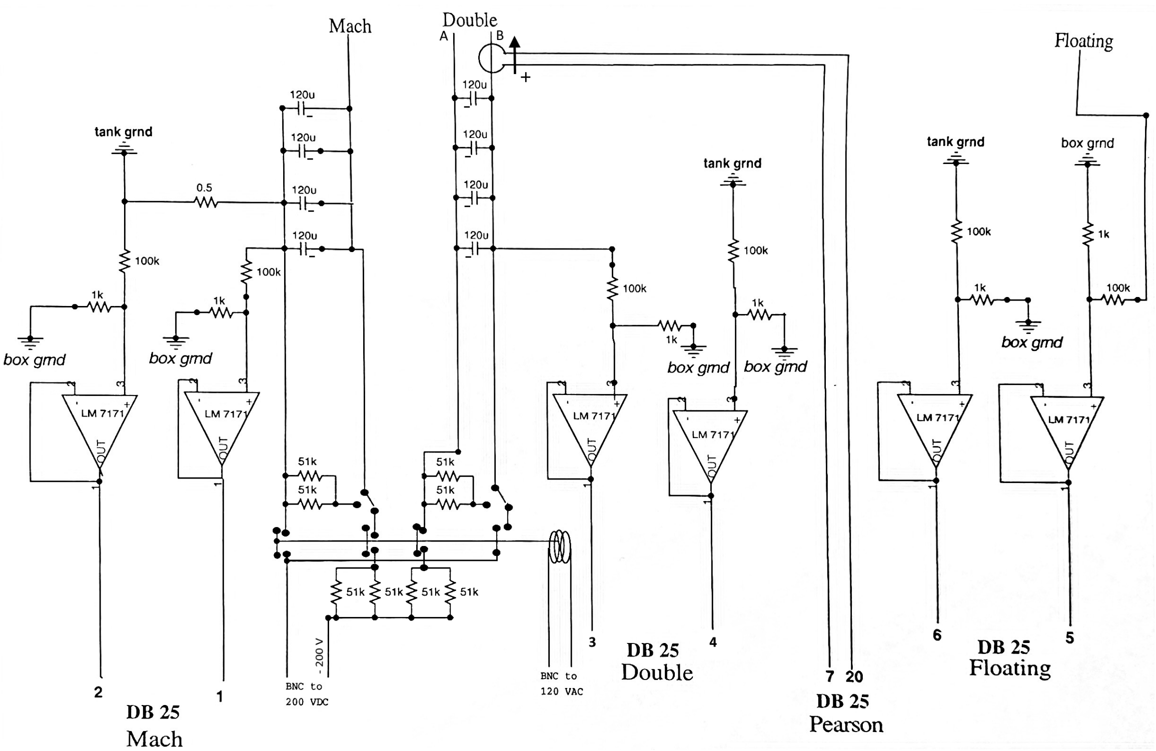

Figure 3.2: Electrical diagram of quadruple Langmuir probe circuit. From left to right are the Mach probe circuit, double probe circuit, and then the floating probe circuit. The Mach probe tip and double probe tip A are biased to collect ion saturation current.

up ground loops. The DC high voltage power supply (HVPS), oscilloscopes, and trigger were all insulated from ground while the experiment was running. While AC power is on and the relays in figure 3.2 are active, the circuit and the DC HVPS are grounded, but these are floating when AC power is off. To avoid charge buildup, alligator grounding clips are attached to the DC HVPS when the experiment is not running.

The probe is physically attached on top of the end chamber 1.13 meters downstream of the inner electrode nose cone (60 cm downstream of the end wall cathode). Using a dial on the end of the probe, the probe tip can extend between the fully retracted position just outside of the vacuum chamber's radius to the fully extended position at R = 32 mm, the same radius as the edge of the spoked end wall's hub. By utilizing this extension, we can determine a radial profile of plasma parameters in the end chamber.

Data are obtained from the Langmuir probe using a pair of Tektronix MDO3014 oscilloscopes. There are four outputs from the Langmuir probe: floating voltage, double probe voltage, double probe current, and Mach probe voltage. Although each oscilloscope has four input channels, the trigger requires use of one of these four channels, necessitating the use of two scopes. To reduce ringing, Mach probe and floating probe voltage measurements are input at 50 Ω impedance. The double probe current uses a Pearson Model 2878 current monitor inside the electronics box to measure current, and is input to the scope at 1 MΩ impedance to back-terminate at the current monitor, which is 50 Ω. As the experiment runs, the scopes are triggered 2 ms before the start of the pulse. Once triggered, each scope collects one million samples in a data record 4 ms long, covering the entire progression of the pulse.

The data from the scopes are transferred to a data storage location via local internet after converting to the voltage and current values at the probe tips. Floating voltage, double probe voltage, and Mach probe voltage are multiplied by 101 to compensate for the voltage dividers in the electronics box, and double probe current is multiplied by 10 to compensate for the voltage divider in the Pearson probe. Mach probe voltage is then divided by 0.5 Ω (seen in the top-left of figure 3.2) to calculate current on the Mach probe, which is the value stored.

3.2 Doppler Shift Spectroscopy Setup

In order to measure plasma velocity with Doppler shift spectroscopy, a component of the observation chord must be parallel to the direction of flow so that some red- or blue-shift in the light spectrum can be measured. To this end, a 1:1 telescope is mounted on the FuZE end chamber at 35° to the $\hat{z}$ direction. This observation chord intersects the centerline at the point exactly below the Langmuir probe, so although the Langmuir probe only extends as far as R = 32 mm, the diagnostics should be measuring plasma at the same distance from the end wall. This measurement is muddied somewhat for the spectroscopy telescope as the 35° observation chord includes half of its length upstream of this point and half downstream, so the telescope will observe light from plasma that is both upstream and downstream of the Langmuir probe. This needs to be taken into consideration when analyzing spectroscopy data.

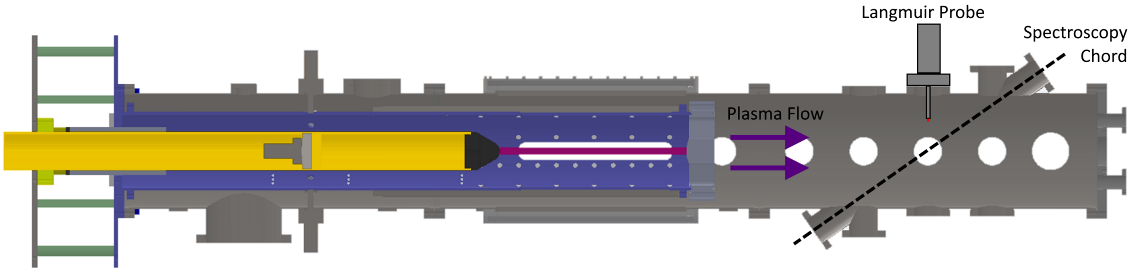

Figure 3.3: Side profile diagram of FuZE with locations of diagnostics installed in the end chamber. Plasma flows out of the acceleration region on the left and into the assembly region, where it forms into a pinch. After exiting the end wall, the Langmuir probe and spectroscopy telescope observe plasma as it travels downstream.

Light from the telescope is passed into a fiber with 20 chords. These chords are arranged laterally, which provides some element of spatial resolution to the spectroscopy measurement. This light is routed to a Princeton Instruments Acton SpectraPro SP-2500 spectrometer with ICCD (the I indicates that an intensifier can be used to amplify signal), where it is recorded with Princeton Instruments' *LightField* software. The spectroscopy measurement is taken at one point in time, which can be adjusted through the *LightField* interface. The gate width (exposure length), intensifier gain, and center wavelength of observation can also be adjusted in *LightField*.

3.2.1 Spectroscopy Calibration

Spectroscopy measurements are especially sensitive. Using equation 2.16 we can see that a Doppler shift of only 0.1 nm in the 468.6 nm He-II spectra corresponds to a flow velocity of 78 km/s. Thus, even minor imperfections in the fiber or connection to the spectroscope can cause large errors in velocity measurement. To ensure precise measurements of peak wavelengths, we need to first calibrate the spectroscope.

To be accurate, calibrations are performed using the same settings on the spectroscope as will be used for data measurement. I intended initially to measure plasma velocity using spectra of carbon-III impurities caught up in the plasma flow. However, the vacuum chamber window the telescope was attached to was Pyrex, which is opaque to light under approximately 280 nm, so we would not be able to measure the major carbon-III line at 228.8 nm. Even once this window was replaced with fused silica (which is transparent to light down to approximately 160 nm), I found little Carbon-III signal in the end chamber. Thus, I decided to look directly at plasma velocity by injecting helium gas into FuZE rather than hydrogen or deuterium. He-II has a strong emission line at 468.6 nm, so calibrations of the spectrometer were performed with the center wavelength set at 468 nm and a diffration grating of 2400 lines/mm. While a diffraction grating of 300 lines/mm is also available, this setting does not provide pixel resolution accurate enough for velocity measurements. The higher resolution grating of 2400 lines/mm provides resolution of 100 pixels/nm; each pixel corresponds to a wavelength shift of 0.01 nm, corresponding to a He-II velocity shift of 7.8 km/s. Calibration at these settings was performed using spectra taken of a neon lamp; Ne-I and Ne-II have eight strong peaks between 464 nm and 472 nm (figure 3.4).

Once the spectrum is recorded, peaks can be found and correlated with known peaks of neon (these can be found on the National Institute for Standards and Technology's Atomic Spectra Database). There is an offset between the observed peak wavelength and the true peak wavelength that depends on the wavelength of light. Depending on the spectroscope, this relation may be nearly constant, a linear function, or a function of some higher power. For the spectrometer used here, a linear correction is accurate. Using a linear fit to relate the wavelength observed and calcu-

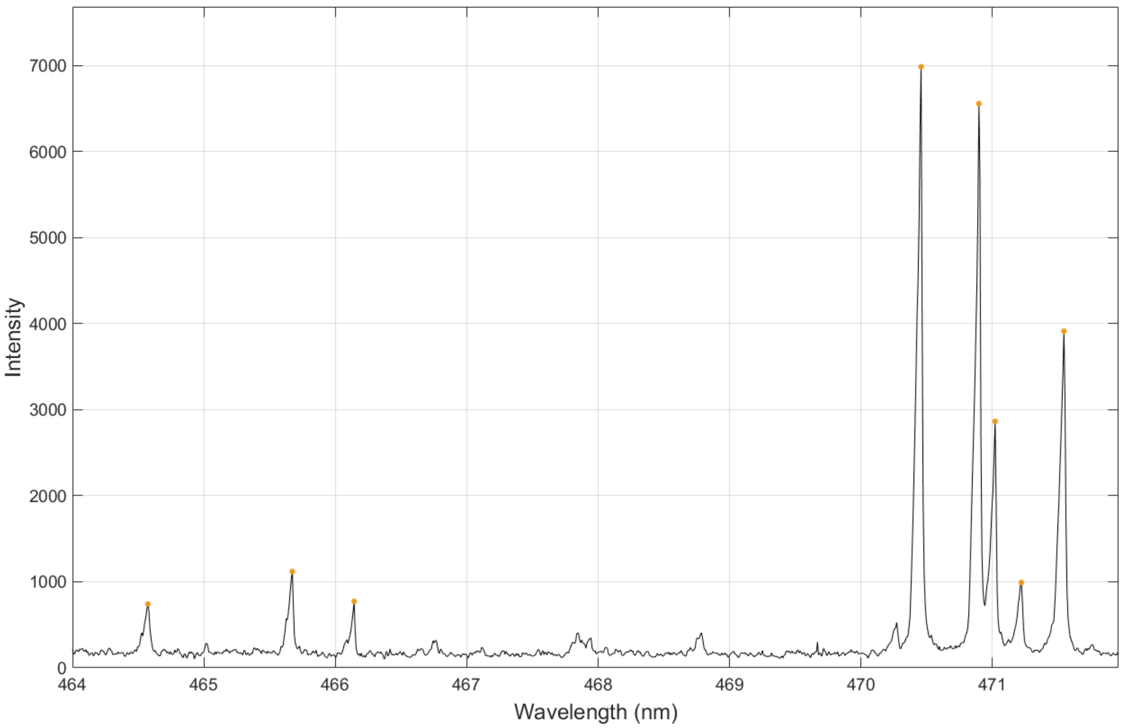

Figure 3.4: Observed line spectra of neon between 464 nm and 472 nm wavelength, taken with spectrometer centered at 468 nm with a 2400 lines/mm grating. Notable peaks are visible at 464.54 nm, 465.64 nm, 466.11 nm, 470.44 nm, 470.88 nm, 471.01 nm, and 471.53 nm.

lated by *LightField* to the true wavelength for each chord yields:

$$\lambda_{true} = m\lambda_{obs} + b \tag{3.1}$$

The twenty different m and b values for each chord, found via the calibration equation above, remain constant for the spectrometer settings, so can then be used to correct any spectra observed at these settings to its true wavelengths. This method of calibration can also be used at coarser grating settings or different center wavelengths, yielding different m and b calibration values.

Chapter 4

EXPERIMENTAL RESULTS

In investigating the plasma plume in the end chamber of FuZE, 202 plasma pulses were taken over the course of six months. Of these, the first 69 pulses were taken using data only from the triple probe electrodes; the rest used the full quadruple probe. The last 79 pulses also included data from the spectroscopy telescope, calibrated to the 468.6 nm He-II line. Plasma current was provided by the capacitor bank with thyristor switches. These pulses used pure hydrogen, pure helium, or a mix of 80% hydrogen and 20% deuterium as injection gas, injected at 3 microseconds before the pulse at a line pressure of approximately 100 PSIA.

As some data are redundant and some data are irrelevant to the outcome of the investigation, not all 192 plasma pulses will be presented here. Instead, this chapter will walk through the data taken that is relevant to the discussion in this investigation. This chapter will present the data itself and note the conclusions made from the data with regards to how well the data was recorded and how well the data reflects the intended goals of the experiment runs. The following chapter will go into further detail on this data, analyzing it to draw conclusions about the nature of the plasma plume.

4.1 Initial Results Using Only Triple Probe

The first sets of data taken used only the first three probe tips of the quadruple probe as a triple probe: the floating probe, and the biased double probe. The intent of these data was to provide an initial view of what probe outputs looked like, and to ensure timing and setup of the diagnostics and data collection instruments was correct. The timing and setup was especially important, as the quadruple probe being used had not been used on FuZE before, and when used before, had only been implemented to record floating voltage.

The first shots were taken with the Langmuir probe retracted out to the edge of the vacuum chamber. At this point, if the plasma is collimated exiting the end wall, there should not be much signal, but signal will be seen if the plasma diffuses out to the edges of the vacuum chamber. Initially, the signal was noisy; enough noise was present that it drowned out any actual signal that was there. This noise corresponds with spikes in the V_{gap} Tuning the scale on the oscilloscopes and setting line termination to 50 Ω on voltage measurements helped damp this noise in preparation for running the full quadruple probe setup.

4.2 Quadruple Probe Results

Once the Mach probe was enabled, the first data run on 9 October 2019 attempted to obtain a radial profile of plasma measurements in the end chamber, at three different points: R = 65 mm (center of end wall gap), R = 77 mm, and R = 89 mm (edge of end wall gap). These positions are shown in figure 4.1 below.

In this profile, notable intermittency in data is observed that is inconsistent with the experiment parameters and the properties of assembly region plasma, which are consistent shot-to-shot. Shots 191009006 and 191009007 were executed at the exact same settings, with the thyristor bank at 3.3 kV and the Langmuir probe extended to the R = 65 mm position, but show drastically different measurements, one high amplitude and one low.

Similar intermittency is seen in other signals on the same day at different positions and different bank charges. At R = 65 mm, three of four shots show higher amplitude signals similar to shot 191009007 in figure 4.2, with one showing a lower signal (shot 006). These four shots covered thyristor bank voltages between 3.0 and 3.6 kV. At R = 77 mm, all four shots show lower signals like shot 006. At R = 89 mm, two of

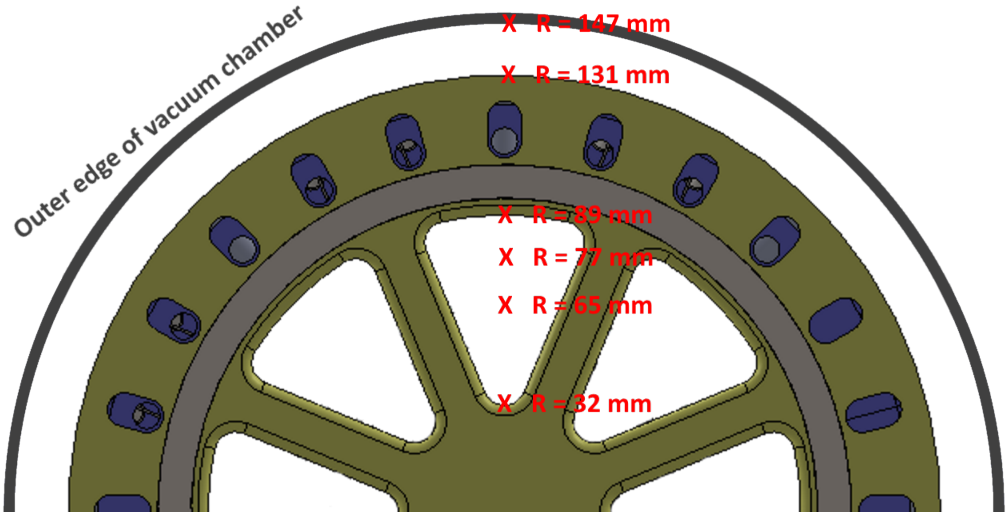

Figure 4.1: Langmuir probe radial profile positions. The probe can extend as far into the chamber as the edge of the central hub of the end wall, at R = 32 mm. The other positions used for data measurement are at R = 65 mm in the center of the spoke gap, R = 77 mm, R = 89 mm at the edge of the gap, R = 131 mm at the edge of the end wall, and R = 147 mm at the edge of the vacuum chamber.

three show the larger signal, with one showing lower. In all shots, there is seemingly no correlation with bank voltage and whether or not the high amplitude or low amplitude signals were observed.

Additionally, intermittency is seen in these signals' arrival time. Signal arrival in the larger signals is inconsistent and does not line up with any notable events in the P45 magnetic field or V_{gap}, as seen in figure 4.3. However, timing does line up in the smaller signals, figure 4.4.

As the calculated plasma parameters are derived directly from probe signals, parameters also show similar intermittency. However, they show different magnitudes, with temperatures of the larger signals reaching nearly 80 eV (as calculated numerically) and temperatures on smaller signals peaking at less than 20 eV. Calculated number densities and flow velocities are more notably different between the smaller and larger probe signals, figure 4.5.

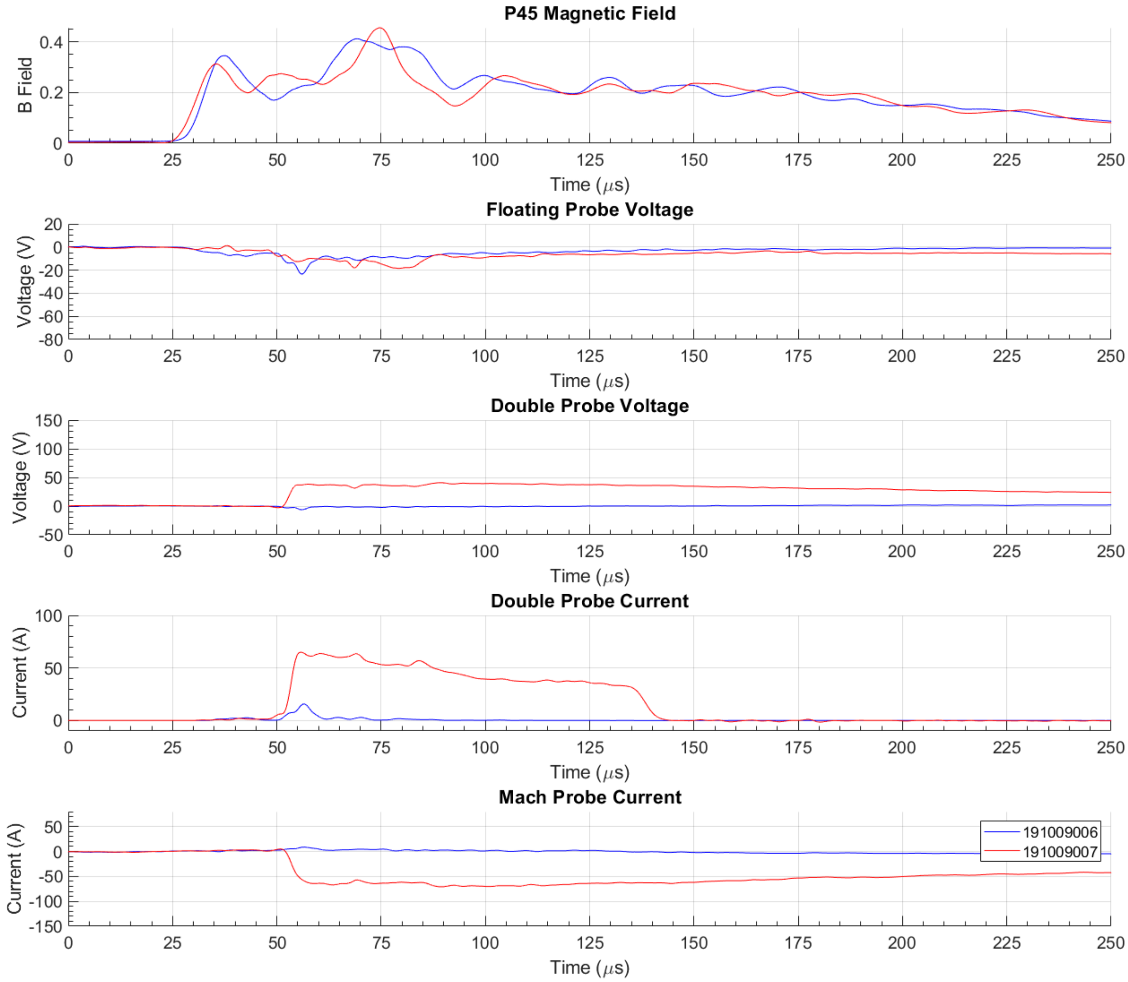

Figure 4.2: Plotting data traces for shots 191009006 & 191009007 side-by-side illustrates intermittency in the Langmuir probe signals, where some pulses produce significantly higher amplitude signals than others. Both of these shots used identical experiment settings with the thyristor bank at 3.3 kV and Langmuir probe position at R = 65 mm.

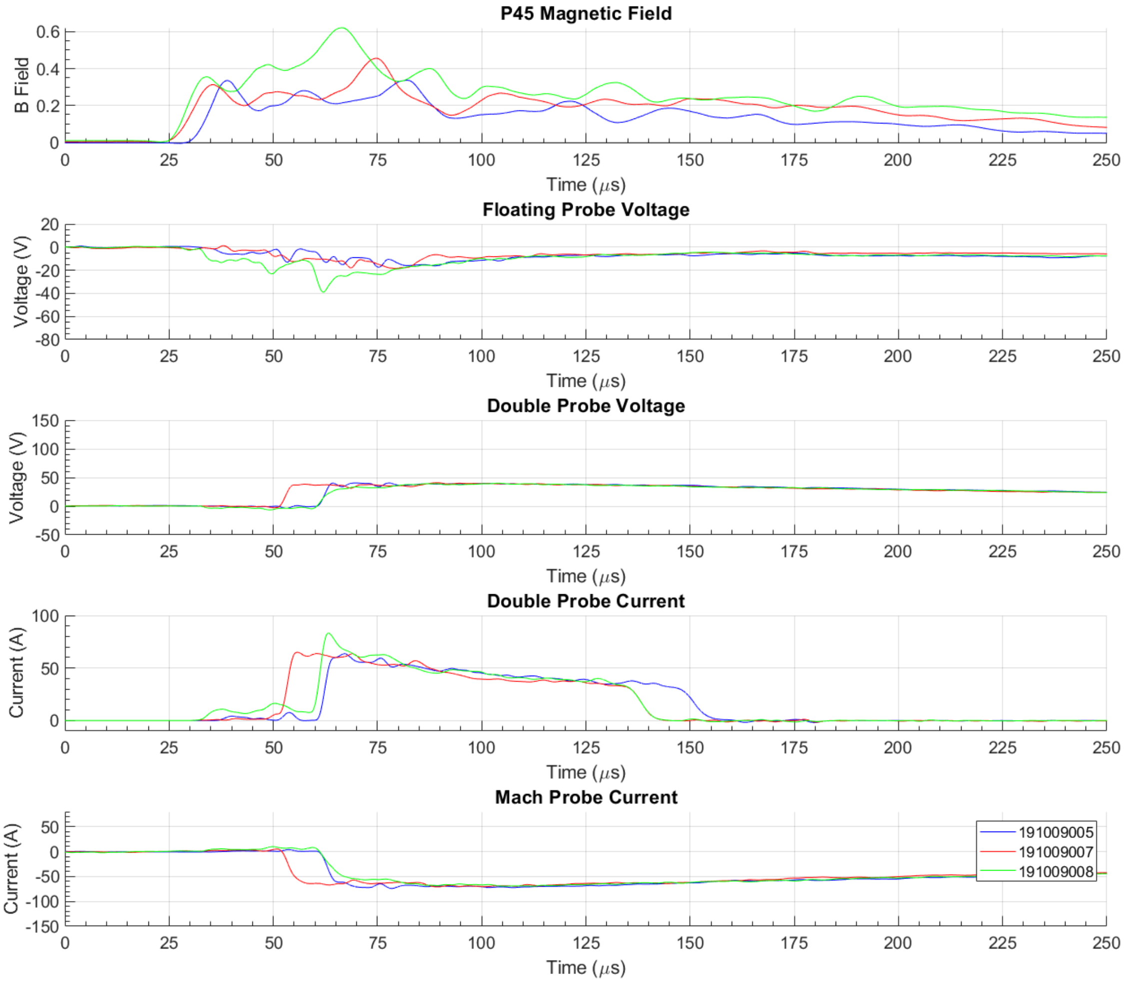

Figure 4.3: Plotting data traces for shots 191009005, 007, & 008 side-by-side illustrates intermittency in the timing of signal arrival. The Z-pinch characteristics are consistent shot-to-shot, yet the timing of signal arrival in these higher-amplitude signals differs by 10 μs. The Langmuir probe was positioned at R = 65 mm, with bank voltages of 3, 3.3, and 3.6 kV, respectively.

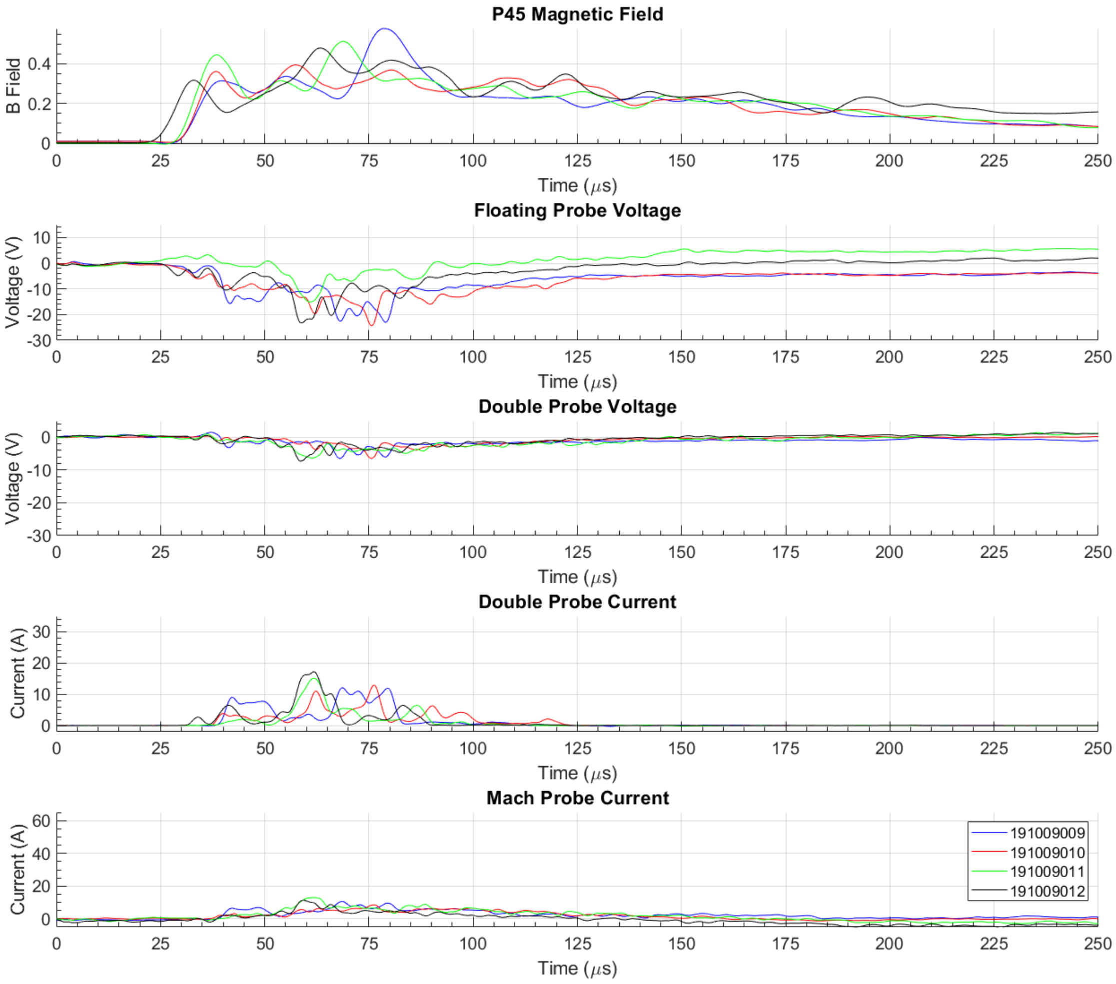

Figure 4.4: Plotting data traces for shots 191009009 through 012 side-by-side illustrates that for the smaller signals, arrival times seem to be consistent at around 40 μs. Amplitudes of these signals are consistent with one another, but some features exist on some signals that aren't present in others (i.e. all peaks in the signals don't necessarily line up).

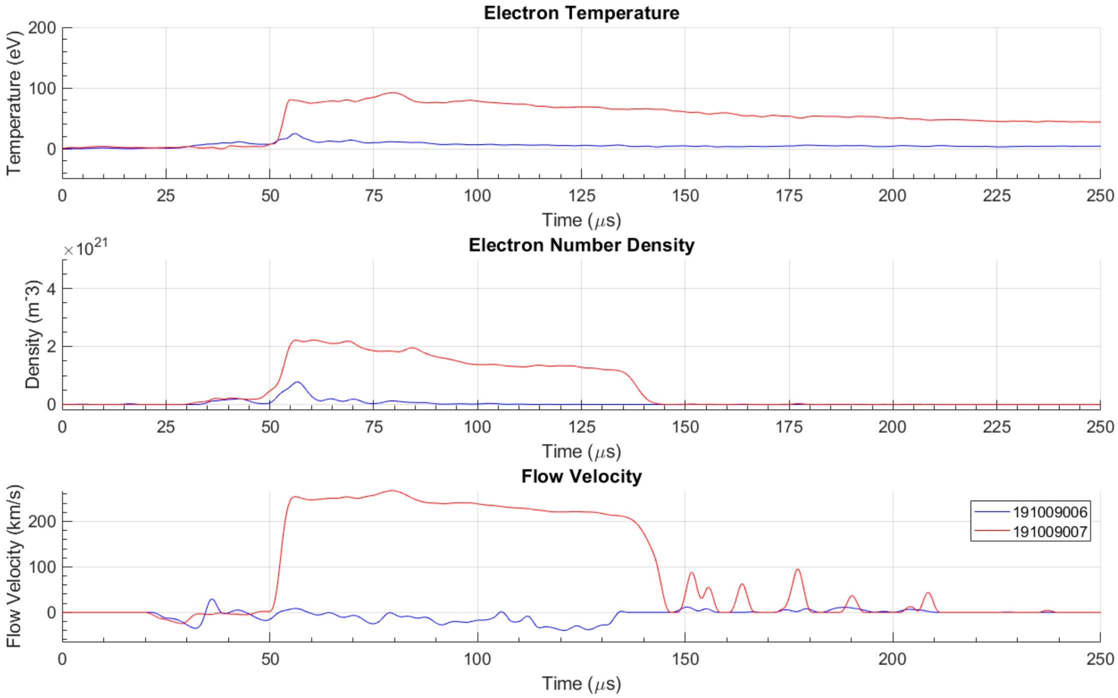

Figure 4.5: Plotting data traces for shots 191009006 & 191009007 side-by-side also illustrates amplitude intermittency in calculated plasma parameters between the smaller and larger Langmuir probe signals. Plasma parameter calculations are especially sensitive to changes in Langmuir probe measurements as they rely on differences and ratios between different signals, which often can be noisy.

Although intermittent, a few common features are noticeable in the higher amplitude data, such as pulse 191009007. First, whereas the main pulse starts and ends by about 150 μs, as seen in the gap voltage trace and in the noise in the voltage traces, the voltages traces themselves take much longer to decrease once the pulse is initially recorded. Second, another feature noticeable in this data a sort of “spike” in the raw data is evident at the time the signals jump in amplitude. This spike is seen on the “voltage” traces — the floating voltage, double probe voltage, and Mach probe current. The Mach probe current is considered a “voltage” trace here because it is calculated by taking the voltage from the Mach probe and dividing by a 0.5 Ω resistor that links the Mach probe to ground. This spike doesn’t seem to consistently line up with any features in the P45 magnetic field or gap voltage, nor does it occur at the same time shot-to-shot. However, it does always occur in the larger amplitude intermittent signals at the point where the amplitude begins to jump.

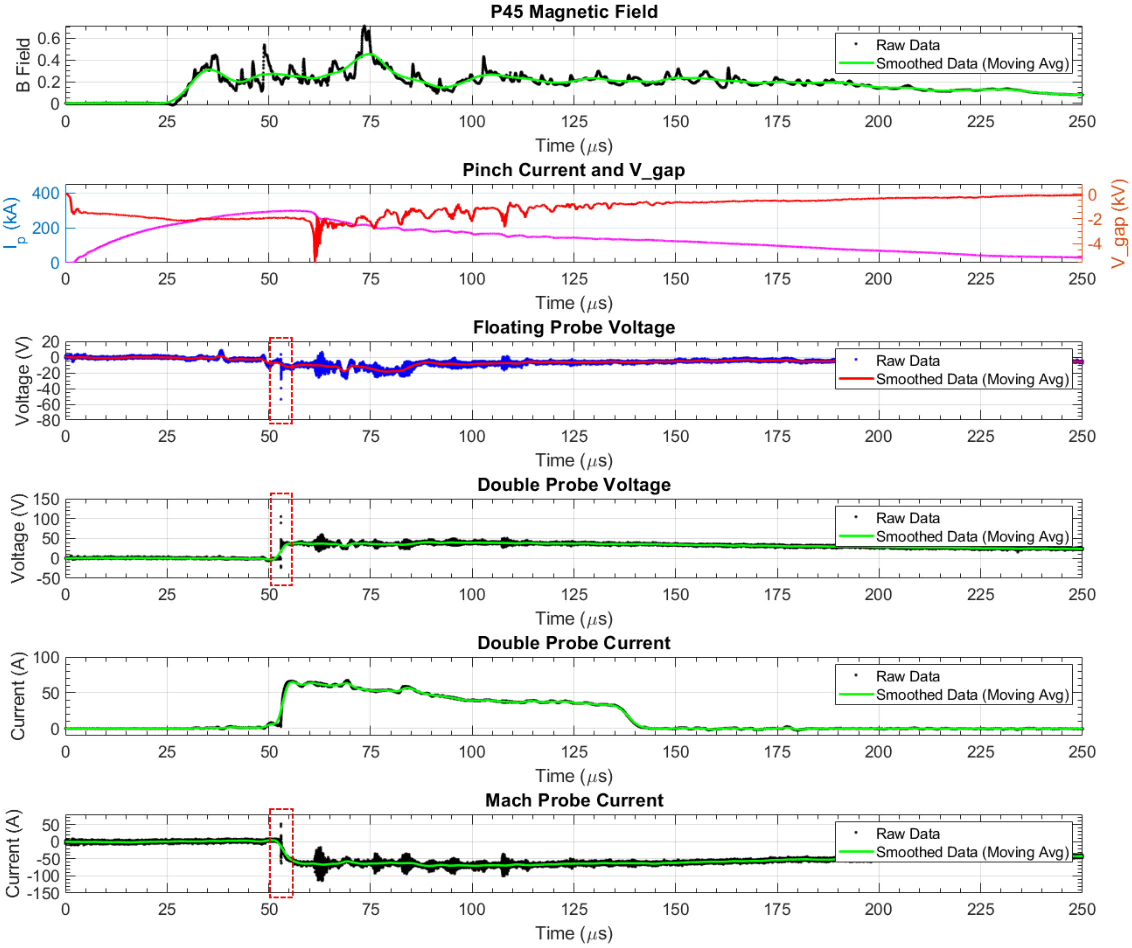

Figure 4.6: A noticeable "spike" in raw data for voltage signals is seen in the larger signal shots such as pulse 191009007. In this case, voltage signals include the Mach probe current, which is calculated using the voltage on the Mach probe tip.

4.3 Quadruple Probe Results with Simultaneous Spectroscopy

Further data taken on 25 November 2019 and 9 January 2020 for the purpose of getting spectroscopy set up show Langmuir probe data with similar intermittency (see appendix B) in timing and amplitude. Five shots on 25 November all have the higher-amplitude style traces and thus don't show the same intermittency in amplitude as the data shown above, but they do show the same intermittency in timing. Four shots on 9 January have intermittency in both timing and amplitude. All of these shots were taken on the thyristor bank at 3.5 kV, using 100% H_2 gas. Additionally, the spectroscopy diagnostic was used for the first time on these pulses, with the intent of analyzing a 228 nm carbon-III impurity line to determine the flow velocity of the plasma. This spectroscopy showed no light, and it was only after the data was taken that I realized that the spectroscopy telescope was attached to a Pyrex window that is opaque to light under 280 nm. This window was subsequently replaced with one of fused silica.

As it turns out, this replacement was not necessary, as data from this point on was taken using pure helium instead of hydrogen in order to directly measure the velocity of bulk plasma ions instead of impurity ions entrained in the flow.

The next data run on 14 January intended to measure velocity of plasma directly and use those measurements to calibrate the Mach probe. In the Langmuir probe signals, similar intermittency was seen in both the first eight shots at 3.5 kV and the last 14 shots at 5 kV. However, with spectroscopy working, I could see plasma present in similar amounts in all of these shots (see table 4.1).

Spectroscopy is a proven diagnostic has been in use for years in the FuZE lab, and for fast, hot plasmas like we see in FuZE, spectroscopy has less noise than direct probes like Langmuir probes. Furthermore, the Langmuir probe in use here has unproven capabilities and more complicated circuitry than a simple spectroscopy measurement. For the purposes of evaluation of Langmuir probe signals, spectroscopy is considered

Table 4.1: Double probe currents and light intensities of shots with intermittency in Langmuir probe signal. Recorded light intensity in this table is normalized by the gain on the intensifier and the gate width, integrated over all wavelengths, and averaged over all 20 chords.

Shot Number	**Maximum Current on Double Probe (A)**	**Integrated Light Intensity**
15	4.70	538.04
16	8.32	533.86
17	64.68	535.93
18	9.02	535.56

to likely be more reliable than the Langmuir probe. Thus, we see from the data on this day that the intermittency in Langmuir probe signals is likely not due to intermittency in the plasma itself but to intermittency in the diagnostic.

Until this point, I believed that plasma was inconsistent in demagnetizing and leaving the end wall, so I thought that the intermittency seen was due to intermittency in the plasma shot-to-shot. However, this spectroscopy data proves otherwise. A second hypothesis explains the "spike" and data intermittency: a discharge is occurring between the probe tips. The Mach probe tip and one of the double probe tips are biased negative, and a possible discharge connects these biased probe tips. Arcing between the probe tips would cause the voltages in the negatively biased probes to jump positive, explaining a negative jump in the Mach probe current (which measures positive current out of the plasma) and a positive jump in the double probe voltage and current (also measuring positive current out of the plasma) as seen in the higher amplitude traces with the "spike."

Although more about discharges will be discussed in chapter 5, at this point it is useful to discuss some notable features of these curves. A lower amplitude signal, representing a “normal” trace for the Langmuir probe, is shown in figure 4.7. A higher amplitude signal, representing an “arcing” trace for the Langmuir probe, is shown in figure 4.8.

In both traces, the magnetic field at P45 and the gap voltage are nearly the same; these are measurements of the Z-pinch plasma in the assembly region and are plotted alongside Langmuir probe traces as a reference for timing and noise. The floating voltage is also similar in amplitude in both traces. Much of the signal in this floating voltage is likely EMI noise corresponding with noise in V_{gap}. The signal in the floating voltage is seen starting at around 25 μs when the first oscillations are visible. This feature is seen on nearly all floating voltage traces, and is possibly an indicator of when first trace plasma arrives, although this is uncertain.

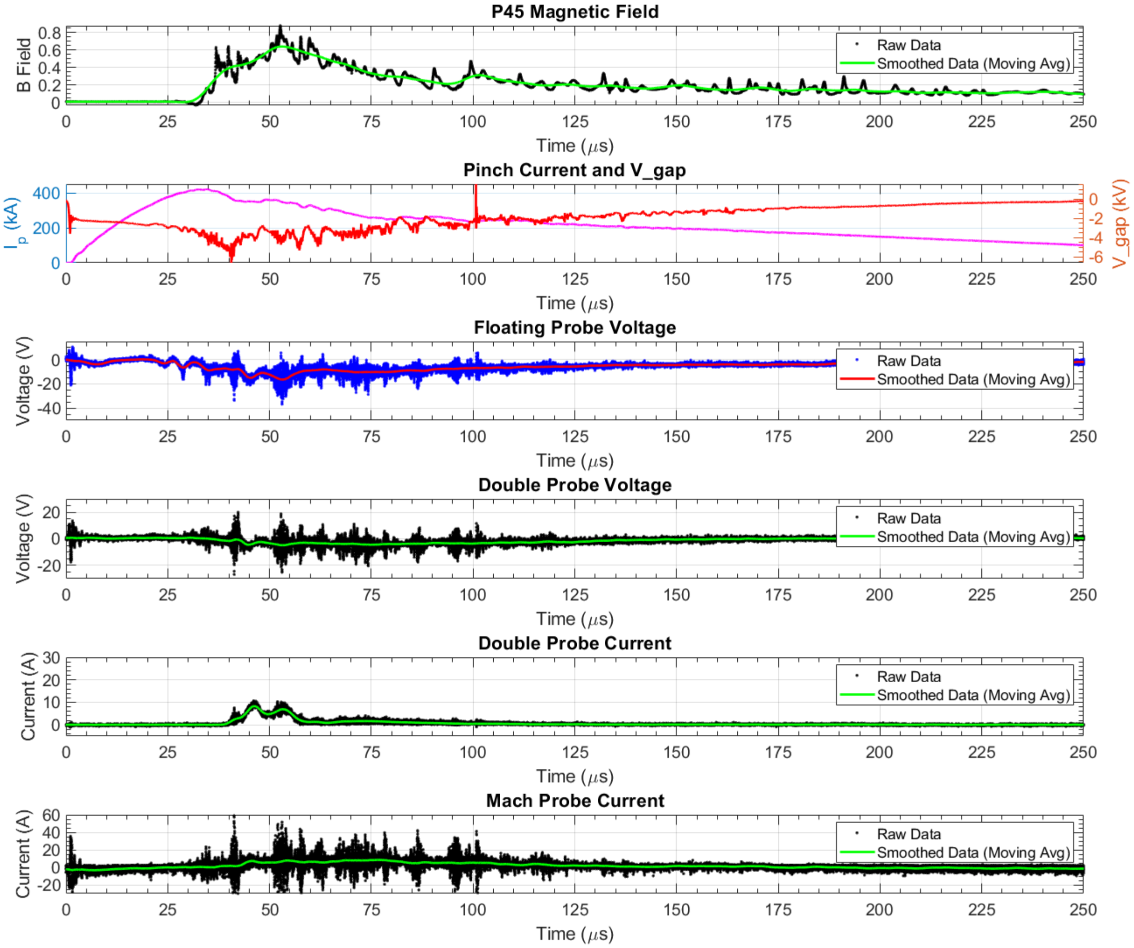

Figure 4.7: Langmuir probe data from shot 200114016, showing one of the smaller-amplitude signals. All small-amplitude signals look similar to this, with similar amplitudes and start times. We see that the double probe current begins to rise at 38 μs, 6 μs after the magnetic field begins to rise, which is consistent with estimates of FuZE plasma speeds at 100 km/s.

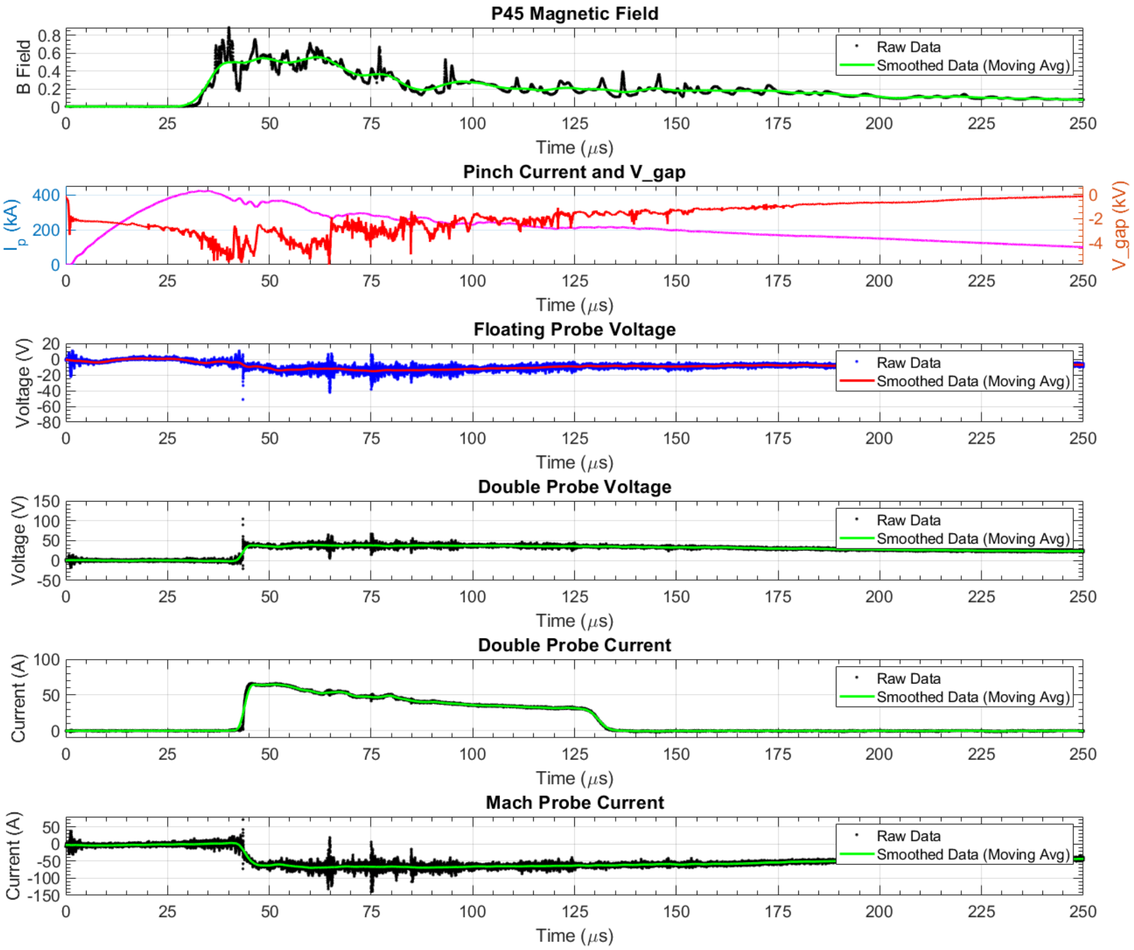

Figure 4.8: Langmuir probe data from shot 200114017, showing one of the larger-amplitude signals. Larger-amplitude signals like this seen in the data have similar shapes and amplitudes but timing can differ slightly of when the large jump occurs. These signals are believed to represent discharges between probe tips.

Looking at the double probe and Mach probe traces are where the “normal” and “arcing” shots differ significantly. In the arcing shots, a similar ramp of signal is seen prior to the jump in amplitude. It’s helpful to focus on the double probe current signal to see this similarity, as the double probe current signal uses a Pearson current monitor and not a voltage measurement from a Langmuir probe, and is less noisy. After this initial ramp of signal that arrives at the same time, the discharge occurs, significantly amplifying the signals on the biased probe tips. The only notable difference in floating voltage between normal and arcing traces is the “spike” in voltage that occurs at the moment of discharge; lingering falloff of signal after the discharge is only seen on the biased probe tips.

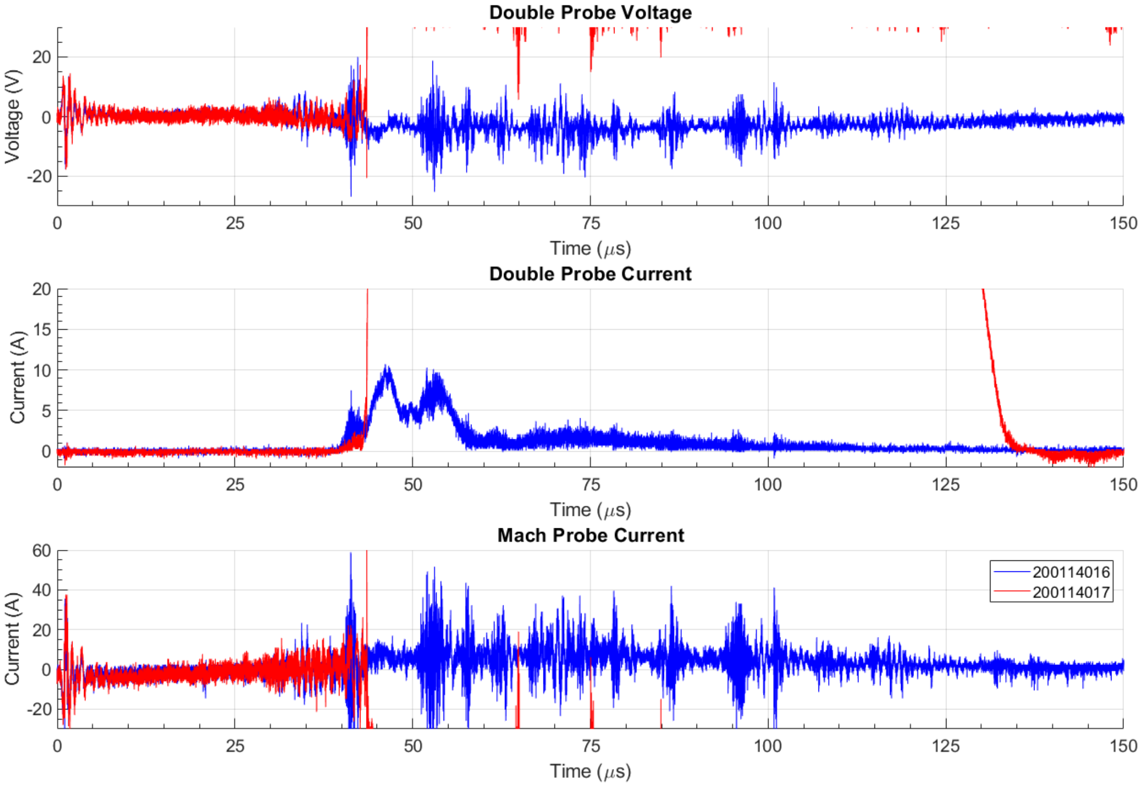

Figure 4.9: Raw data from shots 200114016 and 017, showing the difference between normal and arcing signals on the Langmuir probe. Initial signal is seen at the same time in both traces until the discharge occurs and the arcing trace jumps away.

As mentioned above, the spectroscopy results for these shots don't see similar intermittency. As the spectroscopy diagnostic is recording data for the plasma directly rather than using impurity lines, the signal to noise ratio is large. The expected He-II doublet peak at 468.6 nm is seen clearly, especially for central chords on the fiber, and provides high quality data from which to calculate velocities.

Of the 22 data shots on this day, the first 12 were taken with a diffraction grating of 300 and the last 10 with a grating of 2400. After the initial data is read in, the next step involves calibrating the data with the linear fit equation mentioned in chapter 3. There are different values for this calibration based on the diffraction grating of the spectrometer when the data was taken. As seen in figures 4.10 and 4.11, the 2400 grating and calibration provides a higher resolution data peak for velocity measurements. These shots were taken at 5 kV, with a gate width of 5 μs and a delay of 75 μs, timing the ICCD to take the data after plasma has arrived. Looking at these spectra, besides differences in resolution, possible temperature differences exist too based on the full-width half-max (FWHM) of the gaussian peak form, with the lower resolution, lower grating shots seeming hotter. However, this behavior is consistent shot-to-shot; spectra taken with a diffraction grating of 300 consistently look wider than spectra taken with the 2400 grating.

A double Gaussian curve (to match the helium doublet at 468.6 nm) is fit to all of these chords to determine the magnitude of the wavelength shift from static helium. Once the wavelength shift is determined from the Gaussian fit, velocity is extracted via equation 2.16. Velocities are calculated in the 30 – 85 km/s range, with variation between shots, but are of the same order of magnitude and within a reasonable range. Gate delay has a large effect on velocity observed, as the velocities seen in figure 4.12 were taken at 75 μs, after the initial pulse of plasma hits the end chamber, and are likely measuring a trailing stream of plasma rather than the primary pulse.

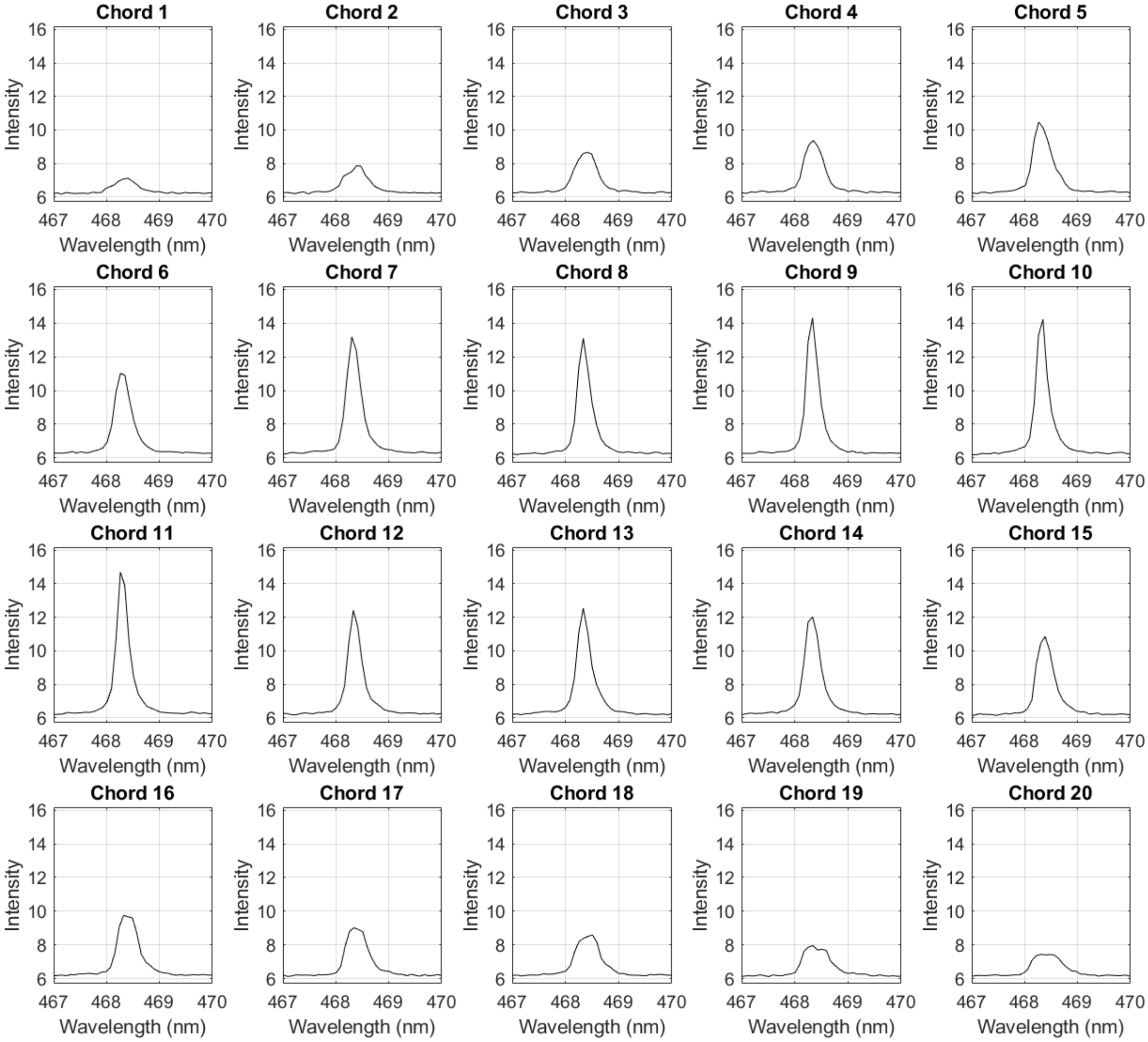

Figure 4.10: Calibrated helium spectrum,shot 200114016. A clear peak at is visible, reflecting the Helium doublet (468.5704 nm & 468.5804 nm) at that wavelength, and the peak is blue-shifted. However, due to the low resolution of the 300 grating centered at 460 nm, the location of this peak varies slightly chord-by-chord.

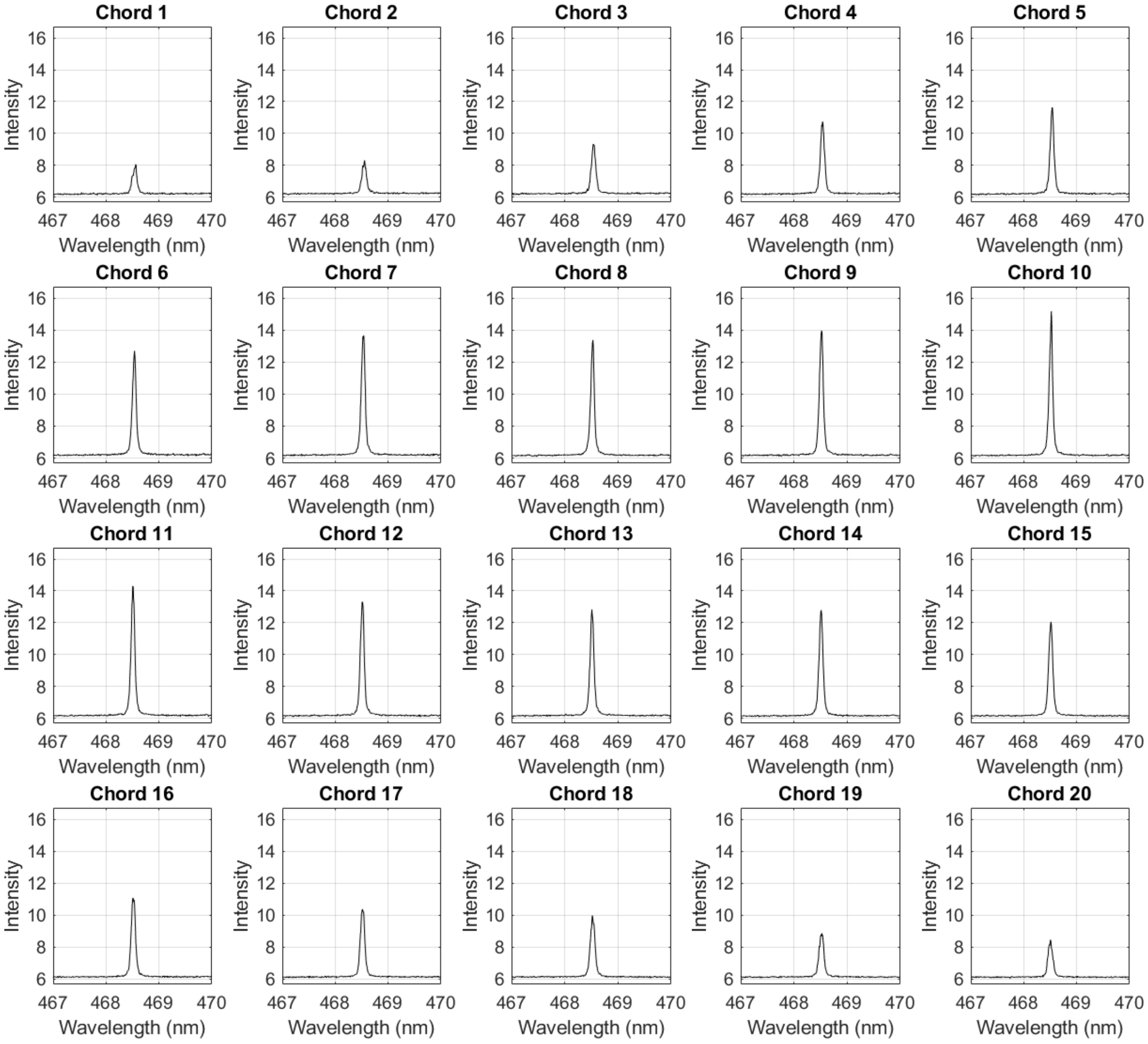

Figure 4.11: Calibrated helium spectrum,shot 200114019. A clear peak at is visible, reflecting the Helium doublet (468.5704 nm & 468.5804 nm) at that wavelength, and the peak is blue-shifted. The higher resolution of the 2400 grating centered at 468 nm provides more consistent peak locations chord-to-chord.

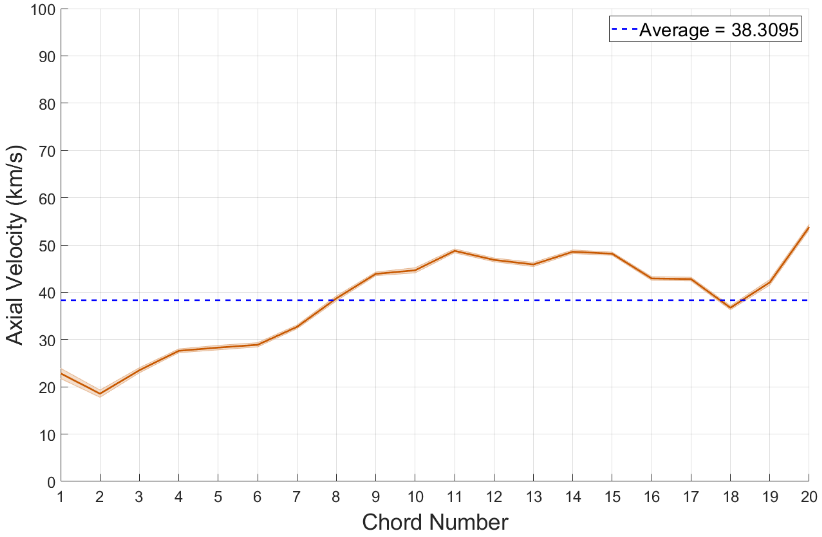

(a) 200114019

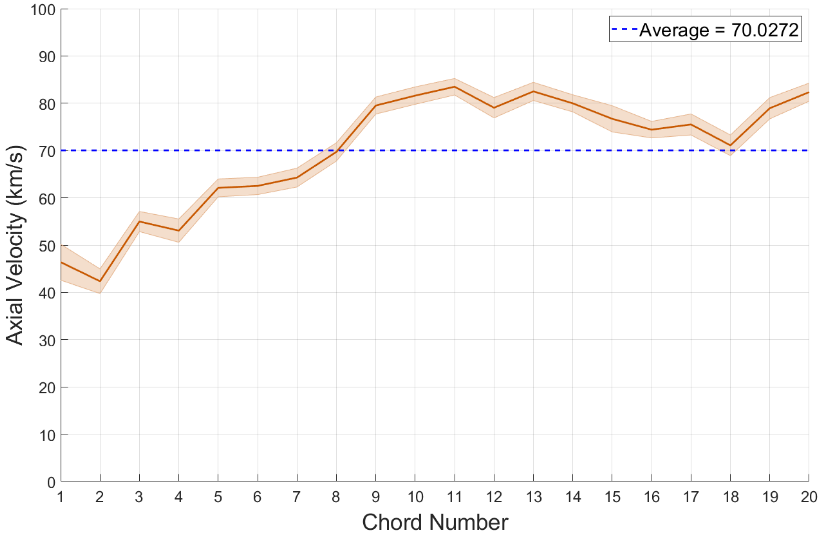

(b) 200114020

Figure 4.12: Plasma velocities from Doppler shift spectroscopy for shots 200114019 & 020. These velocities are reasonable and of a similar order of magnitude, but are taken at 75 μs gate delay so are likely measuring trailing plasma rather than the primary pulse. In these figures the orange shading around the velocity trace represents the confidence interval of the Gaussian fit. Imperfections in the calibration likely lead to the upward trend over chord number noticed in these velocity traces, so results of velocity for one shot will be the average of this curve.

On 10 and 19 February 2020, more data were taken with the objective of obtaining a full radial profile of plasma measurements according to the positions in figure 4.1. Again, the thyristor bank was charged to 5 kV for every shot and helium was used as the input gas to stay consistent with previous shots and to easily use established spectroscopy methods specific to helium.

These shots had a mixture of both normal and arcing shots. Table 4.2 shows the proportion of shots at each radial profile setting where arcing occurred. The data for shots where arcing did not occur are shown in appendix B.

Table 4.2: Number of shots from 10 Feb and 19 Feb 2020 data displaying “arcing” traces for every radial position in the radial profile

Radial Position (mm)	**Proportion of shots where discharge occurs**
32	2/5
65	2/7
89	4/6
131	0/4
147	0/4

While there aren’t enough shots at each radial position to make an accurate statement regarding probability of an arc, there is a definite trend seen in that zero of the shots taken outside the main spoke gap measured arcing. If arcing occurs because enough plasma is present between probe tips to create a short between biased electrodes, then the probability of an arc would be proportional to density. This data indicates that plasma flow is limited to the area following the gaps in the end wall spoke and doesn’t notably expand out to the edges of the chamber; i.e., the plasma plume is collimated.

This conclusion is further reinforced by probe measurements as part of the radial profile. The smoothest of the Langmuir probe measurement traces is the double probe current, which is the upstream ion saturation current according to probe theory. This current is measured by a Pearson current monitor whereas the "voltage" measurements (including the Mach probe current) are measured directly from the potentials of the probe tips, which are subject to EMI noise. A clear radial profile is visible in the double probe current when traces are plotted over one another. This radial profile also falls off steeply, as the current at R = 65 at the center of the spoke gap is nearly half that at R = 32 at the inner edge of the spoke gap.

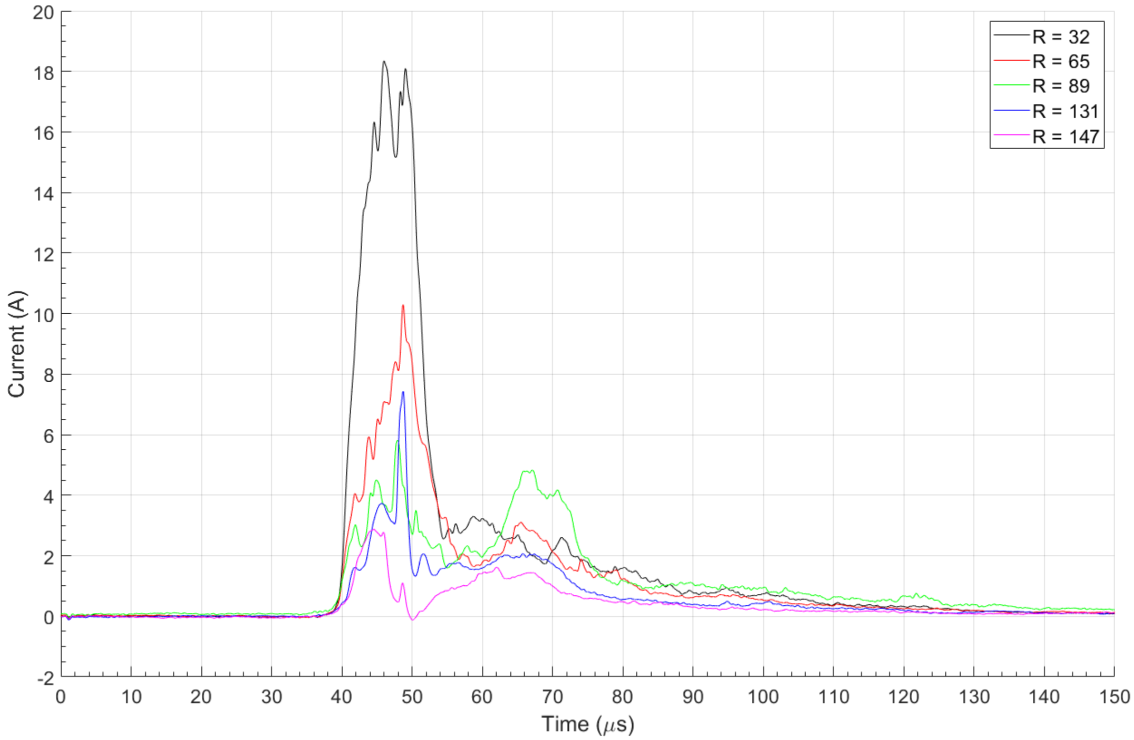

Figure 4.13: Radial profile in double probe current as measured by the Pearson current monitor inside the Langmuir probe at R = 32, 65, 89, 131, and 147 mm. As the least noisy measurement on the Langmuir probe, this shows the clearest radial profile, as the current on the double probe decisively decreases as the probe is retracted.

A radial profile is visible in the voltage measurements, as well, but it is less defined amidst the noise present in these signals. For example, in the floating voltage measurements (figure 4.14), it is difficult to determine if the first peak at approximately 30 μs is signal or noise, as it doesn't show a clear profile and amplitudes shift drastically. However, the second peak at 49 μs likely has some signal in it, evident in the much larger trace at R = 32 mm. Differentiating signal from noise will be discussed further in chapter 5.

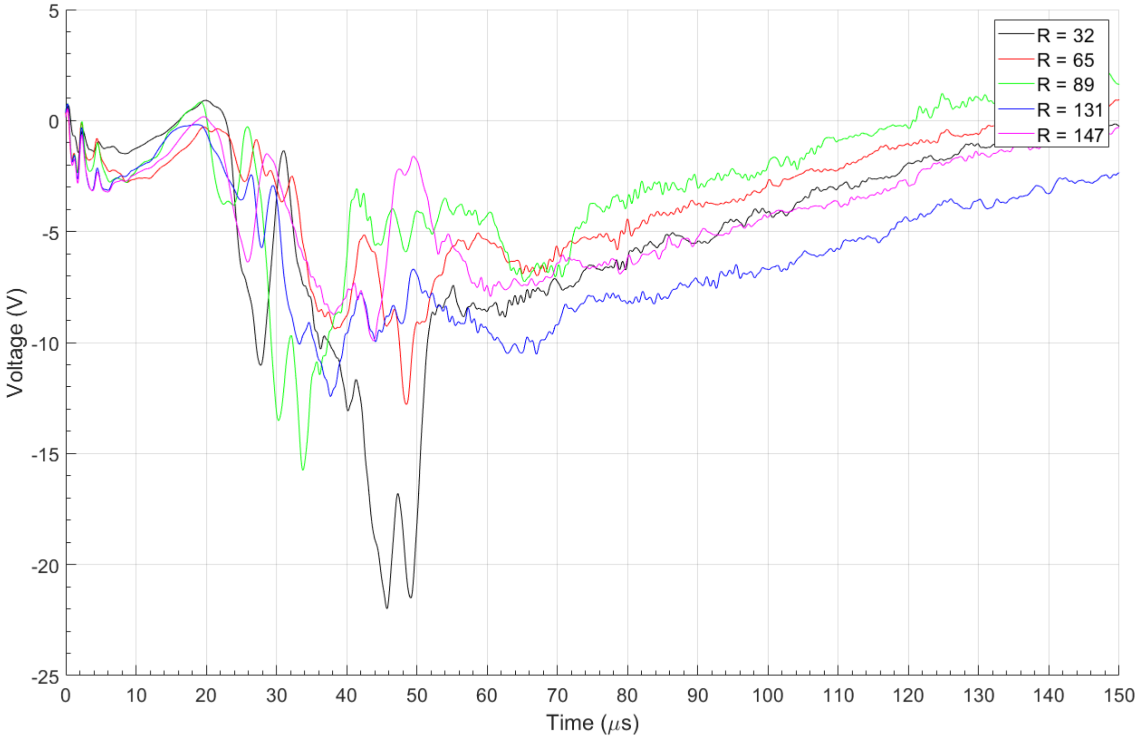

Figure 4.14: Radial profile in floating voltage as measured by the unbiased upstream probe tip on the Langmuir probe. This is a noisy signal; the signal shown in this figure is smoothed three times and still shows noise along the entire trace.

The maximum signal in double probe current (upstream ion saturation current) is seen between 40 μs and 50 μs, so spectroscopy for data shots on 10 and 19 February was recorded at a gate delay of 42 μs and a gate width of 4 μs to capture the light where Langmuir probe signal is the largest. Calculating velocities in the same way as before, using the Doppler shift of Gaussian fits to each chord, yields average plasma velocities for each shot of between 80 and 90 km/s, to a total average of 86.2 km/s.

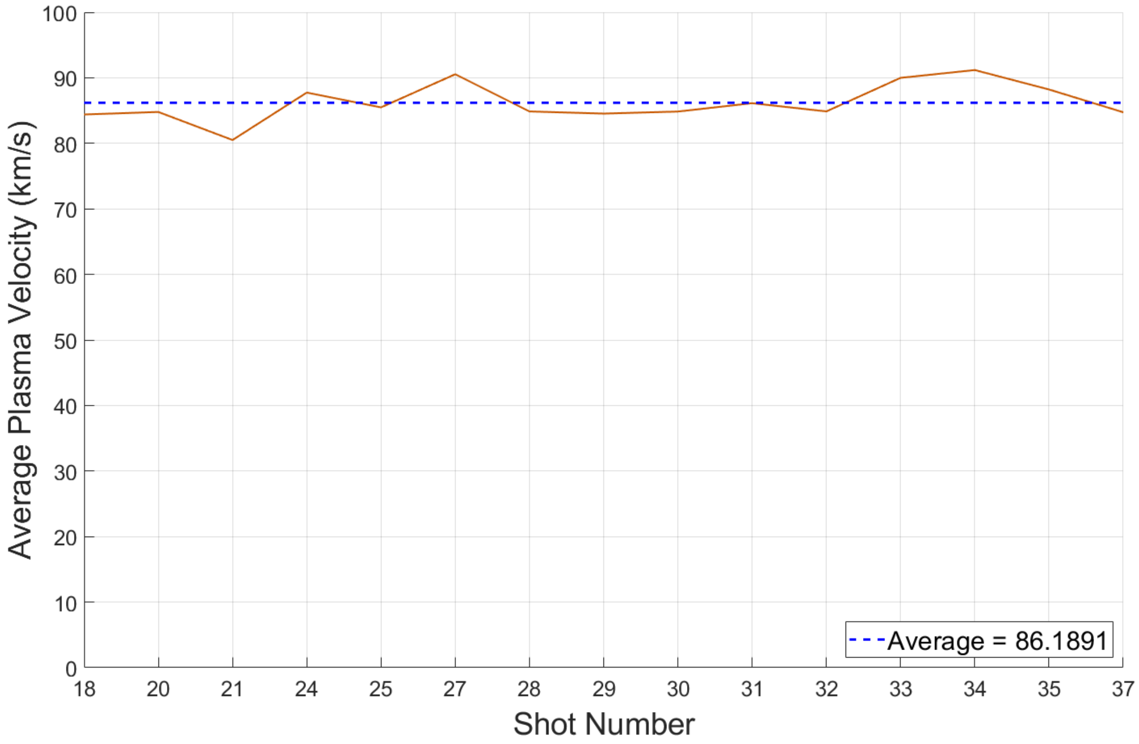

Figure 4.15: Average plasma velocities of FuZE shots during the radial profile scan as calculated by Doppler shift spectroscopy. For each shot, Gaussian fits of the 468.6 nm He-II peak were established and velocity calculated from Doppler shift for each chord. Each chord is then averaged to calculate a velocity for each shot, shown in this figure.

4.4 Corollary Investigations

The primary data campaign to get results for this investigation intended to use the ability of the Langmuir probe to extend and retract into and out of the vacuum chamber to achieve a radial profile of plasma measurements. Running spectroscopy at the same time as these Langmuir probe measurements allows a separate, reliable velocity measurement to correlate with Mach probe measurements. In addition to this primary investigation, other small-scale investigations were pursued to attempt to answer follow-on questions that came up as I proceeded.

4.4.1 Spectroscopy Time Scan

As part of investigations of Langmuir probe intermittency and its relation to spectroscopy measurements, a time scan of spectroscopy measurements was taken, spanning the arrival of plasma at the Langmuir probe. The intent of this investigation was to determine if arrival of plasma at the Langmuir probe correlated with discharges in the probe; I believed that the discharge in the probe is correlated with a region of higher-density plasma near the probe tips providing enough charge carriers to let charge arc between the biased electrodes.

As part of this time scan, I took six pulses, starting at a gate delay of 26 μs with a gate width of 4 μs, and another pulse with a gate delay incremented every 4 μs until the last pulse at 46 μs. All pulses were taken at 5 kV using pure helium gas with the Langmuir probe positioned at R = 65 mm.

This time scan shows that peak normalized intensity for the 468.6 nm helium II line occurs at the same time as the discharge, indicating that the discharge occurs at times when plasma density is higher. Although it is likely that the discharge is creating its own plasma, I believe it is unlikely that this plasma is being viewed through the spectroscope and that is what is causing the high light intensity at 42 – 46 μs. First, the spectroscopy chords do not intersect with the tip of the Langmuir probe; the Langmuir probe is $\sin(55°) * (R = 65 \text{ mm}) = 53$ mm away from the spectroscopy chord. Second, the pulse where spectroscopy light is recorded at 42 – 46 μs is not one of the shots that shows discharge.

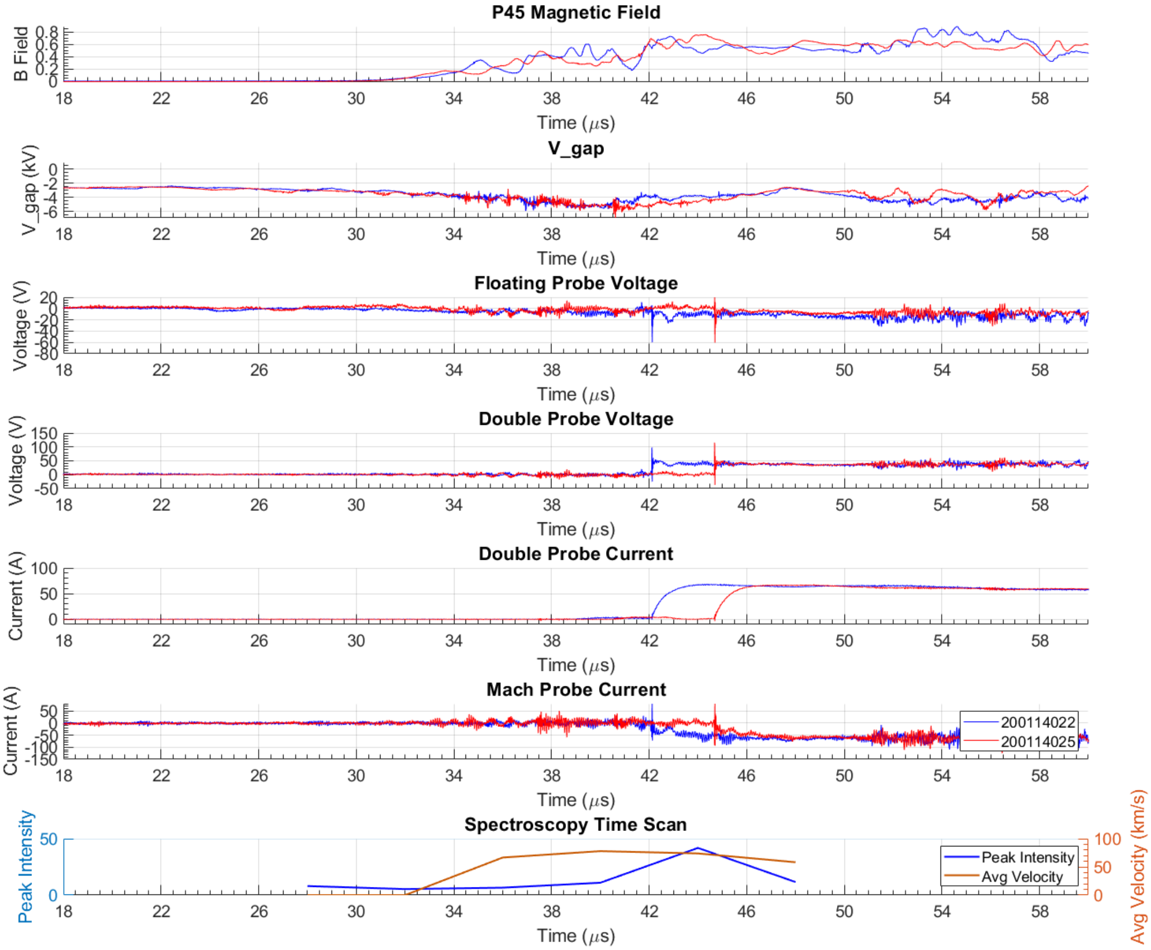

Figure 4.16: Time scan of spectroscopy data shown underneath two raw data traces characteristic of probe discharge. The peak light intensity for the He-II line occurs at the same time as the discharge, with velocity marked in brown and intensity marked in blue on the bottom plot. Probe discharge occurs at 42.1 μs for shot 022 and 44.7 μs for shot 025, with peak He-II intensity seen from 42-46 μs.

4.4.2 Floating Probe Direct-to-Scope Investigation

Voltage measurements on the Langmuir probe are noisy. This is seen in plots like figure 4.7, which shows hashing in the voltage measurements, most of which corresponds to noise in gap voltage. However, hashing isn't the only source of noise in these circuits. Another likely source of noise in Langmuir probe measurements is through pickups of active electronics in the probe's electronics box. Many noise features in the floating voltage trace are present in all of the voltage traces, so in an attempt to narrow down what signal on the voltage traces is from noise caused by active electronics in the box, I disconnected the electronics box and connected the Langmuir probe directly to the oscilloscope through a divide-by-500 probe. I set up the divide-by-500 probe to show as little external noise as possible by twisting the wires, and I reduced the scale on the oscilloscope as much as possible without saturating to achieve higher resolution.

We can see in figure 4.17a that the floating voltage traces with and without the electronics box look mostly similar. The electronics box shows more hashing noise, but the overall shape of the trace is similar. Notably, the larger oscillating peaks are present in both traces. I took identical floating voltage data with a Tektronix divide-by-10 passive probe to see if active electronics were causing these peaks, but the peaks were present with the Tektronix probe as well.

We do see in figure 4.17b, though, that when we look at what happens well after the pulse is over, the electronics box produces a long-period background signal present in the floating voltage. This signal is only present after the pulse and not before, so it is likely some inherent RC time for the electronics box that is causing this signal.

Overall, from this investigation we can conclude that the active electronics in the Langmuir probe box increase the high-frequency, low-amplitude "hashing" noise and produce a background signal reminiscent of RC decay visible as a long-period drift in the pulse amplitude.

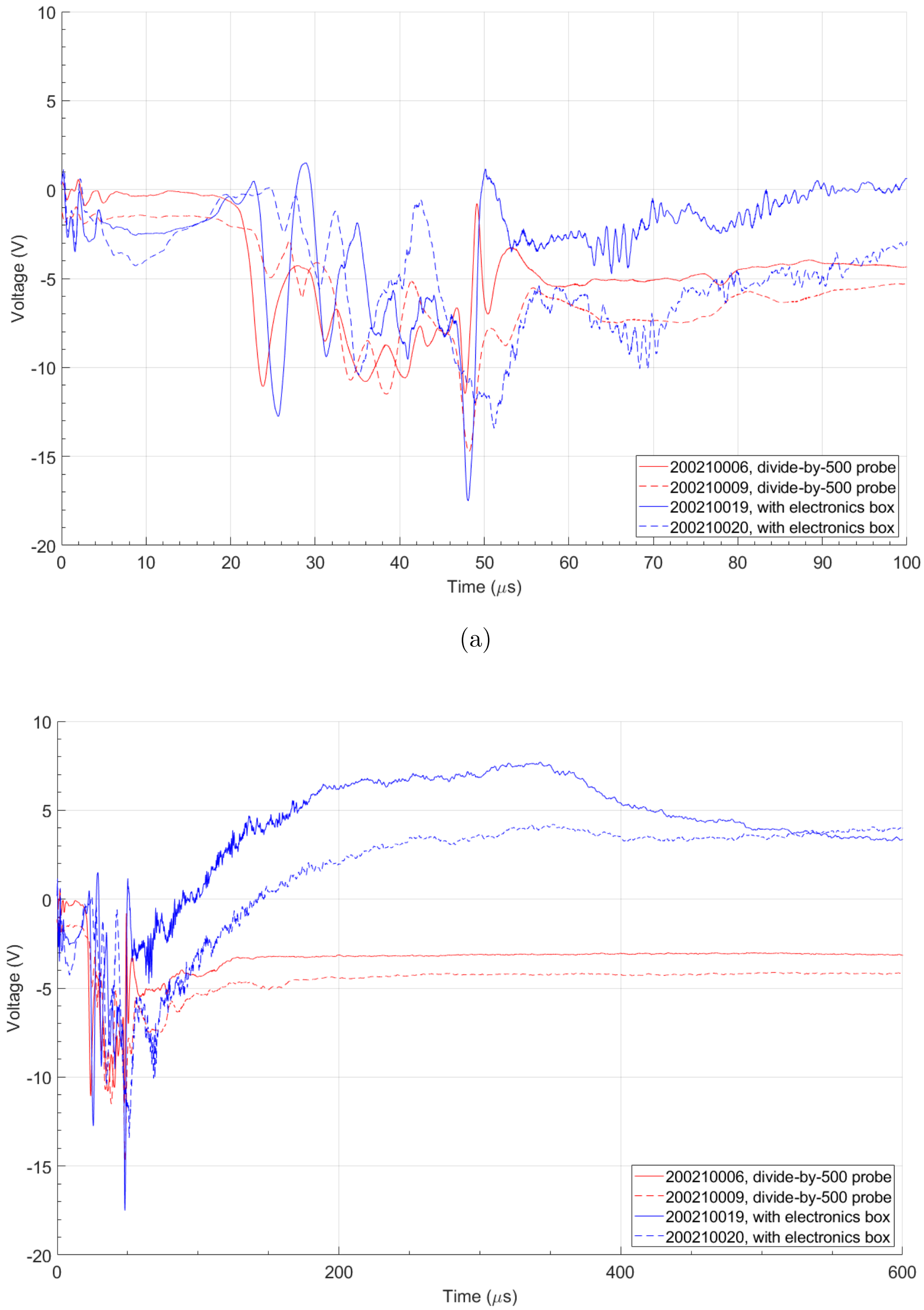

(a)

(b)

Figure 4.17: Floating voltage traces with a divide-by-500 probe with active electronics versus the Langmuir probe electronics box floating voltage circuit. While there is more noise in the electronics box in the form of hashing, overall the traces look similar.

4.4.3 Examination of Effects of Varying Bias Voltage

If indeed the larger-amplitude signals on the Langmuir probe result from discharges between the probe tips driven by the bias voltage, then increasing or decreasing this bias voltage should have an effect on how often the probe discharges. In this short investigation I dropped the bias voltage setting to 100 V (from the 200 V it was for the rest of the data) for four shots and then increased the setting to 300 V for four shots to test this hypothesis.

The capacitors in the electronics box are only rated to 330 V, so in case they had degraded and would fail upon charging to 300 V, these shots were performed last. This did not end up being an issue.

Table 4.3: Number of shots from testing of V_{d3} bias voltage displaying “arcing” traces

V_{d3} **Bias Voltage (V)**	**Proportion of shots where discharge occurs**
100	0/4
200	1/3
300	3/4

Table 4.3 shows a clear change in probability of a discharge as bias voltage increases. This reinforces the idea that discharges are caused by the bias voltage across the capacitors driving a short between biased probe tips.

One concern in varying the bias voltage is in the ion saturation current. If the bias voltage is too low, then the negatively biased electrodes will not be sufficiently biased to collect ion saturation current. As discussed in subsection 2.1.5 on calculating electron temperature, as long as the bias voltage is larger than 2.5 times the actual temperature, calculated values of temperature will be within 10% of their real values. Although electron temperature is not yet decisively known (this will be discussed in chapter 5), we can see if the ion saturation current is affected by looking directly at the measured current. As figure 4.18 shows, there seems to be no statistically significant difference between these pulses, so the probe theory assumption that the biased electrodes are collecting ion saturation current likely still holds.

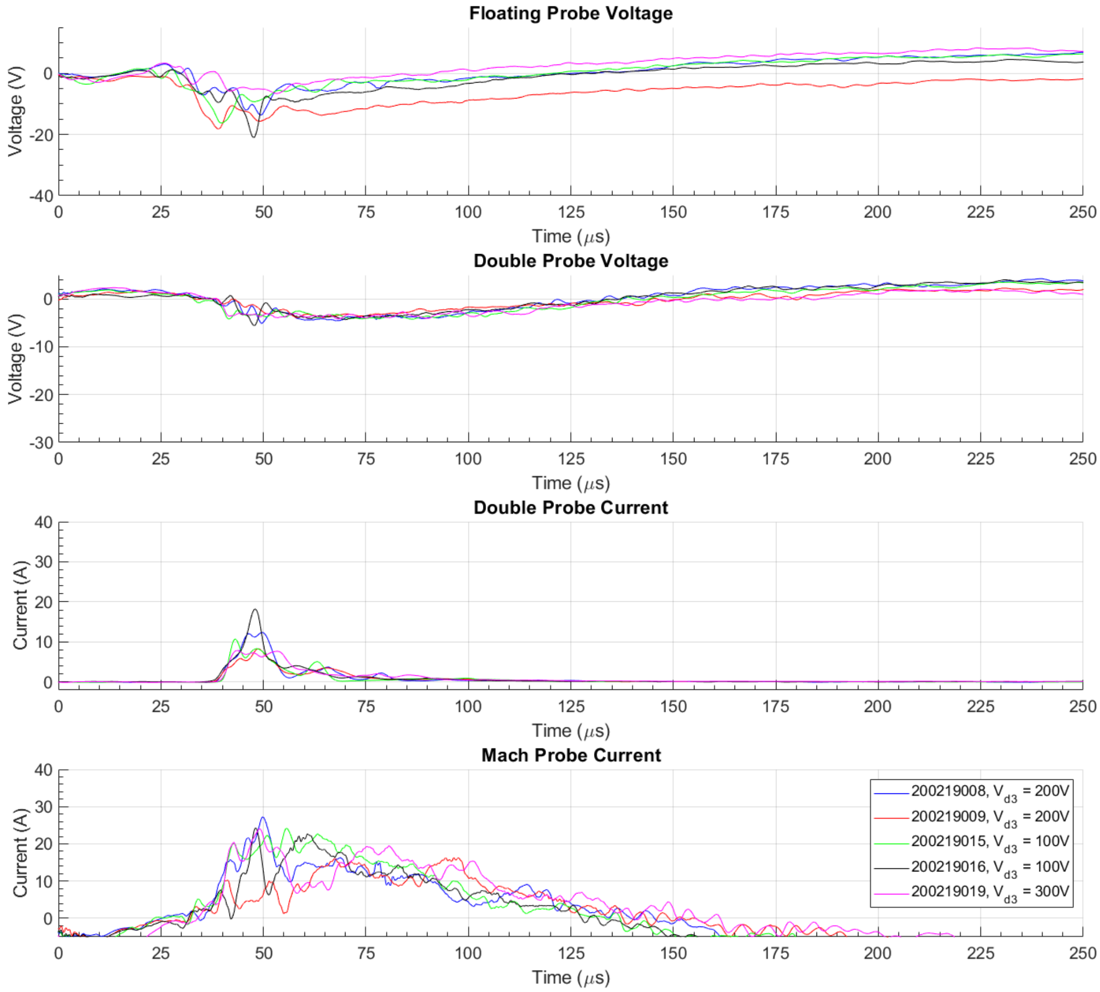

Figure 4.18: Quadruple Langmuir probe data with varying bias voltages. Although variability is seen between the traces, this is typical for shots even with the same settings. There seems to be no statistically significant difference between double probe and Mach probe currents between shots of different bias voltages.

Chapter 5

DATA ANALYSIS AND DISCUSSION

In the previous section I discussed the data measured for the primary investigation of a radial profile of plasma parameters. I explained how we found a clear radial profile in upstream ion saturation currents and less-clear profiles in voltage measurements. Through line-integrated spectroscopy, I observed an average plasma velocity of 86.2 km/s in the end chamber. I also discussed a few corollary investigations: a time scan of spectroscopy data, an examination of bypassing the electronics box for a cleaner floating probe signal, and an analysis of the effects of varying the bias voltage on the double probe and Mach probe. These investigations further implicated the DC bias on the double probe as the culprit of discharges between the probe tips — discharges which show on the Langmuir probe data traces as traces of significantly higher amplitude and long decay time.

In this chapter I will discuss the implications of these measurements. The reliability of the voltage measurements and circuitry will be covered, as will the impact of this reliability or lack thereof on calculated plasma parameters and their radial profiles. I will also further discuss characteristics of the discharges between electrodes. Finally, I will conclude discussion by analyzing how the plume characteristics discovered here educate whether or not a Z-pinch based space propulsion system is plausible.

5.1 Discharges in the Langmuir Probe

Intermittency in Langmuir probe measurements was evident throughout this investigation. About a fourth of all pulses displayed signs of a discharge between the Langmuir probe tips. This discharge is characterized by a quick "spike" in raw signal on voltage measurements (figure 4.6) followed by a rapid increase in double probe voltage and current and a rapid decrease in Mach probe current. The sign of the double probe current indicates the direction of current flow as the discharge arc forms between the negatively biased Mach probe and double probe tips to the double probe tip from which voltage and current signals are recorded.

The traces for shots that show discharge are nearly identical — they all rise to the same height and show exactly the same shape of curve after the rise. This includes the double probe current, which also cuts off back to zero after about 90 μs after the discharge started. This holds no matter the position of the Langmuir probe, indicating that once the discharge starts, it will continue in the same manner regardless of external plasma characteristics (note though that plasma has to be present for discharge to occur, as seen in the radial profile).

If indeed the discharge is driven by the capacitors biasing the double and Mach probes, a quick sanity check is to be sure the total charge expended on discharge does not exceed the charge stored in the capacitors. The charge of the capacitors can be calculated by the equation $Q = CV$; a capacitance of 480 μF multiplied by a bias voltage of 200 V yields a charge of 0.096 C being stored in the double probe capacitors. This is doubled to 0.192 C when including the Mach probe capacitors.

The total charge dissipated during discharge based on a current trace is the area under the curve, so we can calculate the energy of discharge by integrating the double probe current trace. For fifteen of the last shots to arc, this value is nearly the same, an average of 0.00353 C with a standard deviation of 0.00016 C. This value is clearly below the total charge of the capacitors, but when we look at the published

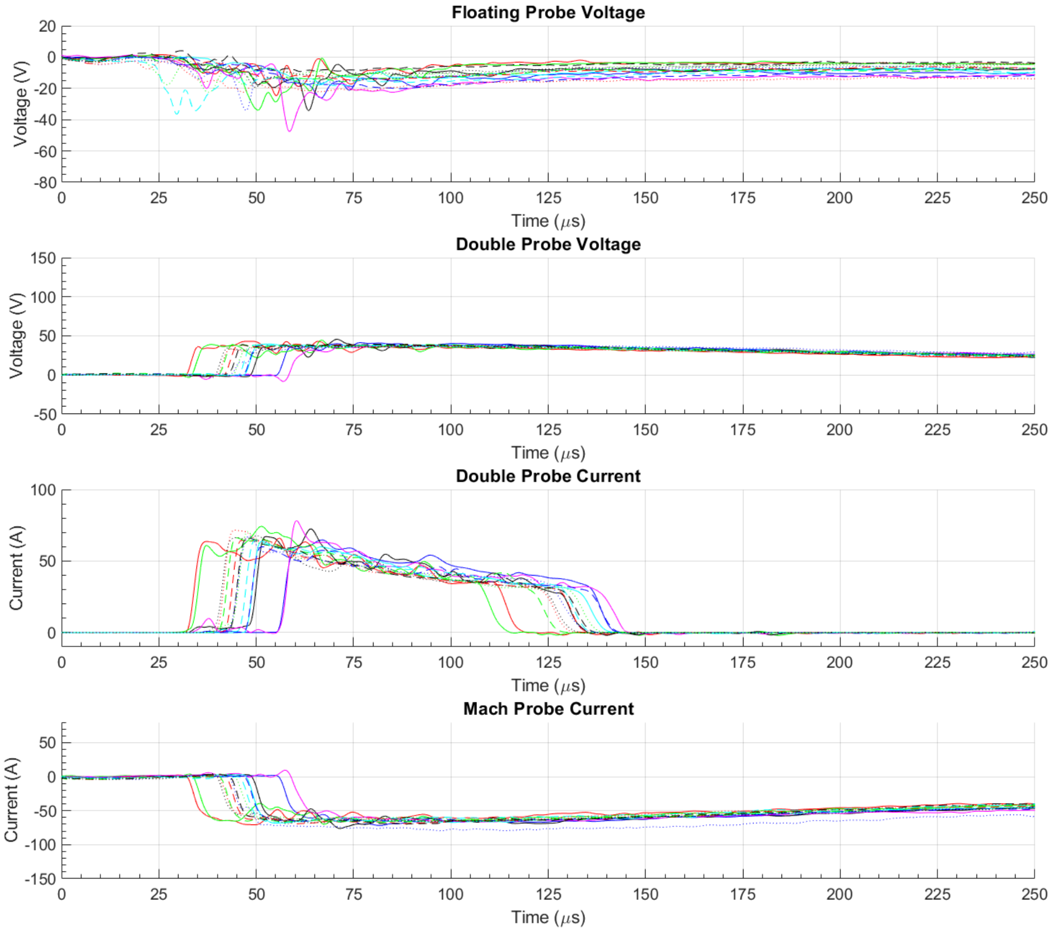

Figure 5.1: Repeatability of discharge traces. We see that once the discharge occurs, Langmuir probe traces look the same, no matter at what radius the probe is positioned. This figure shows the last fifteen shots in which discharge occurred.

specification sheet for a Pearson Current Monitor Model 2878, we see that they are rated to a maximum of 4 mA-sec current time product, or 0.004 C. We see, then, that the discharges are surpassing the limit of the Pearson probe to measure them and the double probe current is not an accurate way to measure the magnitude of the discharge.

In contrast to the double probe current, the voltage traces, while of the same amplitude between discharge shots, do not decay at the same time and instead decay and then drop back to zero at any time between 350 μs and the end of the data record at 2300 μs. The moment of this drop back to zero is likely the moment that the discharge stops, when the potential on the capacitors is no longer enough to drive it. Although the Mach probe current is not measured via a Pearson current monitor, we can still integrate it to determine the total charge expended on discharge. This integration yields an average charge of 0.0244 C passing through the Mach probe circuit resistor, with a standard deviation of 0.0083 C. This is about one eighth of the total charge of the capacitors.

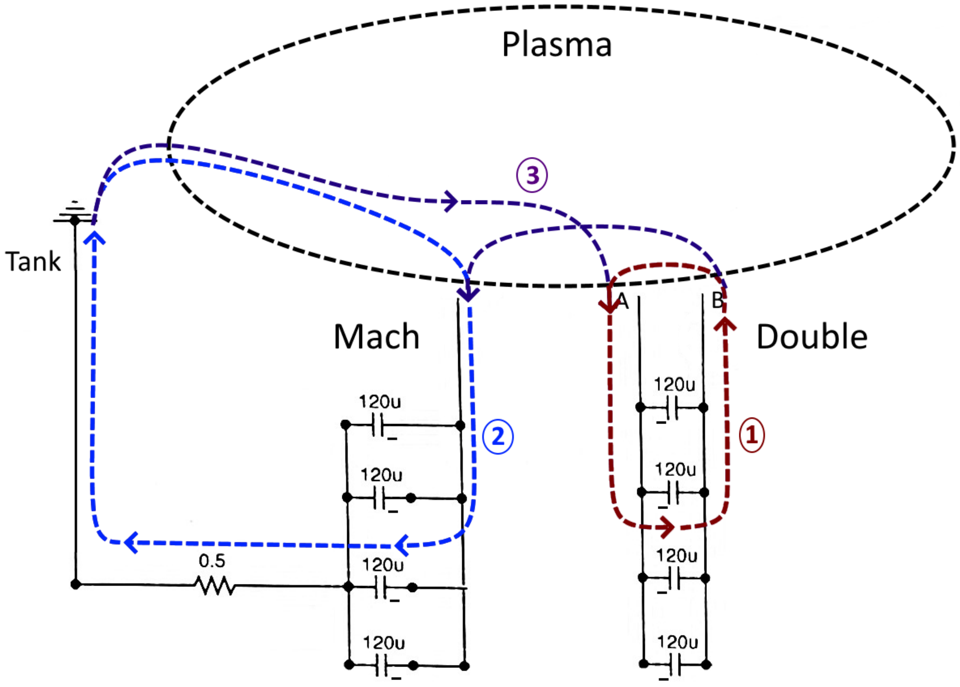

Figure 5.2: Possible Langmuir probe discharge current paths. At sufficiently high bias voltages, the capacitors in Langmuir probe circuitry drive discharge between biased probe tips, possibly along these current paths.

There are multiple ways in which this charge can arc across the probe tips. Charge can flow between the two biased double probe tips, as well as to the Mach probe. When just between biased probe tips (path 2), the circuit is complete. Since the Mach probe is a single biased probe tip that routes current through the capacitors to ground, any discharge flowing through the Mach probe tip (path 2) must then pass through tank ground (the vacuum chamber), through the plasma, and back to the double probe or Mach probe tips. The distance from the tank to the electrodes is large so this return current is unlikely to be part of the arc, but is still part of the total discharge.

There is a 0.264 in horizontal distance between the double probe tips but only a 0.187 in horizontal distance between a single double probe tip and the Mach probe tip. Additionally, there is less insulator between a double probe tip and the Mach probe tip than there is between the double probe tips themselves. Thus, it is more likely for the arc to form between the double probe and Mach probe tips than between the double probe tips (however, once the arc forms, conductivity in the plasma increases so another arc between the double probe tips is subsequently more likely).

Current traces show a maximum of about 60 Amps of current flowing through the Mach probe circuit, and a similar 60 Amps of current flowing through the double probe circuit before the Pearson current monitor saturates. This suggests that the discharge is driving current through the plasma mostly between the Mach probe tip and double probe tip B and not between the double probe tips directly. However, this also relies on the readings of Mach probe voltage being accurate, which they may very well not be, as will be discussed in section 5.3. But, if this reading is indeed accurate and all of the current is flowing through the Mach probe circuit, we can use $Q = CV$ again with a total capacitance of 960 μF and an expended charge of 0.0244 C to calculate that the discharge stops when the capacitors drop 25 V in potential, from 200 V to 175 V.

Integrating the Mach probe currents of the discharges that occurred at a 300 V bias voltage yields a 0.0543 expended charge, over double that of discharges at a 200 V bias. This expended charge correlates to a calculated voltage drop of 56 V, from 300 V to 244 V. Thus, the potential across the circuit capacitors has to drop more at higher bias voltages before the discharge stops, although the final voltage is still higher than the final voltage after discharge at lower initial bias voltages.

Late in the investigation, when re-evaluating the circuitry inside the electronics box to verify Mach probe current signals for section 5.3, we discovered that the solder joints on two of the double probe capacitors had broken off. Perhaps this occurred during the process of tinkering with the circuit and taking it apart to evaluate it, or possibly this happened at another time the electronics box was being adjusted, as these capacitors were connected properly at the beginning of the investigation. However, this reduces the total capacitance in the circuit from 960 μF to 720 μF. This reduction changes the charge calculations above. With a 720 μF capacitance, the total charge on the capacitors is 0.144 C rather than 0.192 C. Additionally, at this new capacitance, the total voltage drop for discharges of 200 V and 300 V bias is 34 V and 75 V, respectively, making final capacitor voltages after discharge 166 V and 225 V, respectively.

The total energy of a capacitor is found via

$$E = \frac{1}{2}CV^2 \tag{5.1}$$

where C is the capacitance and V is the voltage on the capacitors. We can subtract to find the difference in energy between two capacitor states. Using the initial bias voltage for the first state and the change in voltage from the charge expended ($V = Q_{exp}/C$) subtracted from the bias voltage for the second state, we find that the total change in energy on the capacitors after a Langmuir probe discharge is

$$\Delta E = \frac{1}{2}Q_{exp}\left(\frac{Q_{exp}}{C} - 2V_{d3}\right) \tag{5.2}$$

where Q_{exp} is the charge expended in the discharge, calculated by integrating the Mach probe current, and V_{d3} is the initial bias voltage on the capacitors. With this equation we can calculate the energy in the capacitors, and the energy expended on each discharge, assuming all of this energy goes through the Mach probe circuit.

Table 5.1: Charge, voltage, and energy drops on Langmuir probe discharge as calculated from Mach probe current

Capac.	**Bias Voltage**	**Charge Expended (C)**	**Voltage Drop (V)**	**Capacitor Energy Drop (J)**
960 μF	200	0.0244	25	–4.6 (24% of total)
	300	0.0543	56	–14.8 (34% of total)
720 μF	200	0.0244	34	–4.5 (31% of total)
	300	0.0543	75	–14.3 (44% of total)

With sufficiently small capacitors like those in this circuit, the capacitance in the denominator in equation 5.2 is small and the total energy drop at 720 μF and 960 μF is nearly the same. This indicates that at small capacitances, the energy expended in the discharge is dependent more on the plasma parameters the discharge is arcing through and the bias voltage on the capacitors rather than the capacitance of the circuit.

5.2 Distinguishing Signal from Noise in Voltage Measurements

In all voltage measurements, there is notable signal present that is not obviously from the plasma and may be noise. For example, in figure 5.1 we see oscillations in floating voltage that are inconsistent with one another; some shots have a large peak at a certain time while other shots have no peak. This is a property not present in only pulses where the Langmuir probe discharged. Figure 5.3 shows three traces of voltage data taken in the middle of the spoke gap (R = 65 mm), where significant oscillations are also present. These oscillations vary in amplitude and timing.

In the floating voltage, the data start at time zero at 0 Volts, but drift over time.

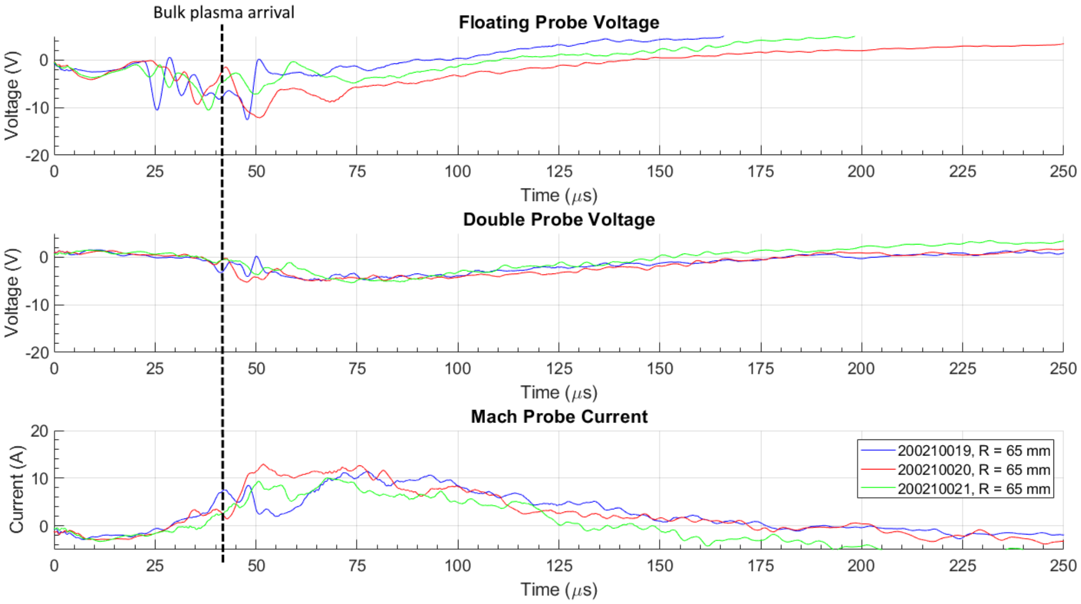

Figure 5.3: Voltage traces showing EMI noise. These data were during the 10 Feb 2020 radial profile scan at position R = 65 mm. Clear peaks are seen in some traces but not in others, suggesting that these large scale oscillations are noise. The time of bulk plasma arrival (42 μs) per the double probe current signal is marked with a dotted black line.

As figure 4.17 shows, this drift is inherent to the electronics box. On a shorter time scale, which elements of the data are noise and which are signal is more difficult to determine. We know from the Pearson current monitor traces that bulk plasma arrives at the Langmuir probe at approximately 42 μs, at which time the floating voltage trace does have a consistent feature, but there are multiple features of the same or greater amplitude before this time as well. These oscillations likely correspond with plasma, as they are not present when the Langmuir probe is retracted. Figure 5.4 compares traces with the probe retracted out of the vacuum chamber (R = 184 mm) to traces with the probe in the plasma stream (R = 65 mm), and while a peak at 40 μs is present that matches the overall trend of the gap voltage, the oscillations seen in the data in the plasma flow are not present in the data with the probe retracted.

These data show that the oscillations seen are likely some element of plasma

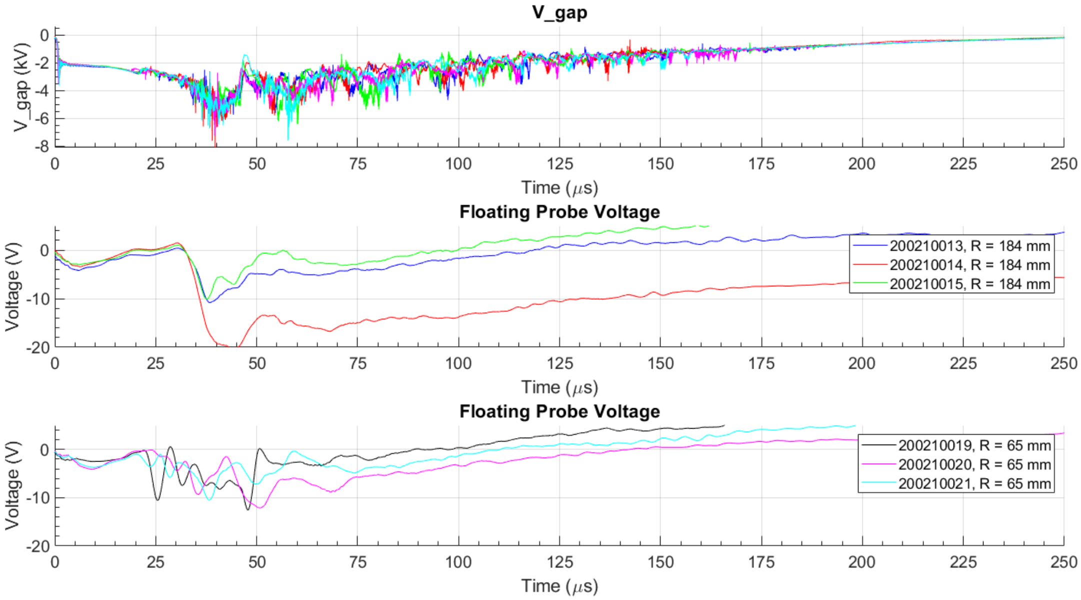

Figure 5.4: Floating voltage at R = 65 mm and R = 184 mm. Data taken outside the vacuum chamber at R = 184 mm lacks the large oscillations seen in the data at R = 65 mm, indicating that these are caused by plasma arrival. However, known arrival of bulk plasma isn't until about 20 μs later, so these are likely some initial elements of plasma.

arrival, but it is unclear what element that corresponds to. Magnetic field at P45 doesn't start to increase notably until 30 μs, after these features start. However, the oscillations are inconsistent with one another, a trait which is often seen in noise. I believe that these features correspond to initial waves of plasma arriving at the Langmuir probe before the main bulk of plasma. These initial elements of plasma are erratic and not strong enough to create notable magnetic fields, but still create signals on electrodes directly immersed within them. The fact that these signals are of the same amplitude as features seen at a logical time of plasma arrival indicates that the signal to noise ratio on these voltage traces is very low.

Figure 5.3 shows that the double probe voltage and Mach probe current (which is derived from voltage) don't show notable oscillations until the expected time of plasma arrival. The bias on the probes seems to screen out some of the initial oscillations, suggesting that these initial oscillations are insignificant to the plasma overall. However, other noise is present in these traces that the floating voltage does not show. Evident as a curve that looks like half of a sine wave of period 200 μs, we see much longer-period background noise in the double probe and Mach probe traces at both R = 65 mm and R = 184 mm. Although the signal is offset to force it to start at zero at time zero, this background noise is high enough frequency to develop further after the pulse begins and skew the data. This noise is likely caused by the capacitors connected to the probe tips, i.e. it is indirectly caused by the DC voltage being applied to the electrodes. It is not present when DC power is disconnected or when AC power is disconnected, which deactivates the relays in the circuit and disconnects DC power from the capacitors. Extracting an average of this background signal and subtracting it from double probe voltage data effectively removes it. However, the subtracted background signal was sourced from the data taken at R = 184, so it may contain real data from plasma that has diffused up into the Langmuir probe itself. As such, the signal isn't entirely physical, although it is mostly physical. It does effectively isolate expected plasma peaks, though.

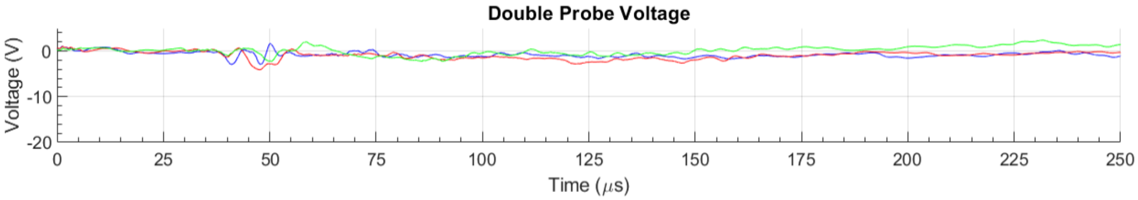

Figure 5.5: Double probe voltage corrected for background DC bias noise. Correction was done by subtracting an average signal of the data at R = 184 mm from this data at R = 65 mm, isolating the data that is due to direct plasma flow.

Noise discussion for the Mach probe voltage/current is discussed in the next section, which also discusses the reliability and trustworthiness of the signal itself.

5.3 Reliability of Mach Probe Measurements

Figure 5.6 highlights another feature: the current calculated from the Mach probe is often higher than the current measured on the double probe. Assuming probe theory holds, the Mach probe current is the downstream ion saturation current and the double probe current is the upstream ion saturation current. It doesn't make physical sense that the downstream current would be higher than the upstream current unless the plasma was flowing backwards, which is certainly not the case for this experiment setup.

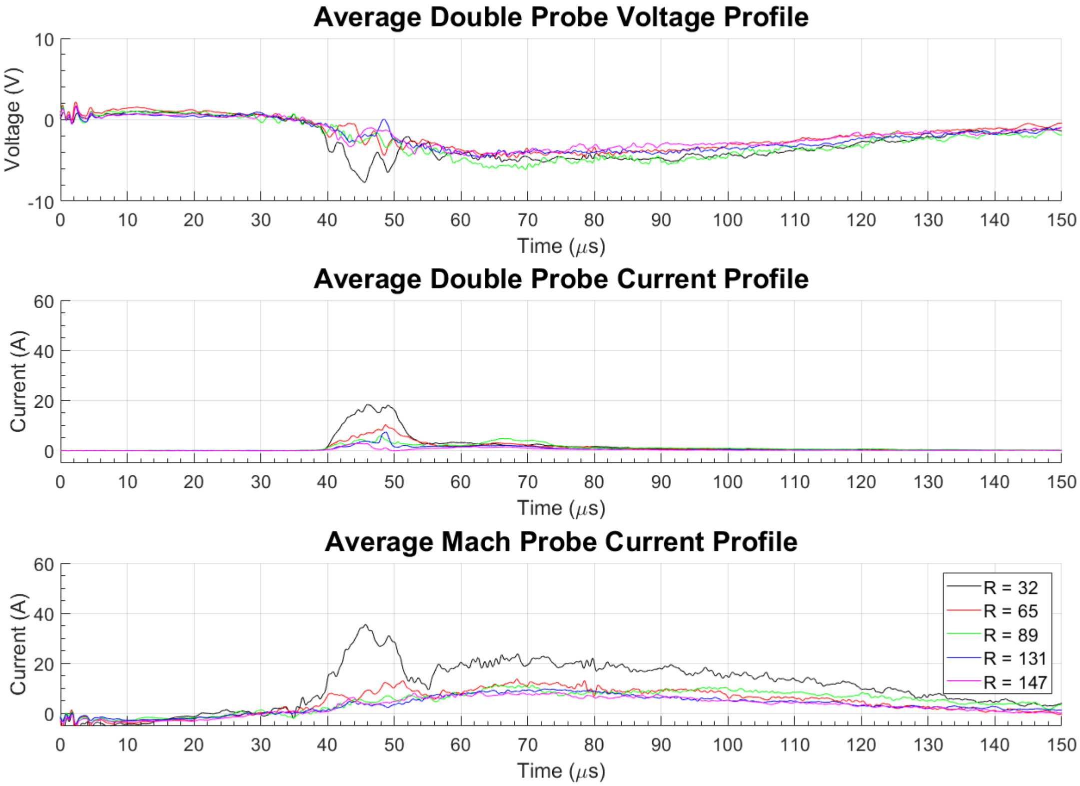

Figure 5.6: Radial profile in average quadruple Langmuir probe measurements of double probe voltage, double probe current (upstream ion saturation current), and Mach probe current (downstream ion saturation current). This shows how the Mach probe current is consistently higher than the double probe current, which doesn't make physical sense for flowing plasmas.

In an attempt to diagnose this, we first took apart the Mach probe to ensure the circuitry was in agreement with the schematic in figure 3.2. To calculate the current on the Mach probe, we take the measured voltage on the Mach probe and divide by a resistance of 0.5 Ω. The measured Mach probe voltage is the voltage across this resistor, which lies directly in the current path from the Mach probe tip to ground (seen in the top left of figure 3.2). We measured this resistance with a multimeter as 0.6 Ω, which is close enough to 0.5 Ω to say that the divisor on the Mach probe current calculation being incorrect is not the primary cause of this signal imbalance. While the box was taken apart, we verified that the rest of the circuitry in the Mach probe was correct, and that there were no other viable current paths for charge on the Mach probe tip to travel down than the one through this resistor. In our other attempts at diagnosing the imbalance, we were unable to find an answer in the hardware setup.

In figure 5.6, we can see that the Mach probe currents have a background signal that looks like half a sine wave of period 200 μs. Because this background signal is not present in the double probe current profile and notable EMI noise is present in the experiment, it is likely this background signal is due to noise on the voltage measurement being used to calculate the current.

Noting that this background signal looks similar to the background signal of the double probe voltage measurement at the top of figure 5.6, I extracted an approximation of this background from the double probe voltage measurement and subtracted it from the Mach probe signal. The Mach probe and the double probe are biased with the same voltage on identical capacitors, so they possibly experience the same background noise. Doing this brings the Mach probe current closer to zero and reduces this difference, but it's irregular; sometimes the "corrected" Mach probe currents are still higher than the double probe currents, and sometimes they drop below zero with the "correction." Either of these solutions are still nonphysical.

The core of this problem likely lies in that the Mach probe current is obtained by measuring voltage on an electrode and calculating current across a resistor, while

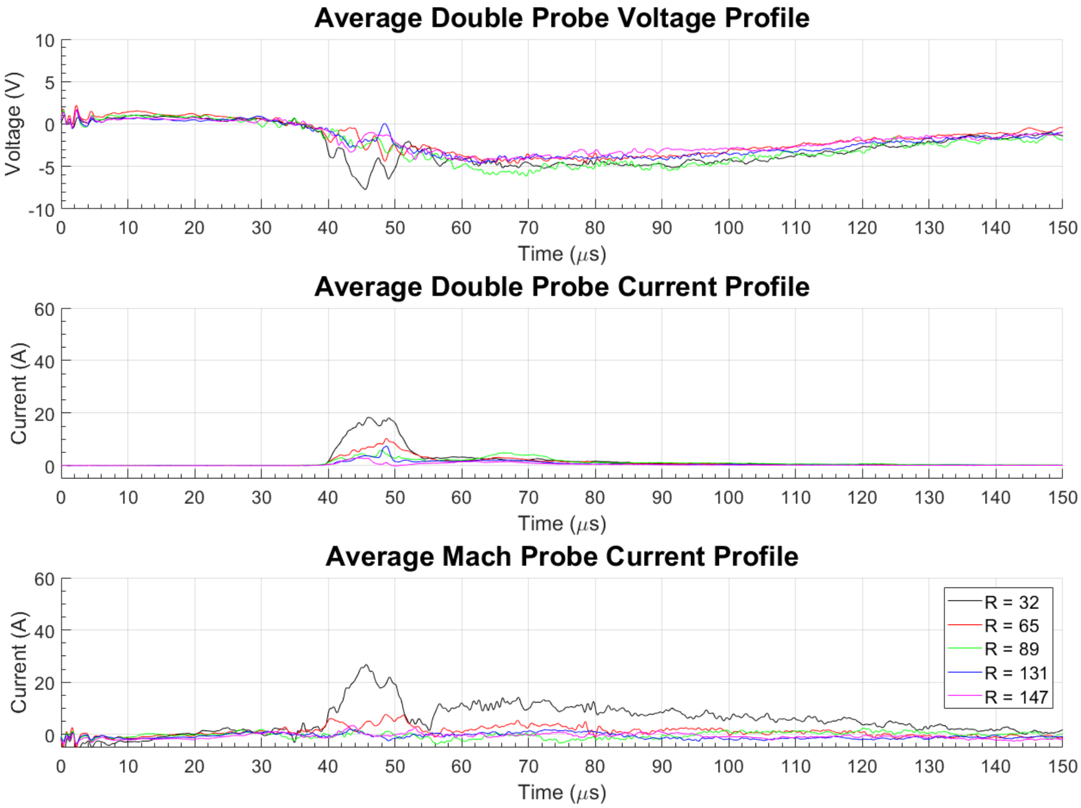

Figure 5.7: Radial profile in average quadruple Langmuir probe measurements of double probe voltage, double probe current (upstream ion saturation current), and "corrected" Mach probe current (downstream ion saturation current). "Corrected" Mach probe current is calculated by subtracting the background signal of double probe voltage from Mach probe voltage before calculating Mach probe current. Clearly this method of "correction" is not correct, because some Mach probe currents are still higher than their double probe counterparts, and some end up going below zero.

the double probe current is obtained directly from a Pearson current monitor. The Pearson current monitor outputs a clean signal, while the Mach probe current as calculated from the circuit has significant noise. The original designer of the electronics box likely did not add a second Pearson monitor to the Mach probe circuit due to cost; however, clearly the quality of the signal has suffered for it.

In an attempt to nail this down as the cause, I took a few data shots with the Pearson current monitor swapped to the Mach probe circuit. The current monitor is

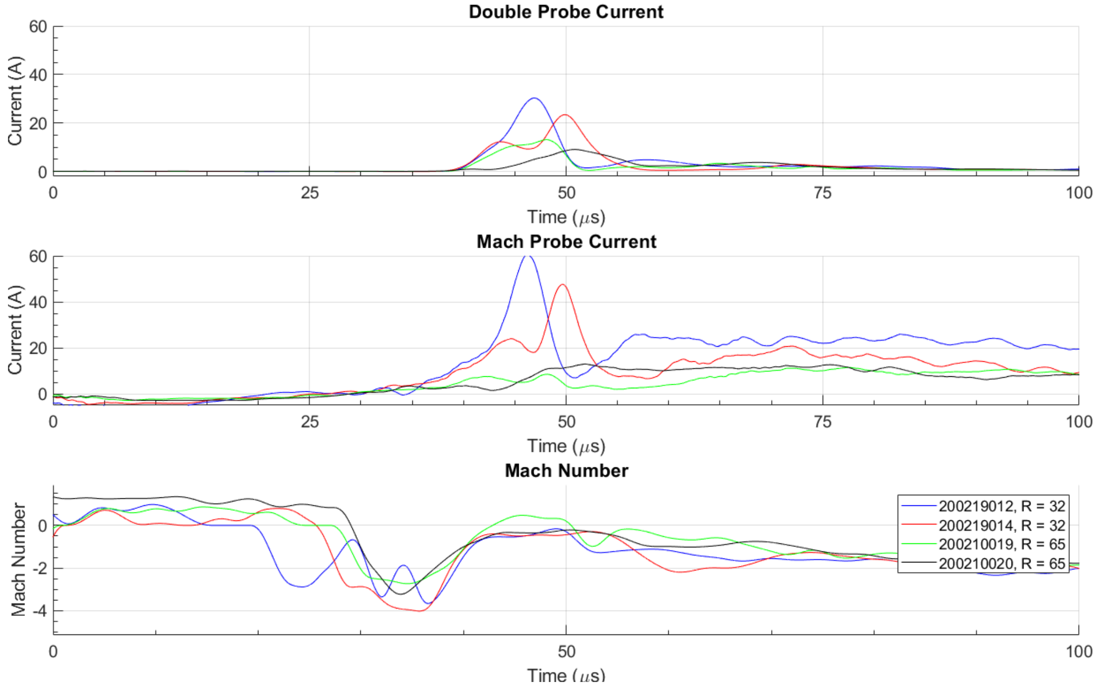

Figure 5.8: Unreliable calculated Mach number for inner radial profile positions. The amplitude of the Mach probe current is nearly double that of the double probe current for the R = 32 traces at their peaks, but not for the R = 65 traces. Calculated Mach number relies on a ratio of double probe current to Mach probe current, which calculates velocities both above and below zero. Mach probe currents, being calculated from a voltage measurement in a system with large EMI noise, contain large noise themselves, which is difficult to accurately remove and throws off calculations of Mach number.

simply a “doughnut” that is threaded around the wire connecting the probe tip to the circuitry, and these wires can be taken on and off in order to remove the electronics box, so the swap was simple enough to do. However, results were initially confusing. After the switch, there was no Mach probe current visible at all, just a flat line at zero Amps.

One could pose that perhaps there is, in fact, no downstream ion saturation current because pressure is low enough and flow speed is fast enough at 86 km/s, and that all of the signal seen on the Mach probe voltage is just noise. This answer doesn't make sense when we consider the radial profile present in Mach probe data, where at least some of the trace seems to be signal, but this profile is from a voltage measurement so it may be noisy anyways. Additionally, the Pearson current monitor registered zero current on the Mach probe even when discharge occurs, which also seems nonphysical as the discharge current flows through the wire the Pearson current monitor is measuring. To verify that the current monitor wasn't damaged in the swap to the Mach probe circuit, I subsequently switched it back to the double probe circuit, where it continued to measure currents reliably.

I conclude from this investigation that data from the Mach probe as it is currently constructed is unreliable at best and nonphysical at worst. Matthews stated that uncertainty for Mach probes can make them "little more than flow direction meters" [20] and it would seem that in hot, fast plasmas like those in FuZE and experiments where significant EMI noise is present, a "direction meter" may be the pinnacle of hope for a voltage-based Mach probe. Furthermore, as the ratio between Mach probe and double probe currents is not consistently positive or negative with these readings, Mach number and flow velocity calculations using the Mach probe are also not consistently positive or negative. As such, accurate calibration of the Mach probe equation constant K between zero and three is not possible either.

Perhaps characterizing the Mach probe traces for tens of shots at a single setting would provide greater insight into the properties of the circuit and the noise within. However, for this investigation, I don't have statistical significance enough to pursue this further. Overall velocity measurements of the plasma are still possible via spectroscopy, which reliably calculates line-integrated velocities of 80 – 90 km/s per figure 4.12. Further conclusions that require a velocity, such as those in section 5.6, will use the 86.2 km/s average velocity as calculated by spectroscopy.

5.4 Determining Plasma Parameters

Plasma parameters are calculated via equations discussed in chapter 2. The primary data used for the radial profile was taken on 10 February 2020, which includes 3 pulses at R = 32 mm, five at R = 65 mm, two at R = 89 mm, four at R = 131 mm, and four at R = 147 mm. Although more pulses were taken at each of these positions, the pulses not included here show the typical characteristics of discharge on the Langmuir probe. Statistical significance is provided at R = 65 mm at the center of the spoke gap; this is the position where most pulses were taken on days besides 10 February 2020.

5.4.1 Electron Temperature

Calculation of plasma parameters starts with calculating electron temperature, as the density and flow velocity both depend on temperature. As discussed in the chapter on theory, electron temperature is found via numerically integrating equation 2.6. Use of equation 2.7 is simpler and does not require integration, but that equation relies on the assumption that $eV_{d3} > 3k_BT_e$, which cannot be guaranteed without first knowing a good estimate of electron temperature.

Using these equations, we find peak electron temperatures in the pulse ranging from 5 eV to 25 eV. The innermost position, R = 32 mm, outputs the highest peak temperature with positions further out reading lower temperatures. However, there is no clear profile between these positions as the radial position increases.

According to the theory, electron temperature is proportional to the V_{d2} difference voltage, or the difference in voltage between the floating probe and the double probe. The background noise in the double probe voltage was due to DC bias was removed to isolate the signals due to plasma. The floating voltage, however, has had no noise removed because it is difficult to determine what of the signal is noise and what is actual signal from the plasma. As such, unconfirmed signal from the floating voltage

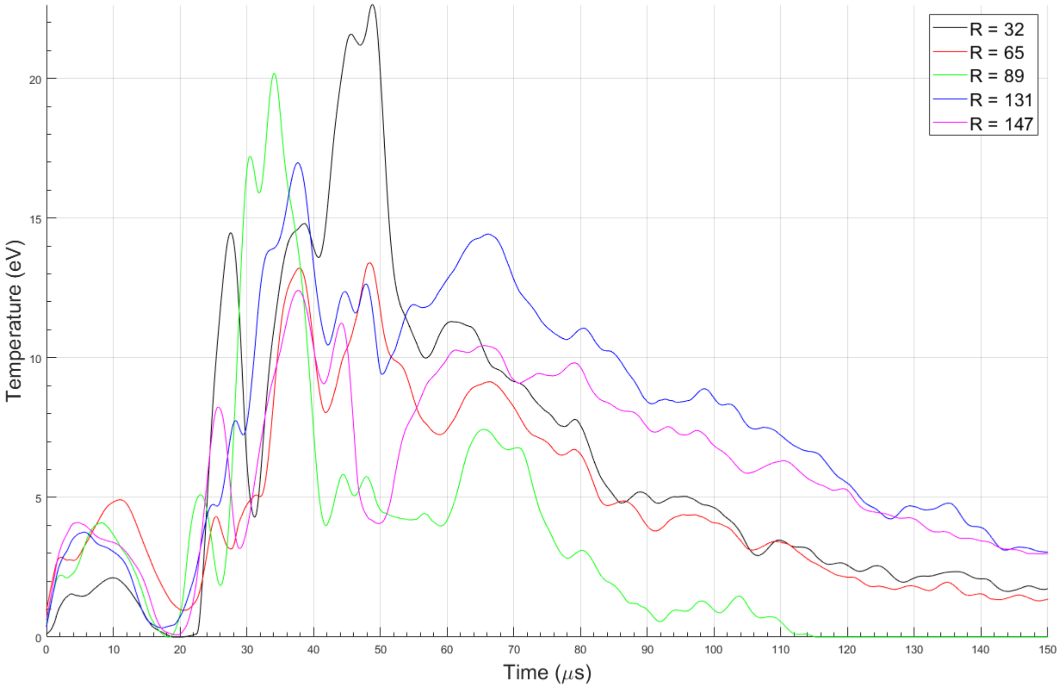

Figure 5.9: Radial profile of average electron temperature for a pulse at a given Langmuir probe position, ranging from the inner edge of the spoke gap to the outside of the vacuum chamber. Temperatures at R = 32 mm peak higher than others, but significant noise in floating voltage affects the accuracy of these measurements and makes it difficult to determine a clear profile.

measurements is visible in the traces for electron temperature. Notable features of this unconfirmed signal include signals prior to 35 μs and the second "hump" of signal near 65 μs that is likely noise because it is also seen in the gap voltage trace. However, for inner radial profile values where there is more plasma (as seen in the clear profile of ion saturation currents, figure 4.13), signal to noise ratio seems to increase at the time when plasma is present, between 40 and 50 μs. These signals will give more reliable measurements of electron temperature.

We know from the radial profile that electron temperature has more reliable signals in the center of the chamber where voltages on the Langmuir probe are larger and signal to noise ratio is higher. However, we don't have statistical significance when we have between two and five pulses at each position, and these vary widely based on the noise in floating voltage signal. Statistical significance for these values comes from measurements at position R = 65 mm, at the center of the spoke gap, where more data were taken. In total, fifteen shots with pure helium and bank charge of 5 kV were taken. Averaging the electron temperatures calculated from these pulses reveals a peak electron temperature of 14.4 eV with a standard deviation of 7.8 eV, about 50%. Original estimates for error of electron temperature were plus/minus 40%.

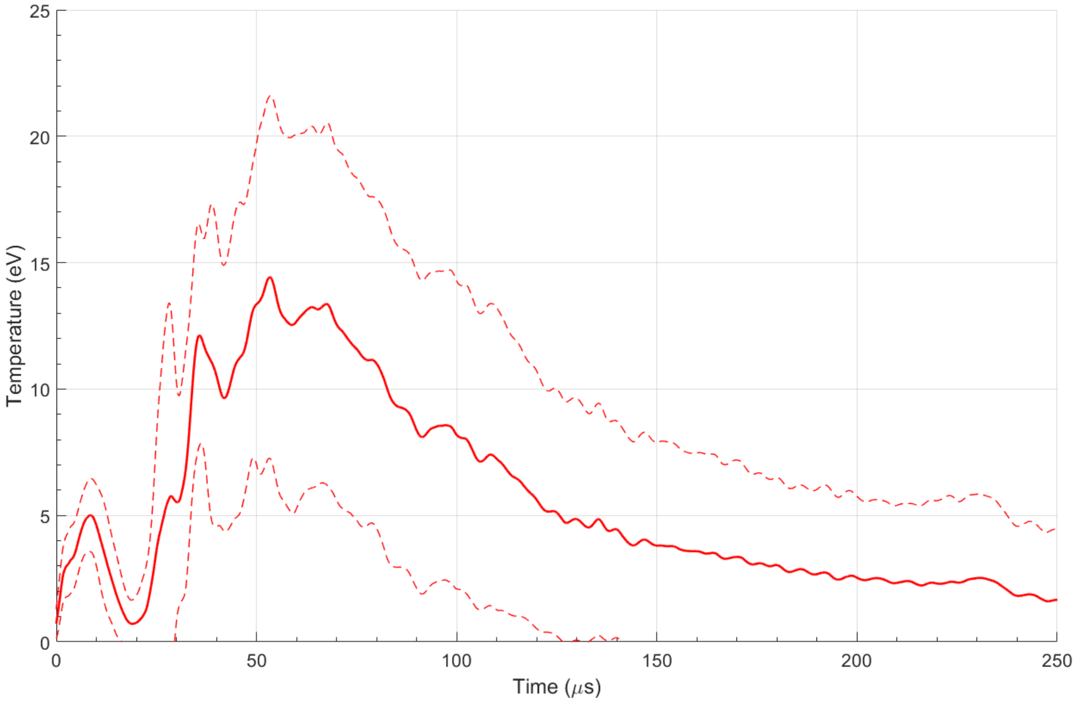

Figure 5.10: Average electron temperature plus or minus one standard deviation for Langmuir probe at R = 65 mm, averaged over 15 pulses. Peak electron temperature of 14.4 ± 7.8 eV is reached at 53 μs.

Although the electron temperature calculated from the Langmuir probe measurements using probe theory assumptions is not precise, we can another method not previously mentioned in this thesis available to double check temperatures. Using the same spectra of light used in the results chapter to determine flow velocity, we can determine ion temperatures from the Gaussian fit. Hotter plasmas will appear as wider Guassian curves as the line broadens; cold plasmas show narrow Gaussians. The square of the full-width half-max (FWHM) of the Gaussian curve fit to the spectra is proportional to the ion temperature according to [29]

$$k_B T_i = \frac{m_i c^2 (FWHM)^2}{\lambda_0^2 8 \ln(2)} \tag{5.3}$$

where m_i is the mass of the ion, c is the speed of light, and λ_0 is the center wavelength of the peak.

I applied this equation to the same shots I analyzed to measure velocity, and found that the average ion temperature of plasma in the end chamber using helium gas and a bank charge of 5 kV is 11.1 eV with a standard deviation of 0.8 eV. This measurement is line averaged, so certain hotter or colder patches of plasma are not accounted for, and neither are any radial profiles of temperature.

For all of these pulses, the spectroscopy recorded light between 42 μs and 46 μs. Assuming that $T_e = T_i$ as we already have before for the sake of probe theory, we see that this value calculated from spectroscopy is nearly the same as the 10.6 eV average electron temperature calculated by the Langmuir probe at 44 μs. This remarkable similarity has some element of coincidence, as the Langmuir probe standard deviation at that time extends down to 4.7 eV and up to 16.4 eV, but the reliable spectroscopy measurement shows that the Langmuir probe measurements are accurate, albeit imprecise.

The imprecision of the Langmuir probe does not easily lend itself to making accurate judgments about a temperature profile, and neither does the line-integrated measurements taken by spectroscopy. This leads to another question that, for the moment, is best answered with educated speculation: how is temperature distributed in the plasma?

There are two likely answers to this question. The first answer is that the temperature is constant throughout the plasma, that the plasma has reached thermal

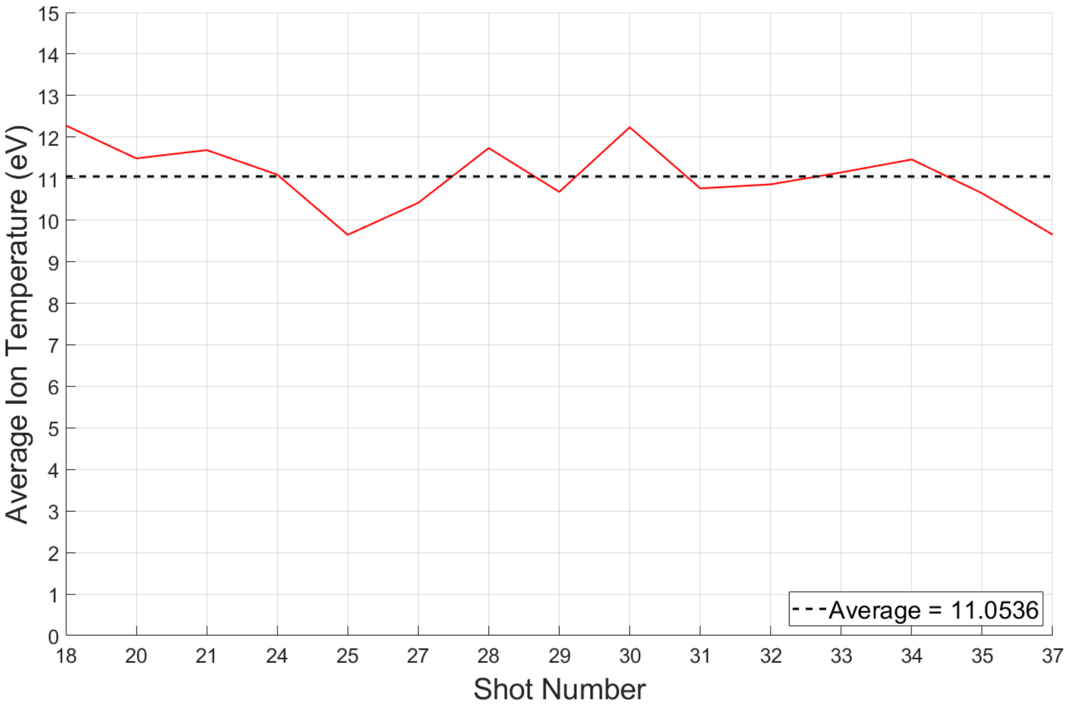

Figure 5.11: Chord-averaged ion temperature calculated from spectrum line broadening. The calculated average, 11.1 eV, is within half of a standard deviation of the electron temperature calculated from the Langmuir probe.

equilibrium. Although amplitude fluctuations are present in the Langmuir probe, 14.4 eV plus or minus a standard deviation of 7.8 eV encompasses much of the data shown in figure 5.9. Thus, a constant temperature throughout is plausible. Additionally, the line-integrated spectroscopy measurements calculated a similar temperature to the Langmuir probe trace in figure 5.10, meaning that either hot and cold plasmas on either side of the spectroscopy chord to the Langmuir probe balance out strangely well, or that the temperature doesn't fluctuate that much across the spectroscopy chord. The second answer is that the temperature distribution, like the ion saturation currents, is hottest at the center and follows a radial profile that drops off as radius increases. Figure 5.9 shows a peak electron temperature of 25 eV at 50 μs on the R = 32 mm data trace. This is nearly double the temperature of the R = 65 mm trace at the same time, and outside one standard deviation from it according to figure 5.10. This suggests a similar radial profile in temperature to the ion saturation current profile. However, after R = 65 mm, there is no similar profile in the Langmuir probe temperature measurements - temperature traces oscillate about this range due to oscillations in the floating voltage. This is dissimilar to the ion saturation current profile, which continues to drop off to zero traveling outward from R = 65 mm to the edge of the vacuum chamber.

To answer this question accurately, more measurements with the Langmuir probe should be taken at each radial position to build more statistical significance to the data, and dampen the floating voltage oscillations with more samples in an average temperature calculation.

5.4.2 Electron Number Density

Per equation 2.11, calculation of electron number density depends on double probe current as measured from the Langmuir probe, the V_{d2} difference voltage between the floating probe and double probe tips, and the electron temperature, which itself depends on the V_{d2} difference voltage. As the electron temperature or the V_{d2} difference voltage approach zero, the numerical calculation for temperature takes a long time to converge, so for analysis of density I set the lower limit for V_{d2} at 0.001 V. Additionally, for points where electron temperature approaches zero, the raw calculation approaches infinity, but these small spikes are removed without noticeably affecting the rest of the signal when it is smoothed twice.

With this procedure, the electron density ranges from 3×10^{20} to 9.5×10^{20} m $^{-3}$. Unlike the electron temperature profile, a clear profile in signal is seen when increasing or decreasing the radial position of the Langmuir probe. This clarity is mostly due to the corresponding clarity in the ion saturation current profile shown in figure 4.13.

After the primary peak, a clear tail with fluctuations is shown in the signal; this is due to the decreased signal to noise ratio caused by dropoff of double probe current

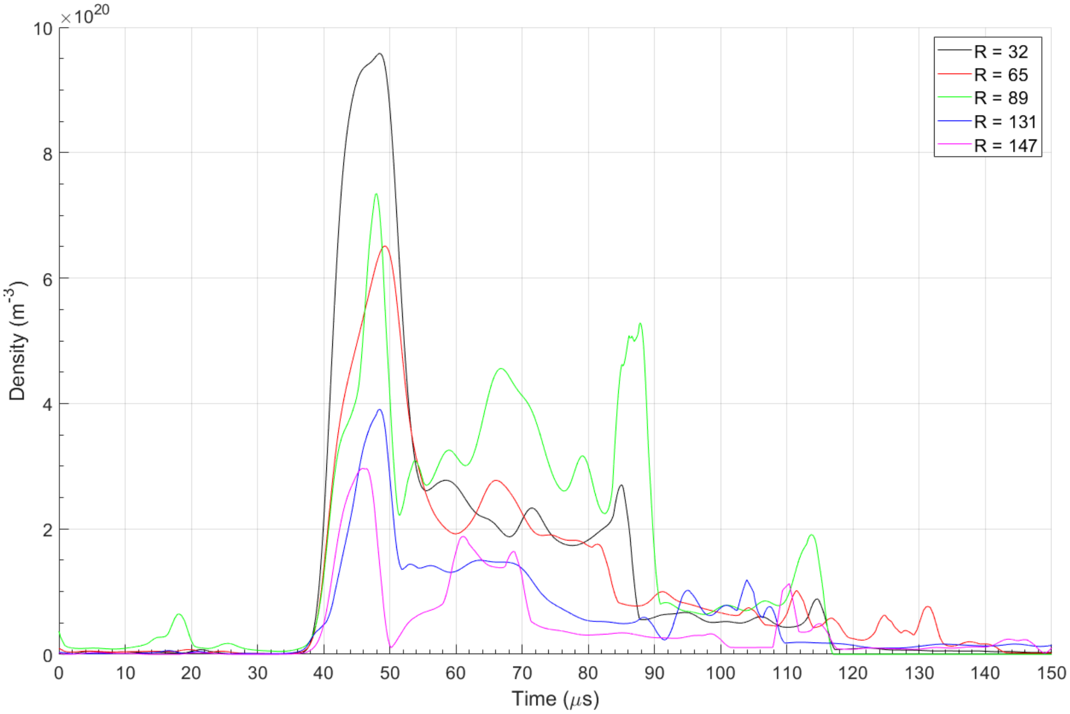

Figure 5.12: Radial profile of average electron density for a pulse at a given Langmuir probe position, ranging from the inner edge of the spoke gap to the outside of the vacuum chamber. Unlike the electron temperature profile, a clear dropoff of density is seen even at positions farther from experiment centerline. The clarity of this signal mostly results from the clarity in the raw double probe current signal as measured by the Pearson current monitor.

while oscillations are still present in the floating voltage feeding the V_{d2} calculation. However, the primary peak occurs at nearly the same time for all signals, owing to the consistent timing of the primary peak in the double probe current data.

More than just showing a clear signal, we see that peak density drops off by 68% between R = 32 mm at the inner edge of the spoke gap and R = 147 mm at the edge of the vacuum chamber, showing evident collimation in the plasma. This collimation isn't logarithmic or quadratic but is nearly linear, apart from a small hitch up at R = 89 mm.

The pulses incorporated into this profile were the same as those used for the

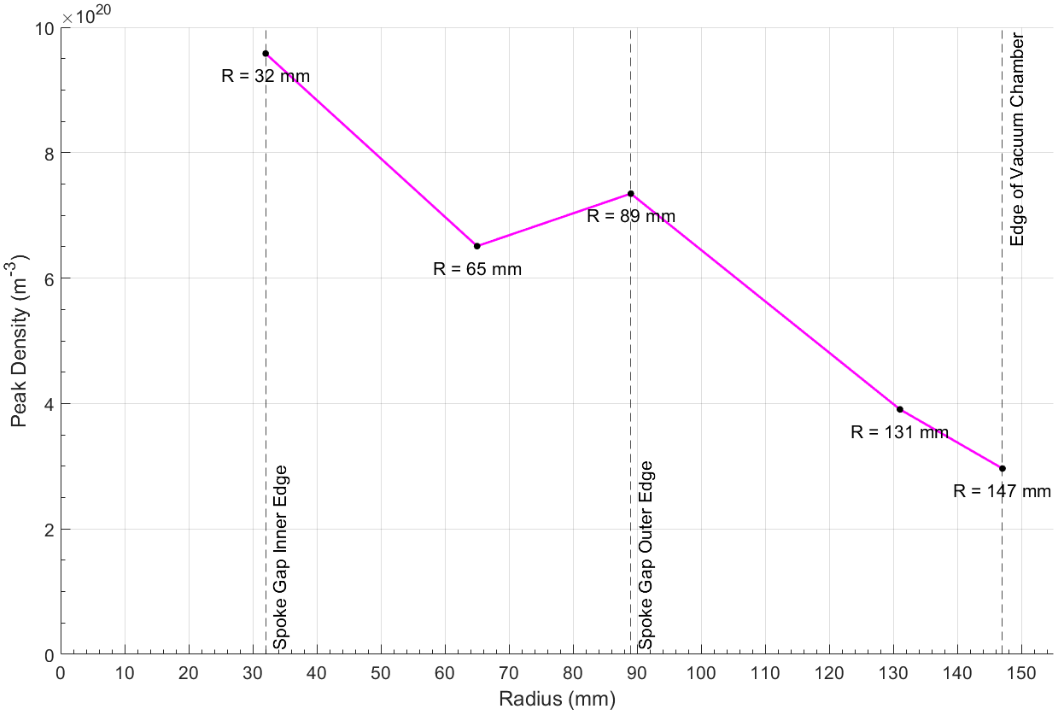

Figure 5.13: Radial profile of peak electron density for a pulse at a given Langmuir probe position, ranging from the inner edge of the spoke gap to the outside of the vacuum chamber. A nearly linear dropoff in density is observed.

electron temperature profile so, like the electron temperature profile, the data lacks statistical significance at some points. Plotting the average and standard deviation of electron density for the same fifteen shots as figure 5.10, it is evident that the average is notably lower for the whole fifteen shots than for the five shots at R = 65 mm incorporated into the profiles for figures 5.12 and 5.13.

Looking at the densities for each individual shot reveals the outliers. Shots 200210019 and 200219008 have peak densities above 8×10^{20} m^{-3}, whereas the rest of the pulses show peak densities at about 6×10^{20} m^{-3} or lower. Both of these shots are included in the data for the density profiles. Delving deeper and looking at individual probe tip data, I found the source of these outlying densities to be the double probe currents. Where shots 200210019 and 200219008 have double probe

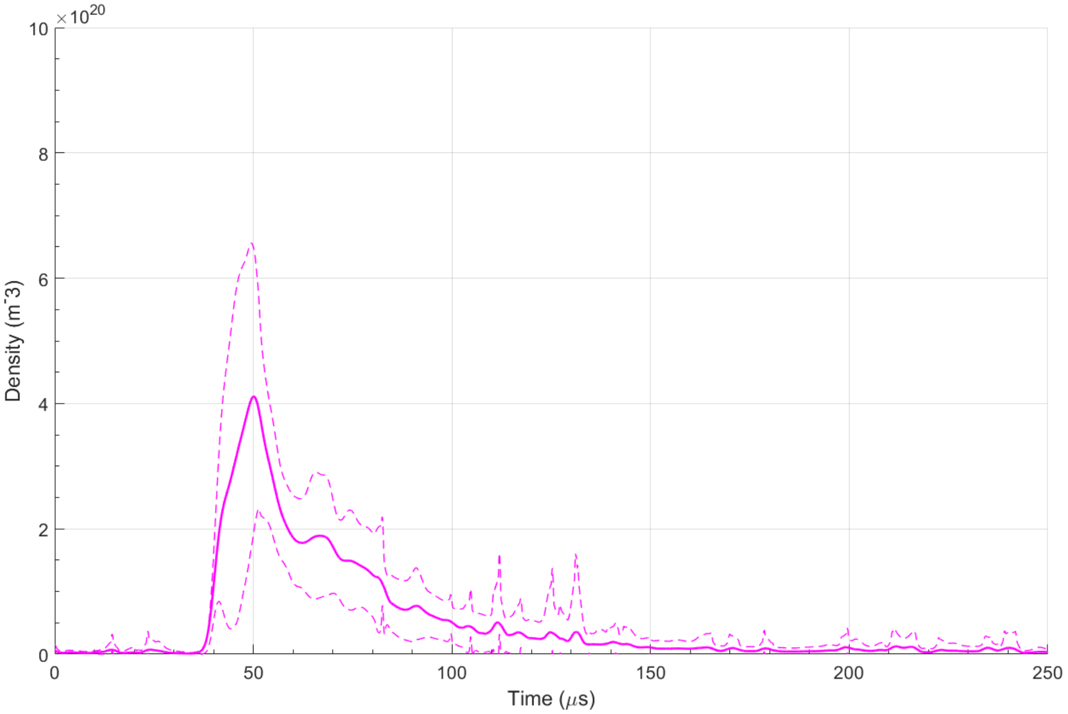

Figure 5.14: Average electron number density plus or minus one standard deviation for Langmuir probe at R = 65 mm, averaged over 15 pulses. This average density is notably lower than the five pulses incorporated into densities in figures 5.12 and 5.13.

currents near 13 Amps, the other three shots of the five used in the radial profile have double probe currents at or less than 9 Amps. One of these outliers, shot 200219008 shows a notably larger Mach probe current than the others, while the other outlier shows a similar current to the others. When removing these outliers from the data, the average density at R = 65 mm in the density profile drops from 6.5×10^{20} m^{-3} to 5.2×10^{20} m^{-3}, more in line with the total average of fifteen shots in figure 5.14. The resulting density profile then looks more cubic than linear. However, the density is at R = 65 mm is still high compared to this total average.

The three pulses at R = 32 mm also show varying data; the average peak density of 9.6×10^{20} m^{-3} has a standard deviation of a full 3.4×10^{20} m^{-3}, about 30% of the average. Densities calculated at outer radii have similar deviations, with peak densities at R = 131 mm having a standard deviation of $1.6 \times 1{-}^{20}$ m^{-3} (40%) of the average peak density) and R = 147 mm having a standard deviation of 3.2×10^{20} m^{-3} (110% of the average peak density).

Clearly, more statistical significance is needed at these radial profile data points to define the profile more clearly. With the data present, the radial profile looks nearly linear. However, with the standard deviations of these data so high (and with the number of data points at each radius lying between two and five), adding more data could would likely reduce the standard deviations. In doing so, it may redefine the curve to something more quadratic or cubic or logarithmic. For the meantime, though, it is clear even with the wide range of data at each radius that there is a dropoff of average density as radius increases, so we can still say that the plasma is collimated.

5.4.3 Flow Velocity

Because of the unreliability of the Mach probe as discussed in section 5.3, no consistent velocity measurements were able to be calculated from Mach probe data. Instead, Doppler shift spectroscopy provides consistent measurements with an average plasma velocity in the end chamber of 86.2 km/s. Spectroscopy calculations are chord-averaged, and given that the line peaks are not inaccurately broad (which would indicate "smearing" of the line between lower and higher velocities), this 86.2 km/s will be assumed constant throughout the plasma, independent of radius.

As a sanity check, we can calculate what the Mach number should be. The speed of sound is found via equation 2.13 to be 16200 m/s for helium gas at a temperature of 11 eV. Thus, the calculated Mach number for a flow velocity of 86.2 km/s should be 5.3. This value is widely outside any calculated values using the ratio of ion saturation currents from the downstream Mach probe. To calculate a Mach number of 5.3 with equation 2.15 and a calibration constant of K = 1.5 requires that the ratio of ion saturation currents be about 2800. This implies that for a Mach 5.3 plasma with an upstream ion saturation current of 20 Amps, the downstream ion saturation current would be 7 mA.

Perhaps, then, the zero signal we see on the pulses where the Pearson probe was moved to the Mach probe circuit is correct. The signal to noise ratios seen with our setup were not high enough to measure currents as low as 7 mA. The background noise measured by the Pearson current monitor regularly reaches ± 0.1 A, so signals below this are indistinguishable from noise. According to a representative I spoke to at Pearson Electronics, the lower limit of current the model 2878 can measure is determined by the thermal noise and the termination of the monitor (50 Ω), and comes out to about 100 nA. Clearly this is well below 7 mA, so I believe the 100 mA noise level we see in the data is from the MDO 3014 oscilloscope and not the Pearson current monitor. Thus, this issue may be fixed simply by decreasing the vertical scale on that scope channel. However, for this data, the noise lies at 0.1 A.

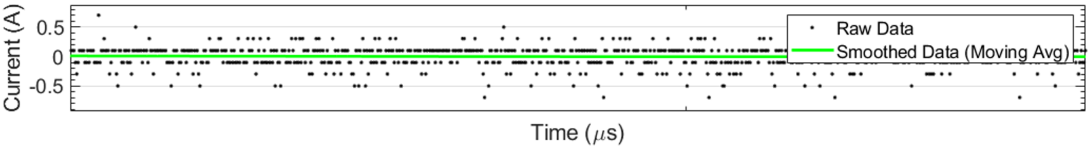

Figure 5.15: Amplitude of noise on the Pearson current monitor. Noise regularly reaches levels of ± 0.3 Amps measured and the current cannot measure points below 0.1 A, thus, any signals below this value are indistinguishable from noise.

Forcing the value of the Mach probe current to be 0.1 A for the purposes of Mach number calculations while leaving the double probe current unchanged shows a more accurate answer for velocity. However, it is still not entirely accurate, partly due to the assumed Mach probe calibration constant, but also due to the assumed Mach probe current of 0.1 A. Perhaps getting more signal to noise ratio from the Pearson probe can be fixed by simply changing the scale of the MDO3014 oscilloscope where the data is collected, or perhaps getting a more sensitive current monitor would be necessary.

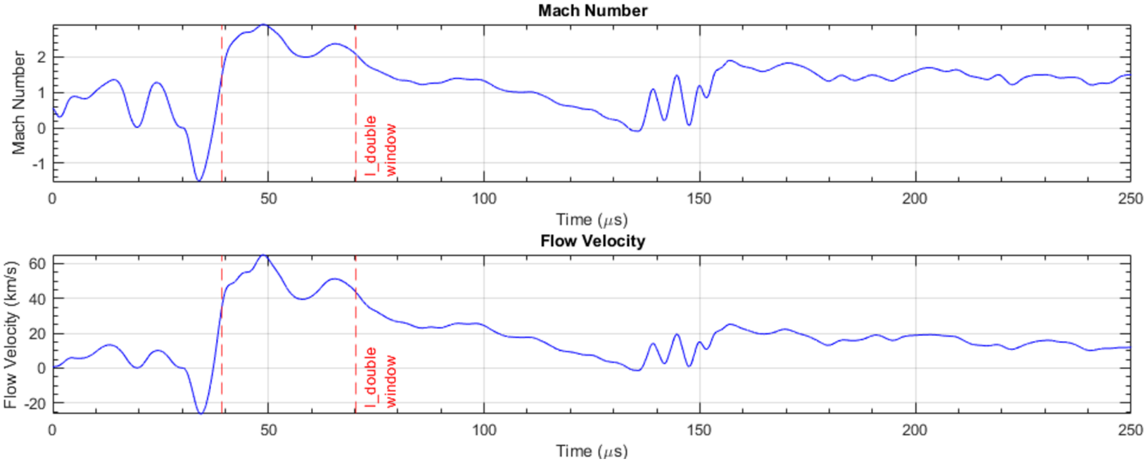

Figure 5.16: Flow velocity calculated with mach probe current set to 0.1 A. These values are much more reasonable, reaching above 60 km/s; however, they are still not quite accurate. Some of this comes down to the assumed Mach probe calibration constant K = 1.5, but most of the inaccuracy is likely a direct result of assuming the Mach probe current.

I conclude that although Mach probe theory may be accurate for slower moving plasmas, it cannot be easily applied to plasmas at hypersonic speeds like those found in FuZE due to the incredibly high signal to noise ratios required for accurate Mach number measurements. Perhaps a different version of Mach probe theory would be applicable here, or perhaps the use of an electric probe to measure flow velocity for fast plasmas is too inherently insensitive. Perhaps using a different current monitor or data collection setup would sufficiently improve signal to noise ratio. However, for the purposes of this thesis, the constant velocity of 86.2 km/s as found by spectroscopy will be used in any calculations moving forward.

5.5 Divergence of Plasma Plume in End Chamber

We see from the density profile that that plasma is clearly collimated. However, as any plume of gas will do, the plasma column expands at some rate and the plume diverges. This is especially applicable for plasma thrusters, as the divergence of the exhaust plume has an effect on the thrust efficiency.

The divergence of the FuZE plasma plume can be estimated with the thermal velocity. Assuming that all initial velocity at the end wall is in the axial direction, any plume divergence present is a result of the plasma thermally expanding. The plasma thermal velocity is found via

$$v_{th} = \sqrt{\frac{k_B T}{m}} \tag{5.4}$$

which for FuZE helium plasma at 14 eV is 18.87 km/s. If a plasma expanding thermally at this velocity is traveling downstream at 86.2 km/s, it will have an expected divergence angle of 12.3°. At 60 cm past the end wall, this plasma will have expanded 13 cm. Thus, if the plasma exits the end wall at R = 65 mm, the center of the spoke gap, then by the time it reaches the Langmuir probe it will have expanded to R = 195 cm.

Per figure 5.13, the plasma shows much more collimation than this, with number densities at R = 32 mm being over three times those at the outside of the vacuum chamber. Clearly there is another mechanism to plume expansion than just the thermal velocity. Perhaps the nature of magnetic separation at the end wall preferentially separates plasma closer to the centerline of the experiment, or at inward radial velocities. If the Maxwellian distribution of plasma temperatures is skewed hot, where some especially hot electrons raise the average temperature but the bulk of plasma is colder, which would result in a decreased divergence angle overall.

The density at R = 32 mm is notably higher than any other density in the profile. At this radius on the end wall, the gaps in the end wall spokes are the smallest, so theoretically less plasma overall would exit here. However, the bulk of plasma is still formed in a pinch inside the assembly region, so it would likely exit the end wall closer to the centerline than not.

Per Zhang, et al. [32], plasma densities in the assembly region of FuZE reach 1.1×10^{17} cm^{-3} inside the pinch, with a pinch radius of approximately 0.3 cm. The linear density of the plasma over the r-θ plane is given as

$$N = \int_0^a n(r) 2\pi r dr \tag{5.5}$$

where $n(r)$ is the volume density at radius r, and a is the maximum radius. Zhang shows that the density in the pinch also falls off approximately linearly, so modeling the density as $n(r) = -2.2 \times 10^{17}(r) + 1.1 \times 10^{17}$ cm^{-3} gives a linear density of 1.87×10^{16} cm^{-1} for a pinch radius of 3 mm. When considering a radius out to 5 mm where Zhang's calculated densities approach zero, the linear density is 2.49×10^{16} cm^{-1}.

In the end chamber, density also falls off approximately linearly. Modeling density as as $n(r) = -1.09 \times 10^{14}(r) + 1.90 \times 10^{15}$ cm^{-3} over a radius of 14.7 cm, the linear density is 5.65×10^{17} cm^{-1}, an order of magnitude larger than the linear density in the assembly region. This is reasonable when considering the plasma parameters and that linear density scales inversely with temperature and volume density. As the plasma expands out of the assembly region, temperature and volume density decrease while linear density increases.

5.6 Plausibility of a Z-Pinch-Based Space Propulsion System

One of the goals of this thesis is to determine the plausibility of using a sheared-flow stabilized Z-pinch-based thruster as a space propulsion system. As such, this section intends to characterize the plasma exhaust plume of FuZE as it relates to potential thruster performance.

One of the primary appeals in using electromagnetic thrusters as opposed to chemical thrusters or using potential fusion-based rockets over current EM thrusters is efficiency. Efficiency of a thruster system is often measured and compared to other systems as specific impulse, which can be found via

$$I_{sp} = \frac{F_T}{\dot{m} g_0} = \frac{v_e}{g_0} \tag{5.6}$$

where F_T is the thrust of the engine, $\dot{m}$ is the mass flow rate, g_0 is the gravitational acceleration at sea level, and v_e is the exhaust velocity. For FuZE, using an average exhaust velocity of $v_e = 86.2 \pm 2.8$ km/s, I_{sp} is 8790 ± 290 seconds.

The mass flow rate is the measure of how much fuel is accelerated out of the thruster. Once we know the mass flow rate, we can calculate the theoretical thrust of the engine.

To find mass flow rate, first we need to find the amount of mass expended in a single effective pulse. For the purposes of this analysis, the effective pulse will be considered to be the average length of time in which the density is nonzero, which according to figure 5.14 is about 120 μs. Assuming the plasma is neutral, the electron density equals the ion density, which equals the total particle density. According to figure 5.13 (which includes the two high outliers), peak density falls of approximately linearly, so the average peak density across the FuZE cross section is the average of this value, $6.06 \times 10^{20} \pm 1.05 \times 10^{20}$ m^{-3}. Mass density equals the number density times the mass of one particle, which in this case is pure helium at 6.65×10^{-27} kg, so we're left with an average peak mass density across the FuZE plume cross section of $4.03 \times 10^{-6} \pm 0.70 \times 10^{-6}$ kg/m^3.

Now we need to figure how much volume is expended in one pulse. A pulse is 120 μs long and plasma travels at 86.2 ± 2.8 km/s. Distance equals rate times time, so over a pulse the plasma travels 10.3 ± 0.34 m. Multiplying the average peak mass density by a cylinder of this length and radius 0.147 m yields a total pulse exhaust mass of $2.83 \times 10^{-6} \pm 0.50 \times 10^{-6}$ kg. Over a pulse time of 120 μs, this gives a peak mass flow rate of 0.0236 ± 0.0042 kg/s. Multiplying by the exhaust velocity yields a peak thrust (without pressure effects) of 2030 ± 370 N.

This calculated thrust is true only if the peak density holds for the entire pulse, which it does not. Instead, the average density over the course of the pulse is the proportional to the average of the curve in figure 5.14 divided by the peak density of that curve, which yields a multiplier of approximately 0.66 to be applied to the peak values to convert to average values. Using this multiplier, the average mass flow rate of the pulse is 0.0156 ± 0.0028 kg/s, yielding an average thrust (without pressure effects) of 1350 ± 250 N.

These thrusts don't include the pressure term to the thrust equation:

$$F_T = \dot{m}v_e + (P_e - P_0)A_e \tag{5.7}$$

where P_e is the thruster exit pressure, P_0 is the outside pressure, and A_e is the area of the thruster exit. Assuming the plasma exhaust behaves as an ideal gas, the pressure can be calculated via $P = nk_BT$ to be 1070 ± 190 pA. Multiplying by the cross section area of FuZE yields a pressure differential force of 72.5 ± 13 N, which can be added to both the peak instantaneous thrust and the average thrust.

Thus, our peak instantaneous and average thrusts for FuZE are 2100 ± 380 N and 1420 ± 260 N, respectively.

These values for peak and average thrust used a few important simplifying assumptions:

- Density varies linearly by radius in the FuZE end chamber.
- Total pulse length is 120 μs and gas only escapes during this pulse.
- Exit velocity of 86.2 ± 2.8 km/s is constant over the pulse and over the radius of the end chamber.
- Plasma is neutral, so mass density is the ion and electron number density multiplied by the mass of neutral helium.
- Plasma behaves as an ideal gas.

With these assumptions in mind, we can double check the initial calculation of specific impulse, which used only the exhaust velocity as calculated by spectroscopy, using the first equivalency of equation 5.6:

$$I_{sp} = \frac{F_{T,avg}}{\dot{m}g_0} = \frac{(1420 \pm 260\ N)}{(0.0156 \pm 0.0028\ kg/s)(9.81\ m/s^2)} = 9280 \pm 2400\ s \tag{5.8}$$

While the error bars are somewhat large at about 25% of the value itself, the value itself is only 490 N different than the initial calculation of specific impulse at 8790 ± 290 s, a percent difference of only about 5%. This shows that while the assumptions above simplify the calculations significantly, they still produce accurate results, so they must not be far off the truth. Additionally, because the spectroscopy diagnostic is trustworthy, these calculations show that the measurements of density from the Langmuir probe are also likely trustworthy, albeit not to quite the same extent based on the magnitude of the error bars.

These thruster parameters are notably different than those predicted in Shumlak's paper [27], which placed estimates of specific impulse in the range of 10^6 seconds and thrust in the range of 10^5 N. However, these estimates were of thrusters of a significantly larger scale, with scale lengths between 1.5 and 18 meters and exhaust velocities in the thousands of kilometers per second, whereas FuZE only has velocities near 100 km/s and a pinch length of less than half a meter.

Calculated FuZE thruster performance parameters lie far above current-day electromagnetic thruster parameters, which have thrusts in the hundreds of millinewtons as opposed to a kilonewton or more. Also, although efficient, even the most efficient electrostatic and Hall-effect thrusters have specific impulses less than half that of FuZE, due to FuZE's relatively high exhaust velocities.

Although fuel efficient and with a considerable amount of thrust, a space propulsion system based on the sheared-flow stabilized Z-pinch like FuZE has some drawbacks. First, radiation shielding is a concern dependent on fuel. If using deuterium and He^3 for fuel, no neutrons will be directly produced in the fusion reaction so shielding can be minimal, but some neutrons are still present when D-D reactions occur.

Table 5.2: Comparison of thruster performance for known and theoretical space propulsion systems (known system performance found at [30])

Thruster Name	**Thrust (N)**	$\mathbf{I}_{sp}$ **(s)**
Existing Thrusters		
Aerojet MR-501B EHT	0.37	303
Aerojet MR-510 Arcjet Thruster	0.25	600
XIPS 25cm Electrostatic Thruster	0.165	3500
Aerojet BPT-400 Hall-effect Thruster	0.254	2076
Theoretical or Planned Thrusters		
NASA Advanced Electric Propulsion System (40 kW Hall-effect)	0.6	2900
VASIMIR VX-200 Electrothermal Engine	5.4	5000
FuZE	1420	8790
Shumlak's Theoretical D-He^3 Engine	3.3×10^5	360000

Second, the method of power generation is unclear. Somehow the excess energy produced by the fusion reaction inside the pinch needs to be converted to usable energy for the spacecraft. Possible schemes to do this efficiently via direct energy conversion have been theorized. For example, a traveling-wave direct energy converter generates power through oscillating waves measured by grids through which the fusion products travel [17]. However, direct energy conversion methods have not yet been extensively tested or engineered, so their applicability to use in a space propulsion system is unknown.

Despite these obstacles, though, it seems clear from this investigation that a sheared-flow stabilized Z-pinch like FuZE has potential as a space propulsion solution. The high specific impulse means less fuel has to be carried, high thrust provides a faster time-to-destination than current electromagnetic thrusters, and assuming the issue of energy conversion can be solved, the power output of the system should be high enough to offset the power required to accelerate the plasma at least in part.

5.7 Plasma Separation at the End Wall

Due to the rapid pace of my thesis program and the availability of other problems to investigate, my work did not delve deeply into examining how plasma separates from magnetic fields at the end wall. However, I will present a basic analysis here that may educate further research into this process.

In the assembly region, a strong magnetic field exists as a strong pinch current is present. The plasma may very well be magnetized in this field. When the plasma is magnetized, it will gyrate around the field lines per the Lorentz force and will follow the field lines as they curve. Particle drifts will be present on longer timescales if an electric field is present or if the magnetic field lines curve, but as a whole the plasma stays attached to field lines. This pinch current flows inward along the spokes in the end wall, creating a magnetic field around the end wall spoke. For a magnetized plasma to diffuse past the end wall and be observed by the Langmuir probe and spectroscopy telescope, it must be able to demagnetize and separate from the field lines. A plasma that is already demagnetized will freely move through the end wall without worrying about the magnetic field.

Figure 5.17 shows that density starts increasing at about 37 μs. Taking into account a travel speed of 86.2 km/s, the plasma reaching the Langmuir probe at this time would pass P45 8 μs earlier at 29 μs. This is the time at which the P45 magnetic field also starts to rise, suggesting that the plasma is not initially blocked from reaching the Langmuir probe and that it is sufficiently demagnetized to move through the end wall without issue.

If at some point in the pulse the magnetic field becomes strong enough to force the plasma to break free from it to move into the end chamber, then perhaps the

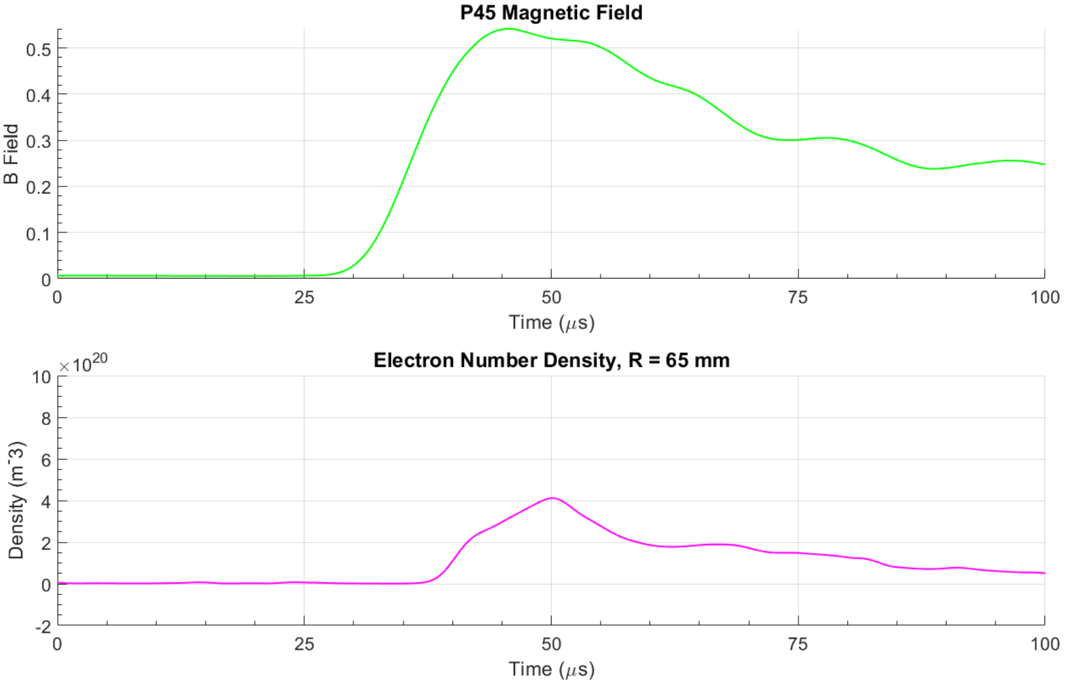

Figure 5.17: Magnetic field at P45 vs End Chamber Density at R = 65 mm. These data are an average of data from the fifteen shots used for statistical significance.

method of this separation is through a pressure balance. We can investigate this on a surface level by comparing magnetic field pressure and flow ram pressure.

Knowing that plasma velocity in the end chamber is 86.2 ± 2.8 km/s and average peak density across the FuZE cross section is $4.03 \times 10^{-6} \pm 0.70 \times 10^{-6}$ kg/m^3 (as found in section 5.6), we can calculate the peak ram pressure via

$$P_{ram} = \rho v^2 \tag{5.9}$$

to be approximately 29.9 kPa, where ρ is the mass density and v is the flow velocity. Magnetic pressure at P45 can be calculated from the P45 magnetic field via

$$P_{mag} = \frac{B^2}{2\mu_0} \tag{5.10}$$

where B is the magnetic field strength and μ_0 is the permeability of free space. From this we find a peak magnetic field pressure at P45 of 116 kPa. This is much greater than the ram pressure, suggesting that even when the magnetic fields are strong, plasma can escape from the end wall. But to what degree, and where is the cutoff?

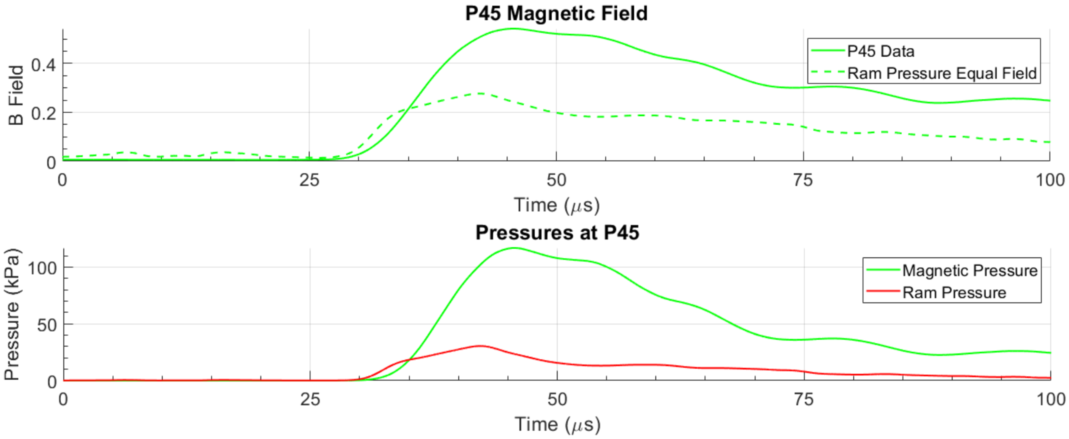

Figure 5.18: Magnetic field, magnetic pressure, and ram pressure at P45. A magnetic field creating magnetic pressure equal to the ram pressure is also plotted to compare to the actual magnetic field at P45.

Assuming the ram pressure is the same at the Langmuir probe and at the end wall, we can use equations 5.9 and 5.10 to calculate the strength of a magnetic field that exactly opposes this pressure.

These two field strengths line up until a field strength of about 0.2 T is reached, at which point the rate of increase of the ram pressure decreases to about one sixth that of the magnetic pressure. This indicates that if magnetic field strengths are below 0.2 T in the assembly region, the plasma is sufficiently unmagnetized to pass through the end wall without hindrance. At greater magnetic field strengths, the magnetic field begins to meaningfully oppose the passage of plasma through the end wall. If ram pressure before the end wall actually continues to increase at the same rate whereas ram pressure after the end wall increases at a sixth of the rate, this may suggest that if sufficiently magnetized, five sixths of the excess ram pressure goes towards separation from the magnetic fields and the rest can then go into the flow.

However, this is all speculation. The plasma may behave differently entirely, and perhaps the ram pressure upstream of the end wall actually does see a notable decrease in its rate of increase and that isn't an event characteristic of separation. To know for sure, specific analysis of plasma just before and just after the end wall should be performed.

Chapter 6

SUMMARY, CONCLUSIONS, AND FUTURE WORK

While Z-pinches are geometrically simple and their design, construction, and maintenance is easier than other magnetic confinement fusion schemes, they have not been largely pursued in the past due to the m = 0 and m = 1 instabilities. By exploiting sheared-flow in the plasma, the Z-pinch can be stabilized. The Fusion Z-pinch Experiment, or FuZE, was set up as a test of this concept on fusion plasmas. While the acceleration and assembly regions of FuZE have been extensively diagnosed, the region downstream of the end wall has not. This thesis investigation sought essential plasma parameters and behavior of plasma flow downstream of the end wall in order to make determinations on plasma detachments from magnetic fields, plume divergence, and potential performance of a sheared-flow Z-pinch-based space thruster. This chapter summarizes the experimental setup and procedure for this investigation and the results and conclusions drawn from it as well as possible avenues for future work.

6.1 Summary of Experimental Setup and Procedures

The first of two diagnostics used to measure the downstream plasma is a quadruple Langmuir probe. The quadruple Langmuir probe measures upstream floating voltage on an unbiased probe tip and on connected double probe electrodes biased to collect ion saturation current as well as the ion saturation currents themselves on both the upstream double probe and a downstream Mach probe tip. Using these measurements, calculations can be made of electron temperature, electron number density, and ion flow velocity.

The probe used for this investigation was inherited from the student who built the probe a number of years ago who left little documentation of its function or construction. The probe is mounted to the top of the vacuum chamber approximately 60 cm downstream of the end wall, and can extend and retract into and out of the chamber. The range of this extension is from 32 mm off-axis to a point inside the probe at 184 mm off-axis.

In other experiments not at the University of Washington, triple and quadruple Langmuir probes have been mostly used to diagnose cold, slow-moving plasmas. In the assembly region of FuZE, plasmas reach temperatures greater than 1 keV and velocities in the range of 100 km/s, far hotter and faster than any previous measurements seen using quadruple Langmuir probes. Although this investigation measured plasmas downstream of the assembly region, these plasmas are still traveling quickly and likely carry residual heat from the Z-pinch, thus the plasmas measured are likely outside the realm of previous use of Langmuir probes. Langmuir probes, being electrodes physically immersed in the plasma, are especially sensitive to hot and fast plasmas that vary rapidly like those in FuZE and are similarly sensitive to EMI noise.

The second diagnostic used in this investigation is Doppler shift spectroscopy. This diagnostic measures the light spectrum of the plasma and uses its wavelength shift relative to static ions to determine the velocity of the plasma. It can also measure ion temperature using the width of the Gaussian peak of the wavelength lines observed in the plasma. Spectroscopy has a much more reliable history in the FuZE lab than Langmuir probes, and being a passive experiment measuring only the light coming from the plasma, it is less sensitive to noise than the quadruple Langmuir probe.

A 35° angled port downstream of the end wall was used as the location for Doppler shift spectroscopy. This port's line of sight extends straight through the axial location of the Langmuir probe, and the angle of the port allows a parallel velocity component to be observed as blue-shift of the light. In contrast to the Langmuir probe's ability to extend into and retract out of the plasma to measure different points in 1-D space, the spectroscopy measurements are chord-averaged along the line of sight of the telescope.

Measurements of the plasma were taken with these diagnostics over a six month period in late 2019 into early 2020. Initial measurements intended only to properly set up the diagnostics, a procedure especially important for the Langmuir probe and its sparse experimental history on FuZE. After taking initial measurements and understanding the signals, Langmuir probe measurements were taken at five radii in the end chamber, ranging from the inner edge of the gap in the spoked end wall out to the edge of the vacuum chamber.

6.2 Summary of Results and Conclusions

Signals in the Langmuir probe show intermittency; about one fourth of pulse measurements show a sharp increase in signal at about the time of plasma arrival, varying by up to 10 μs, with a following slow decrease in signal over hundreds of microseconds until a sudden drop-off back to zero. The rest of the pulses show a significantly lower amplitude signal, starting at about the time of plasma arrival, and decaying back to zero within tens of microseconds.

Initially, the larger signals were assumed correct, because they showed consistent amplitude and initial measurements of plasma parameters using these signals were in the reasonable range for FuZE of $50 - 60$ eV temperature and 2×10^{21} m^{-3} number density. However, later I determined that all of these larger amplitude signals were indicative of an electrical arc between biased Langmuir probe tips, driven by the bias capacitors in the double probe and Mach probe circuits. Evidenced for this includes a rapid and brief spike in voltage measurements at the time of signal rise and the direction of current flow and voltage change on each probe tip. The rapid spike in voltage measurements is not visible in any of the smaller signals. Simultaneous spectroscopy measurements showed consistent presence of plasma shot-to-shot, suggesting that the intermittency in Langmuir probe signals is due to the electronics of the probe itself and not the plasma. Furthermore, increasing the bias voltage on the capacitors significantly increases the likelihood of a discharge. On shots where discharge occurs, the consistent 0.00353 C current time integral under the double probe current measurement shows that the Pearson current monitor consistently saturates during discharges. The Mach probe current integral yields consistent drops in capacitor energy of 4.6 Joules at 200 V Langmuir probe bias, or 24% of the total energy in the capacitors. For plasma parameter calculations, pulses that show discharge are neglected.

Calculations of plasma parameters using Langmuir probe measurements show temperatures ranging from 5 eV to 25 eV, but this calculation inherits significant variation due to large amplitude oscillations in the floating voltage. Because of these oscillations, a clear profile in temperature is not visible, possibly indicating a constant peak temperature throughout the plasma independent of radius. Averaging fifteen shots at position R = 65 mm provides more statistical significance than the two to five pulses at each probe position taken for the radial profile investigation. This reveals a peak electron temperature of 14.4 ± 7.8 eV.

Density calculations reveal a far more defined radial profile and a collimated plasma. The clarity in these calculations is due to the direct proportionality of electron density on the double probe current, a measurement made by a Pearson current monitor with high signal to noise ratio. The radial profile reveals a nearly linear drop-off in electron number density as radius increases from R = 32 mm, ranging from 3×10^{20} to 9.5×10^{20} m^{-3}. Recalculating average density with the same fifteen shots at position R = 65 mm shows a notably lower value than the five pulses at R = 65 mm as part of the radial profile, revealing that high variation in these measurements can create outliers.

Ion Mach number calculations using the Langmuir probe are unreliable at best or nonphysical at worst when using the Mach probe as it is set up. The core problem of these measurements is that the downstream Mach probe current signal is unreliable. It is measured not by a Pearson current monitor, as the upstream signal is, but by measuring the voltage across a 0.5 Ω resistor. Thus, it is subject to the same EMI noise as the other voltage measurements where the Pearson current monitor is not. Additionally, despite the noise, the current measured by the Mach probe is often higher than the current measured on the double probe, sometimes nearly double the value, suggesting that flow is moving in reverse at supersonic speeds, which is a nonphysical answer.

Calculations of flow velocity using Doppler shift of the 468.6 nm helium-II line are fortunately much more reliable and precise, showing flow velocities of 86.2 ± 2.8 km/s. A time scan of spectroscopy shows that the main pulse of plasma arrives between 42 μs and 46 μs, confirming the arrival time that the Langmuir probe measurements imply. Because these measurements are chord-averaged and the spectroscopy line peaks are not overly broad (which would indicate "smearing" of low and high velocities), this 86.2 km/s is considered constant throughout the plasma.

This flow speed sheds more light on the issues in the Mach probe. For a Mach number of 5.3, the ratio of upstream to downstream ion saturation currents is 2800. The Pearson current monitor was unable to give accurate measurements below 100 mA due to the scope setup, much less the 7 mA required for this current ratio. It seems that for fast flowing plasmas, the required signal to noise ratio is too high for our current setup and using a second Pearson current monitor on the Mach probe circuit with a small vertical scale on the scope may show clearer signals.

The Langmuir probe calculated electron temperatures were also verified by the spectroscopy measurements, which via the full-width half-max of a fit Gaussian doublet at the 468.6 nm He-II line reveal an ion temperature of 11.1 ± 0.8 eV at 44 μs. The Langmuir probe calculated electron temperature at this time is 10.6 ± 5.9 eV, which is within one standard deviation of the spectroscopy calculated ion temperature. For FuZE, ion temperature and electron temperature are considered equal. Spectroscopy is the more trusted diagnostic, so equating the temperatures calculated by spectroscopy and the Langmuir probe shows that the Langmuir probe measurements are likely accurate as well, albeit imprecise.

To summarize, FuZE plasma plume parameters are shown in table 6.1.

Table 6.1: Summary of plasma parameters in the FuZE downstream plasma plume

Parameter	**Value**	**Behavior**
Peak Electron Temperature	14.4 ± 7.8 eV	Assumed constant throughout plasma, peak at 48 μs
Peak Electron Number Density	$9.5 \times 10^{20} \pm 3.4 \times 10^{20}$ m^{-3}	Linear falloff with radius, peak at 50 μs
Plasma Flow Velocity	82.6 ± 2.8 km/s	Constant throughout plasma, peak at 46 μs

Comparing ram pressure in the end chamber to magnetic field pressure at the end wall shows that these two pressures line up until the magnetic field strength at P45 reaches 0.2 T, suggesting that below 0.2 T, the plasma is sufficiently unmagnetized to pass through the end wall unhindered. At larger magnetic fields, the magnetic pressure may grow large enough to oppose some of the ram pressure of the flowing plasma so that only a portion of the plasma in the assembly region escapes into the end chamber.

Converting a sheared-flow stabilized Z-pinch experiment like FuZE into a thruster concept essentially only involves removing the end wall and the downstream chamber to allow accelerated plasma to flow directly out as exhaust, assuming it separates from the magnetic fields without hindrance. I calculated theoretical thruster performance parameters using plasma parameters as calculated by probe theory and spectroscopy. For these calculations a few reasonable simplifying assumptions are made; apart from the assumptions about radial profiles of plasma parameters, I also assume that the entire effective length of the pulse is 120 μs (based on the average length of double probe current signal) and that the plasma acts as an ideal gas. Modeling each pulse as a wave of isothermal plasma with density that falls off linearly with radius and a constant velocity, I found that FuZE, if a thruster, would have a specific impulse of 8790 ± 290 s, average mass flow rate of 0.0156 ± 0.0028 kg/s, and average thrust of 1420 ± 260 N. These parameters, while far below the theoretical estimates for a larger scale sheared-flow stabilized Z-pinch fusion engine, are also notably better than other more traditional EM thrusters currently in production. The current disadvantage to the use of a Z-pinch engine is in low power efficiency and lack of flight history or engineering precedent.

Fast, collimated plasma exhaust as seen in FuZE can act directly to provide thrust for an engine rather than provide power for a separate thruster as other fusion based spacecraft concepts involve. This plasma exhaust also provides sufficient thrust to propel spacecraft to a destination in significantly less time than traditional electromagnetic propulsion can. Additionally, the simplicity of the Z-pinch geometry is appealing for spacecraft construction and weight management. While there is much work still to be done in researching fusion space propulsion and many questions left to ask, the sheared-flow stabilized Z-pinch provides one plausible answer.

6.3 Future Work

The measurements taken as part of this investigation provided some important answers, but also provided more questions. To pursue these questions, there are a few notable paths for future work that I will suggest here:

1. More pulses should be taken to provide further statistical significance for the temperature and density radial profiles. The variation in Langmuir probe measurements between pulses can be significantly reduced with more data points in the average, and this may reveal that the temperature does have a radial profile or that the density profile cannot be assumed linear.

2. A second Pearson current monitor should be installed onto the Mach probe circuitry. The Pearson model 2878 current monitor proved itself as a reliable way to measure current in the double probe, far better than the “voltage across a resistor” method used by the Mach probe circuit. However, the signal to noise ratio of the Pearson current monitor as used is still too low for accurate measurements of Mach probe current; I believe this can be rectified by simply decreasing the scale on the oscilloscope, as the current monitor theoretically can read nanoamp currents.

3. Pulses should be taken at radii in between the ones taken here to further flesh out the plasma parameter radial profiles. As it lies now, a clear profile is visible in density, but more data in between the data presented here would provide more accuracy to the profile and possibly reveal more fine details.

4. Pulses should be also be taken with the Langmuir probe positioned at a different location on the experiment. There are 4 5/8 inch conflats along the side of the FuZE end chamber at P113 (where the probe currently is), P96, P80, and P60. These can all be used as mounting points for the Langmuir probe. The end wall has a spoke gap horizontally as well as vertically, so the Langmuir probe would still be in the plasma stream. By measuring different axial locations, more data points can be taken to define plume divergence and collimation.

5. Revealing more details about background noise in voltage measurements due to EMI interference of the experiment could assist in removing this noise from the signal and cleaning up the temperature measurements. One possible way to do this would be to position similar electrodes at points around the laboratory to measure EMI noise that is not confined to the vacuum chamber.

6. Data should be taken with different gas pressures and mixtures. Both of these

parameters change the way the pinch behaves and whether or not nuclear fusion occurs, so in changing these the way the plasma separates from the magnetic field lines at the end wall may also change.

7. An investigation into plasma behavior just downstream and just upstream of the end wall should be performed. Due to the rapid pace of my program, I was unable to take a deep look at detachment of plasma from magnetic fields at the end wall. Basic analysis reveals efficient separation below 0.2 T field strength and partial separation above, but this analysis is base level and relies on a few major assumptions.

8. Another possible method for future work is to reevaluate the plasma in the end chamber with a third diagnostic. Although spectroscopy is reliable, it does not have the ability to measure specific points in the plasma as the Langmuir probe does. The use of laser interferometry and magnetic field probes would both help reinforce or refute Langmuir probe measurements and make further judgments about the plasma that Langmuir probes and spectroscopy cannot educate.

BIBLIOGRAPHY

[1] A. Ando, T. K. Watanabe, T. Makita, H. Tobari, K. Hattori, and M. Inutake. Mach probe measurements in unmagnetized plasmas with subsonicand supersonic flow. *Contributions to Plasma Physics*, 46(5-6):335–340, 2006.

[2] R. L. Burton, S. G. Delmedico, and J. C. Andrews. Application of a quadruple probe technique to mpd thruster plume measurements. *Journal of Propulsion and Power*, 9(5):771–777, 1993.

[3] R. Chapman, G. H. Miley, W. Kernbichler, and M. Heindler. Fusion space propulsion with a field reversed configuration. *Fusion Technology*, 15(2P2B):1154–1159, 1989.

[4] S.-L. Chen. Studies of the effect of ion current on instantaneous triple-probe measurements. *Journal of Applied Physics*, 42(1):406–412, 1971.

[5] S.-L. Chen and T. Sekiguchi. Instantaneous Direct-Display System of Plasma Parameters by Means of Triple Probe. *Journal of Applied Physics*, 36:2363–2375, August 1965.

[6] Y. Choi, H. Woo, K. Chung, M. Lee, D. Zimmerman, and R. McWilliams. Determination of Plasma Flow Velocity by Mach Probe and Triple Probe with Correction by Laser-Induced Fluorescence in Unmagnetized Plasmas. *Japanese Journal of Applied Physics*, 45:5945, July 2006.

[7] V. I. Demidov, S. V. Ratynskaia, and K. Rypdal. Electric probes for plasmas: The link between theory and instrument. *Review of Scientific Instruments*, 73(10):3409–3439, 2002.

[8] R. Eckman, L. Byrne, N. A. Gatsonis, and E. J. Pencil. Triple langmuir probe measurements in the plume of a pulsed plasma thruster. *Journal of Propulsion and Power*, 17(4):762–771, 2001.

[9] R. F. Eckman. Langmuir Probe Measurements in the Plume of a Pulsed Plasma Thruster. Master's thesis, February 1999.

[10] U. Fantz. Basics of plasma spectroscopy. *Plasma Source Science and Technology*, 15(4):1299–1304, 2006.

[11] R. J. Groebner, N. H. Brooks, K. H. Burrell, and L. Rottler. Measurements of plasma ion temperature and rotation velocity using the He-II 4686-A line produced by charge transfer. *Applied Physics Letters*, 43(10):920–922, 1983.

[12] M. Hudis and L. M. Lidsky. Directional langmuir probe. *Journal of Applied Physics*, 41(12):5011–5017, 1970.

[13] I. H. Hutchinson. A fluid theory of ion collection by probes in strong magnetic fields with plasma flow. *The Physics of Fluids*, 30(12):3777–3781, 1987.

[14] I. H. Hutchinson. The invalidity of a mach probe model. *Physics of Plasmas*, 9(5):1832–1833, 2002.

[15] I H Hutchinson. Ion collection by a sphere in a flowing plasma: I. quasineutral. *Plasma Physics and Controlled Fusion*, 44(9):1953–1977, aug 2002.

[16] I. H. Hutchinson. *Principles of Plasma Diagnostics*. Cambridge University Press, 2 edition, 2005.

[17] H. Katayama, K. Sato, and F. Miyawaki. Direct Energy Conversion for D-3He Reactor. *Fusion Technology*, 27(3T):563–566, 1995.

[18] J. Khachan and S. Collis. Measurements of ion energy distributions by Doppler shift spectroscopy in an inertial-electrostatic confinement device. *Physics of Plasmas*, 8(4):1299–1304, 2001.

[19] S. H. Maslen. Fusion for space propulsion. *IRE Transactions on Military Electronics*, MIL-3(2):52–57, April 1959.

[20] G. F. Matthews. Tokamak plasma diagnosis by electrical probes. *Plasma Physics and Controlled Fusion*, 36(10):1595–1628, oct 1994.

[21] R. L. Merlino. Understanding Langmuir probe current-voltage characteristics. *American Journal of Physics*, 75(12):1078–1085, 2007.

[22] B. J. Peterson, J. N. Talmadge, D. T. Anderson, F. S. B. Anderson, and J. L. Shohet. Measurement of ion flows using an “unmagnetized” Mach probe in the interchangeable module stellarator. *Review of Scientific Instruments*, 65(8):2599–2606, 1994.

[23] A. Qayyum, N. Ahmad, S. Ahmad, Farah Deeba, Rafaqat Ali, and S. Hussain. Time-resolved measurement of plasma parameters by means of triple probe. *Review of Scientific Instruments*, 84(12):123502, 2013.

[24] C. Riccardi, G. Longoni, G. Chiodini, and M. Fontanesi. Comparison between fast-sweep Langmuir probe and triple probe for fluctuations measurements. *Review of Scientific Instruments*, 72(1):461–464, 2001.

[25] S. Shinohara. Response to “The invalidity of a Mach probe model” [Phys. Plasmas 9, 1832 (2002)]. *Physics of Plasmas*, 9:1834–1834, 05 2002.

[26] U. Shumlak, R. P. Golingo, B. A. Nelson, and D. J. Den Hartog. Evidence of stabilization in the Z-pinch. *Phys. Rev. Lett.*, 87:205005, Oct 2001.

[27] U. Shumlak, R. Lilly, C. Adams, R. Golingo, S. Jackson, S. Knecht, and B. Nelson. Advanced Space Propulsion Based on the Flow-Stabilized Z-Pinch Fusion Concept. *Collection of Technical Papers - AIAA/ASME/SAE/ASEE 42nd Joint Propulsion Conference*, 6, 07 2006.

[28] U. Shumlak, B. A. Nelson, E. L. Claveau, E. G. Forbes, R. P. Golingo, M. C. Hughes, R. J. Oberto, M. P. Ross, and T. R. Weber. Increasing plasma parameters using sheared flow stabilization of a Z-pinch. *Physics of Plasmas*, 24(5), 2 2017.

[29] G. Vogman and U. Shumlak. Deconvolution of Stark broadened spectra for multi-point density measurements in a flow Z-pinch. *The Review of scientific instruments*, 82:103504, 10 2011.

[30] Mark Wade. Encyclopedia Astronautica.

[31] Th. Welzel, Th. Dunger, H. Kupfer, and F. Richter. A time-resolved Langmuir double-probe method for the investigation of pulsed magnetron discharges. *Journal of Applied Physics*, 96(12):6994–7001, 2004.

[32] Y. Zhang, U. Shumlak, B. A. Nelson, R. P. Golingo, T. R. Weber, A. D. Stepanov, E. L. Claveau, E. G. Forbes, Z. T. Draper, J. M. Mitrani, H. S. McLean, K. K. Tummel, D. P. Higginson, and C. M. Cooper. Sustained Neutron Production from a Sheared-Flow Stabilized Z Pinch. *Phys. Rev. Lett.*, 122:135001, Apr 2019.

[33] J. C. Zwahlen. Investigation of a Pulsed Plasma Thruster Plume Using A Quadruple Langmuir Probe Technique. Master's thesis, November 2002.

Appendix A

PHOTOS OF EXPERIMENTAL SETUP

This appendix contains pictures of the experimental setup in the FuZE lab, including the physical location of the diagnostics on the machine and the equipment supporting the diagnostics.

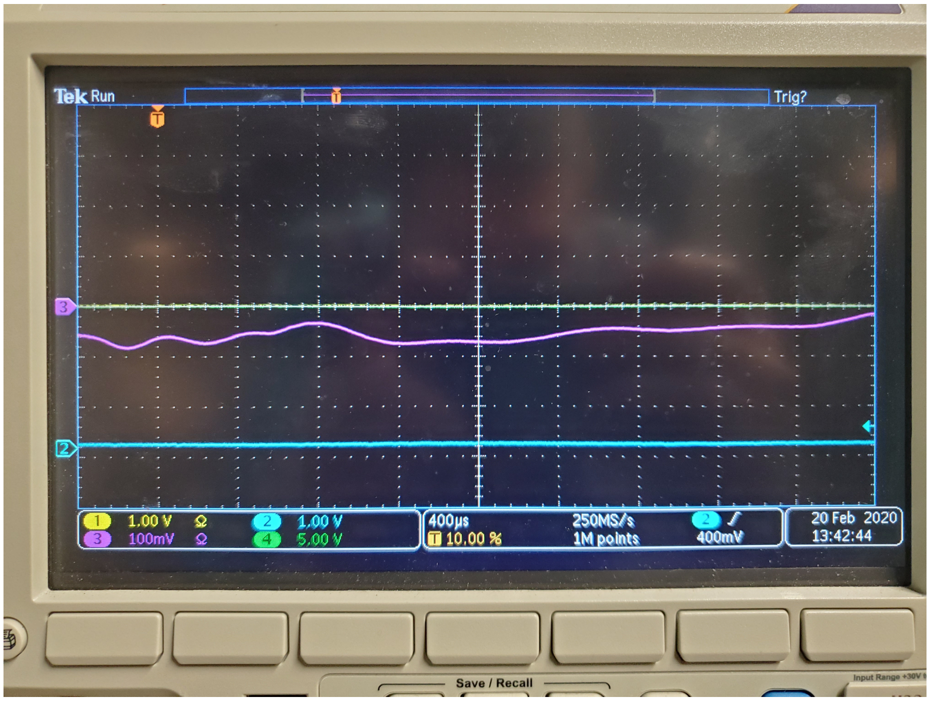

Figure A.1: Long-period background oscillations of about 80 mV in double probe voltage at 50 Ω input impedance due to active electronics. These oscillations are not present when AC power to the probe is turned off. When AC power is turned off, the double probe does not receive a voltage bias, either, as AC power activates relays that need to be on for the DC bias to be connected to the circuit.

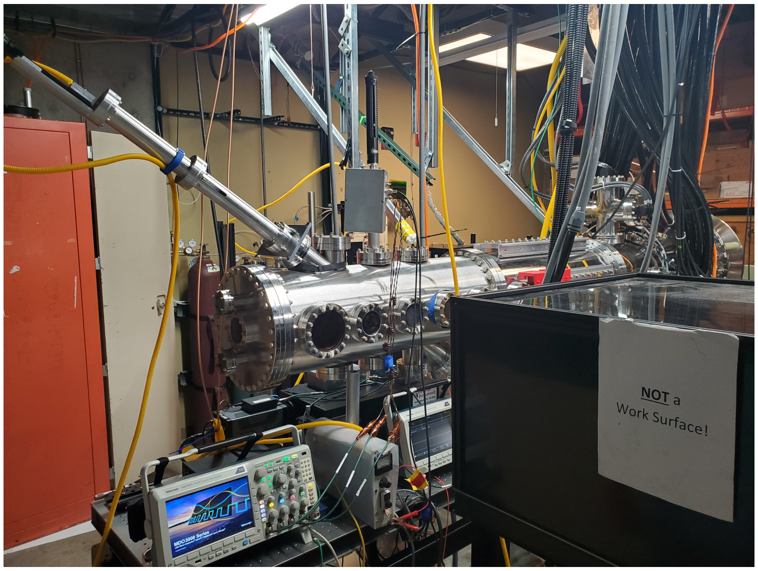

Figure A.2: Right-side view of experimental setup on end chamber of FuZE. The Langmuir probe is positioned vertically on the top of the end chamber, and the spectroscopy telescope is fixed to a 35° port. Oscilloscopes used for data collection are visible on the table beneath the machine, as well as the high voltage power supply for DC bias in the probe.

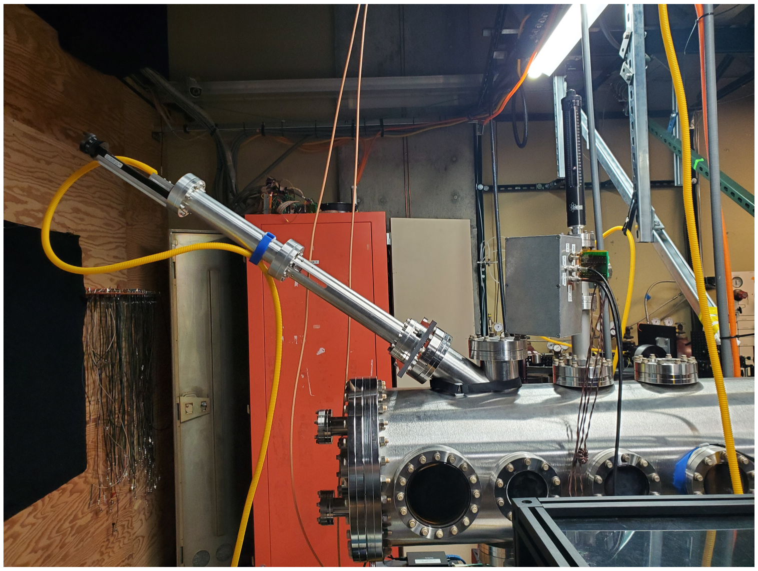

Figure A.3: View of spectroscopy telescope and Langmuir probe from the left side of the machine (looking downstream). Here the yellow plastic-wrapped fiber carrying light from the telescope to the PI spectroscope is clearly visible.

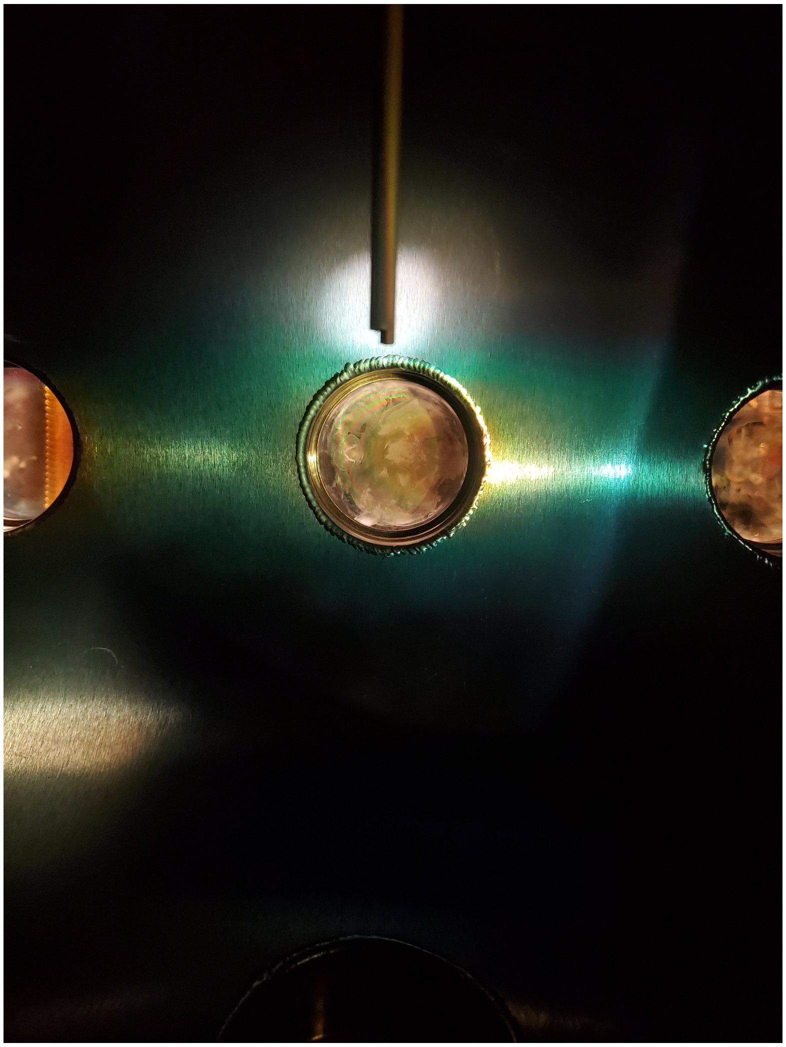

Figure A.4: The Langmuir probe tip can extend into the vacuum chamber as far as R = 32 mm from the centerline of the machine. Here the probe tip is pictured from a window on the right side of the machine (looking downstream). The "step" in the probe tip is the insulator shielding the Mach probe from direct flow.

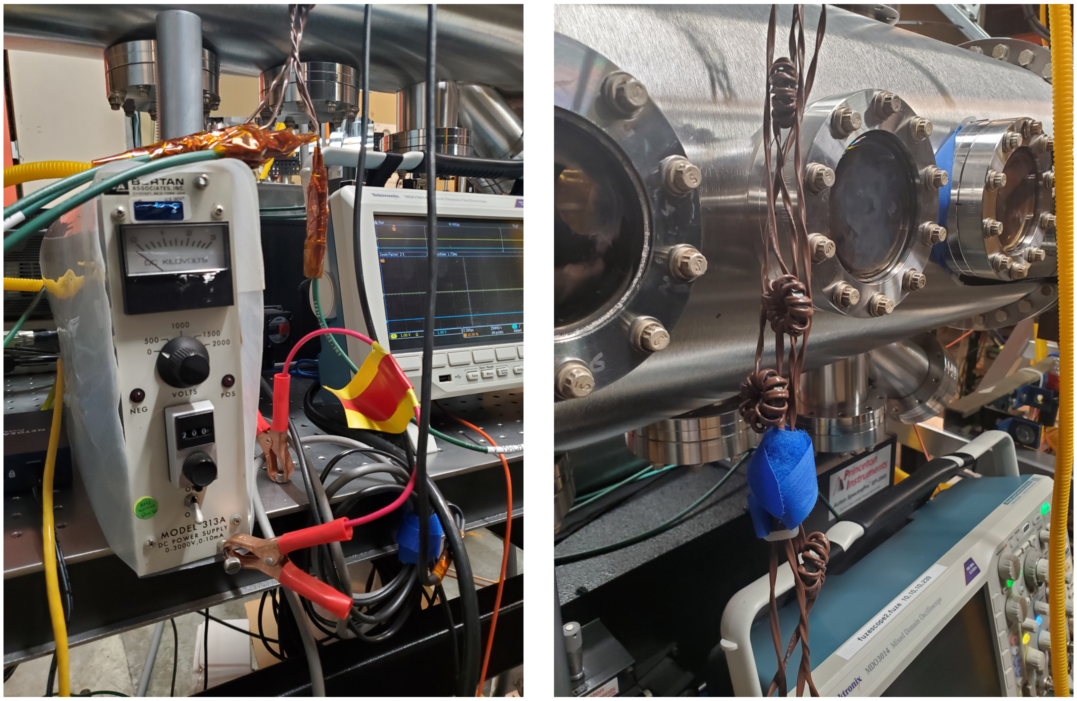

(a) High voltage power supply used to supply DC bias on double probe and Mach probe electrodes. Red and yellow-flagged alligator grounding clips are attached to the power supply whenever the experiment is not running.

(b) Four data cables run from the Langmuir probe to the MDO3014 oscilloscopes, carrying differential measurements of floating voltage, double probe voltage, double probe current, and Mach probe voltage. Cables are a combination of BNC and twisted pair, and are wound around ferrite cores to reduce noise.

Figure A.5: Supporting cabling and power supply for Langmuir probe.

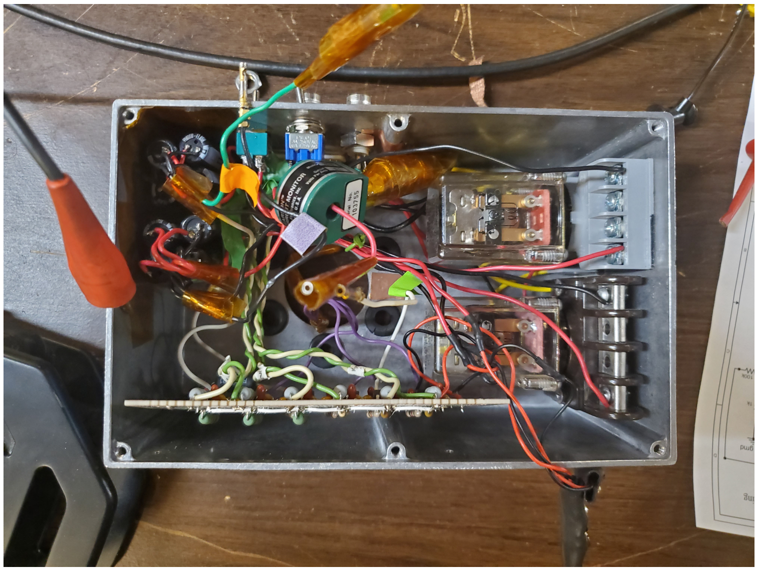

Figure A.6: The inside of the electronics box for the Langmuir probe is messy. Fishing through this box to find the correct cables for probe circuits and to verify the circuit diagram was a challenge.

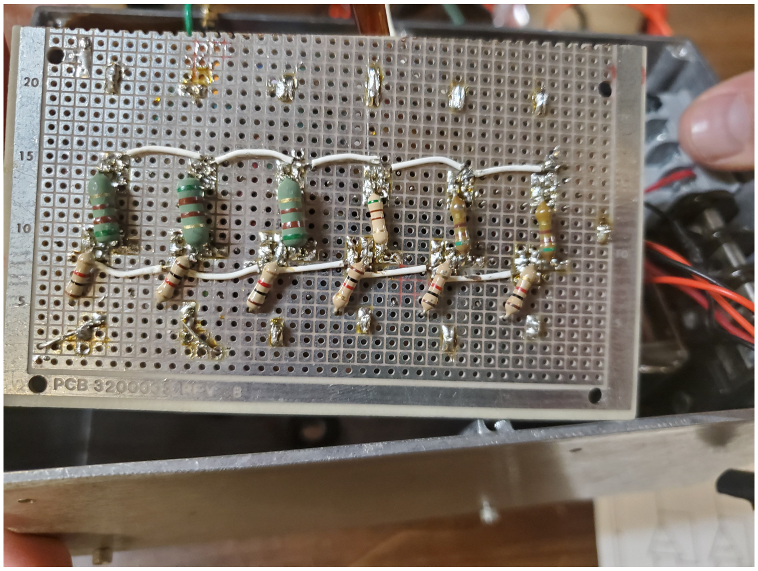

Figure A.7: Rear view of the circuit board in the Langmuir probe electronics box. This board contains much of the resistors and circuitry for the probe as well as the op-amps used as buffers.

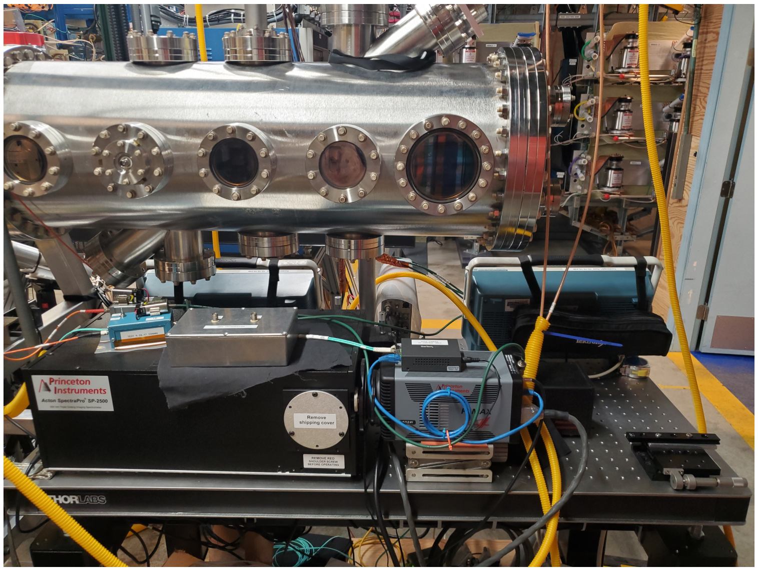

Figure A.8: Princeton Instruments spectrometer setup on bench, including spectrometer and ICCD controller. The spectrometer is the large black box on the left, and the ICCD and camera controller are on the right side behind the blue coil of cabling.

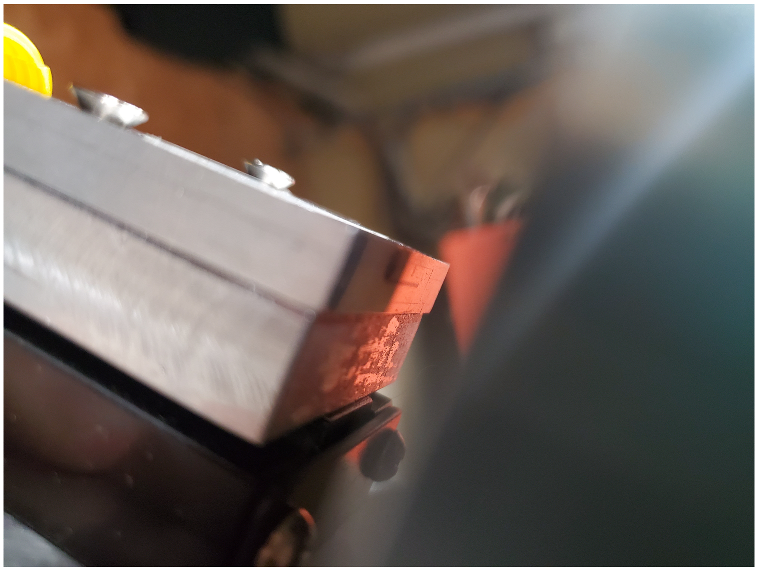

Figure A.9: View of spectroscopy fiber bundle at telescope, showing twenty light chords arranged horizontally.

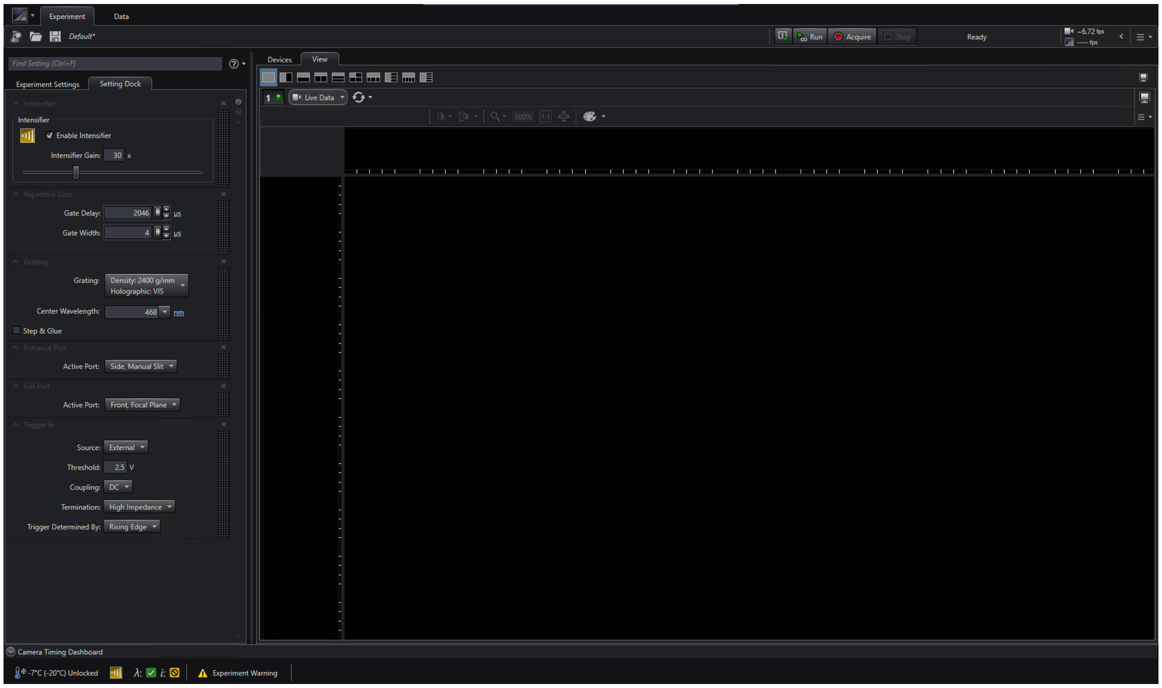

Intensifier

☑ Enable Intensifier

Intensifier Gain: 30 x

Repetitive Gate

Gate Delay: 2046 µs

Gate Width: 4 µs

Grating

Grating: Density: 2400 g/mm Holographic: VIS

Center Wavelength: 468 nm

☐ Step & Glue

Entrance Port

Active Port: Side, Manual Slit

Exit Port

Active Port: Front, Focal Plane

Trigger In

Source: External

Threshold: 2.5 V

Coupling: DC

Termination: High Impedance

Trigger Determined By: Rising Edge

-7°C (-20°C) Unlocked

Figure A.10: GUI interface of Princeton Instruments' *LightField* program, used to define camera parameters for spectroscopy. Important settings controlled here include the diffraction grating, ICCD gate width, ICCD gate delay, intensifier value, and center wavelength.

Appendix B

SUPPLEMENTAL FIGURES TO EXPERIMENTAL RESULTS

Supplemental data plots to the experimental results chapter are shown here. Not all 202 pulses of data are shown in this section, only the data plots helpful for understanding of experimental results but redundant to other data plots in chapter 4.

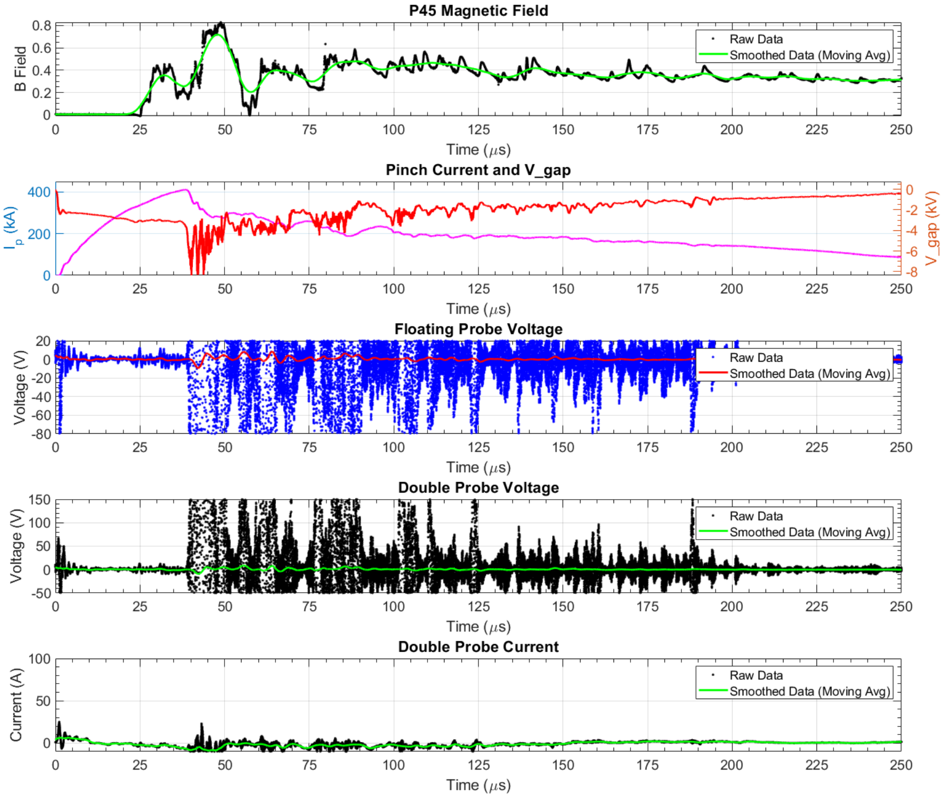

Figure B.1: Shot data obtained using the triple Langmuir probe at the edge of the vacuum chamber, R = 147 mm. Data was taken using the thyristor bank at 5 kV charge with pure hydrogen gas. Noise drowns out any active signals for these first pulses. Changing scope scale and line termination to 50 Ω later helped reduce this.

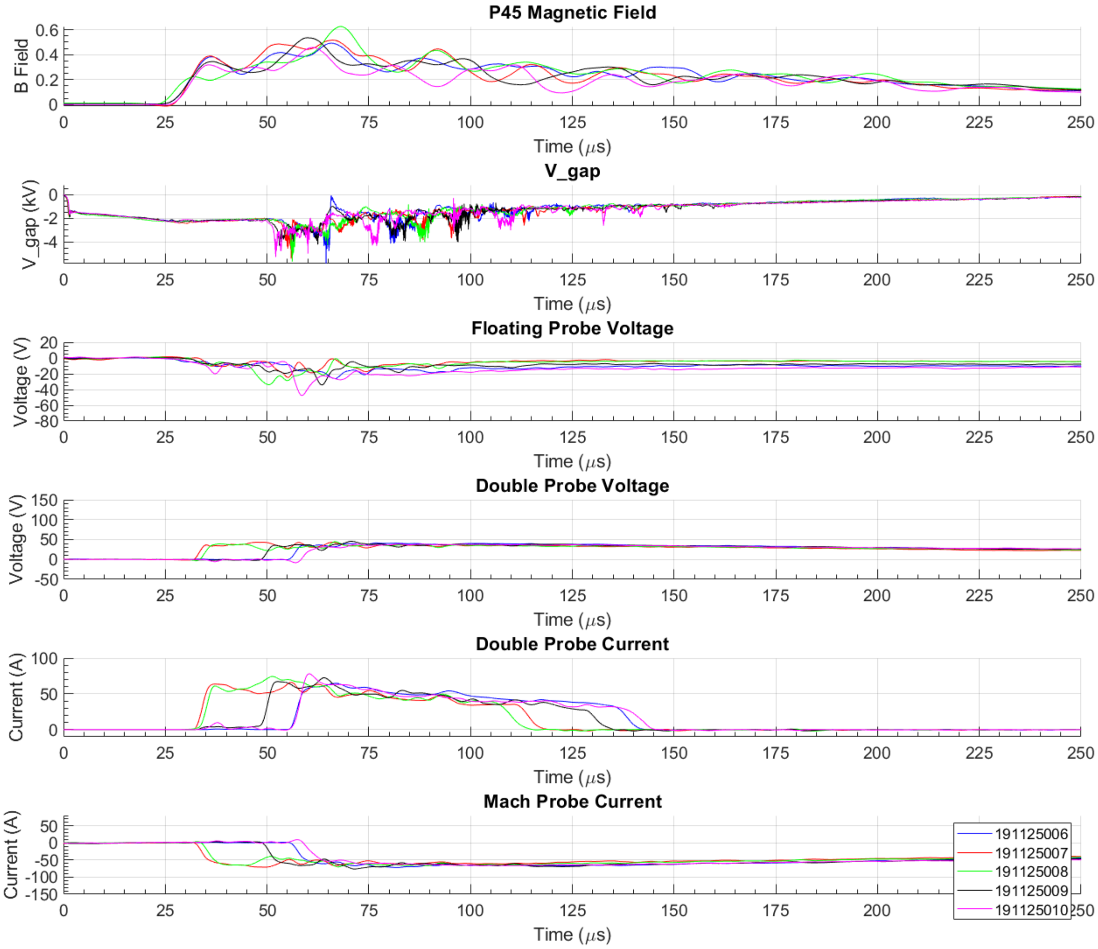

Figure B.2: Quadruple Langmuir probe data for five shots on 25 November 2019, taken with the thyristor bank charging to 3.5 kV, 100% H_2 gas, and the Langmuir probe positioned at R = 65 mm. These shots don't show intermittency in amplitude, but do show a wide range of timings, even though the magnetic field at P45 and the gap voltage don't show this timing intermittency.

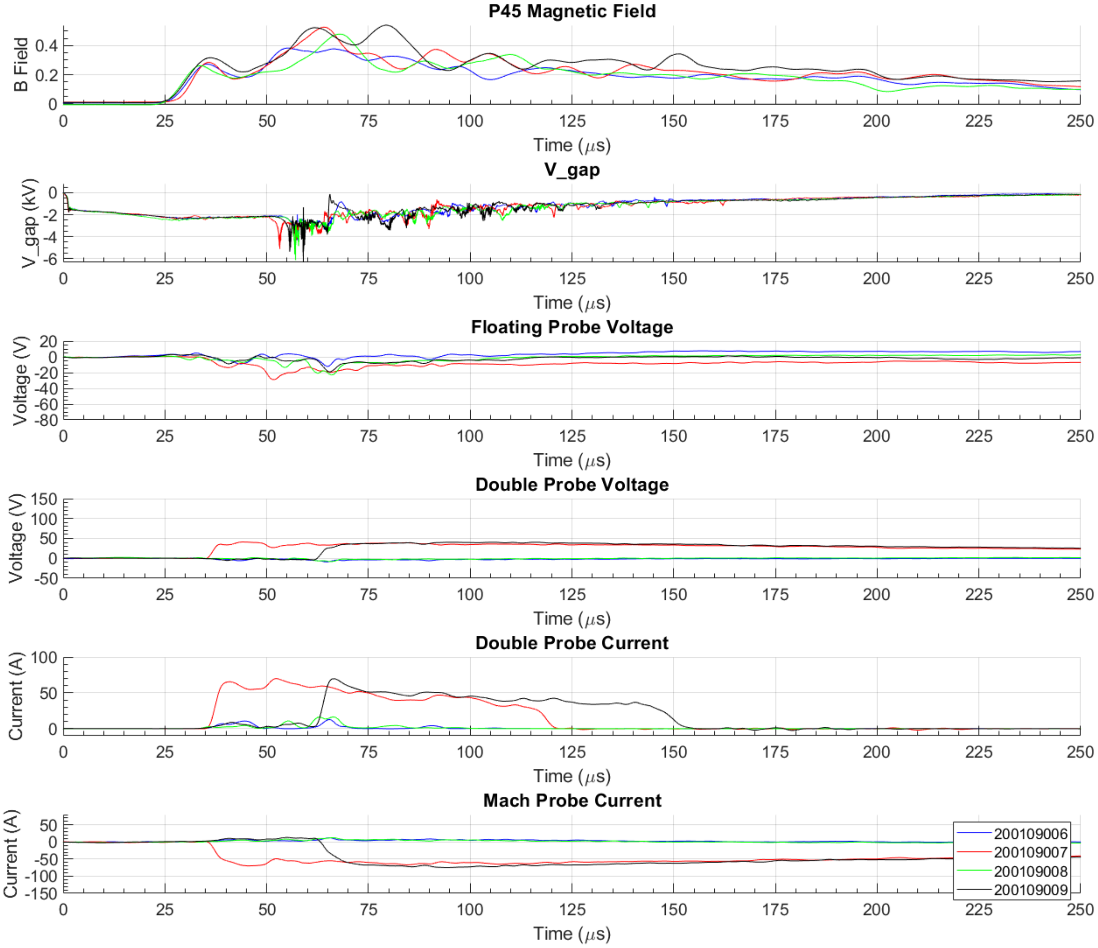

Figure B.3: Quadruple Langmuir probe data for four shots on 9 January 2020, taken with the thyristor bank charging to 3.5 kV, 100% H_2 gas, and the Langmuir probe positioned at R = 65 mm. These shots show intermittency in both timing and amplitude.

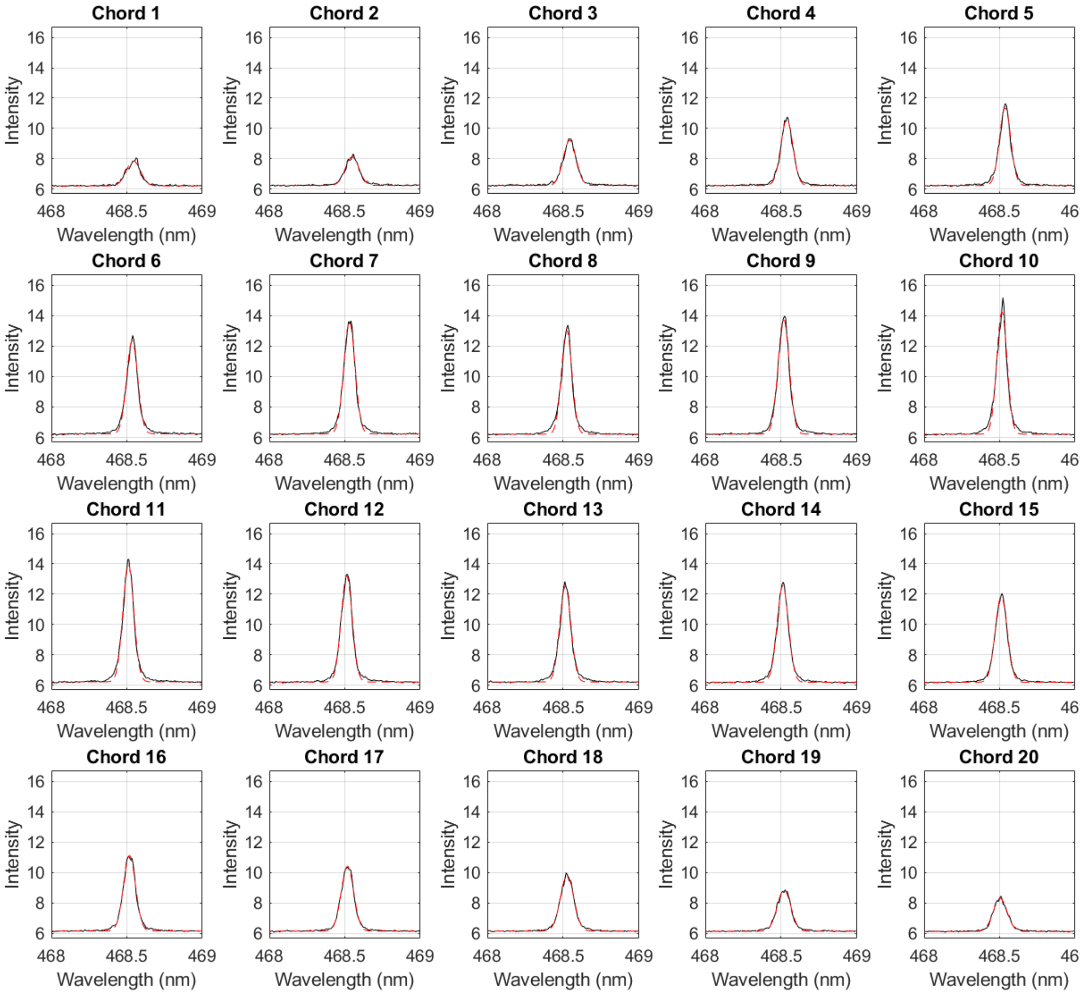

Figure B.4: Calibrated helium spectrum, shot 200114019, with Gaussian fits to data. The Guassian fits are marked in red and the data in black. The double-Gaussian fit to these peaks has two peaks, 0.01 nm apart, to match with the static helium doublet at 468.57 nm and 468.58 nm.

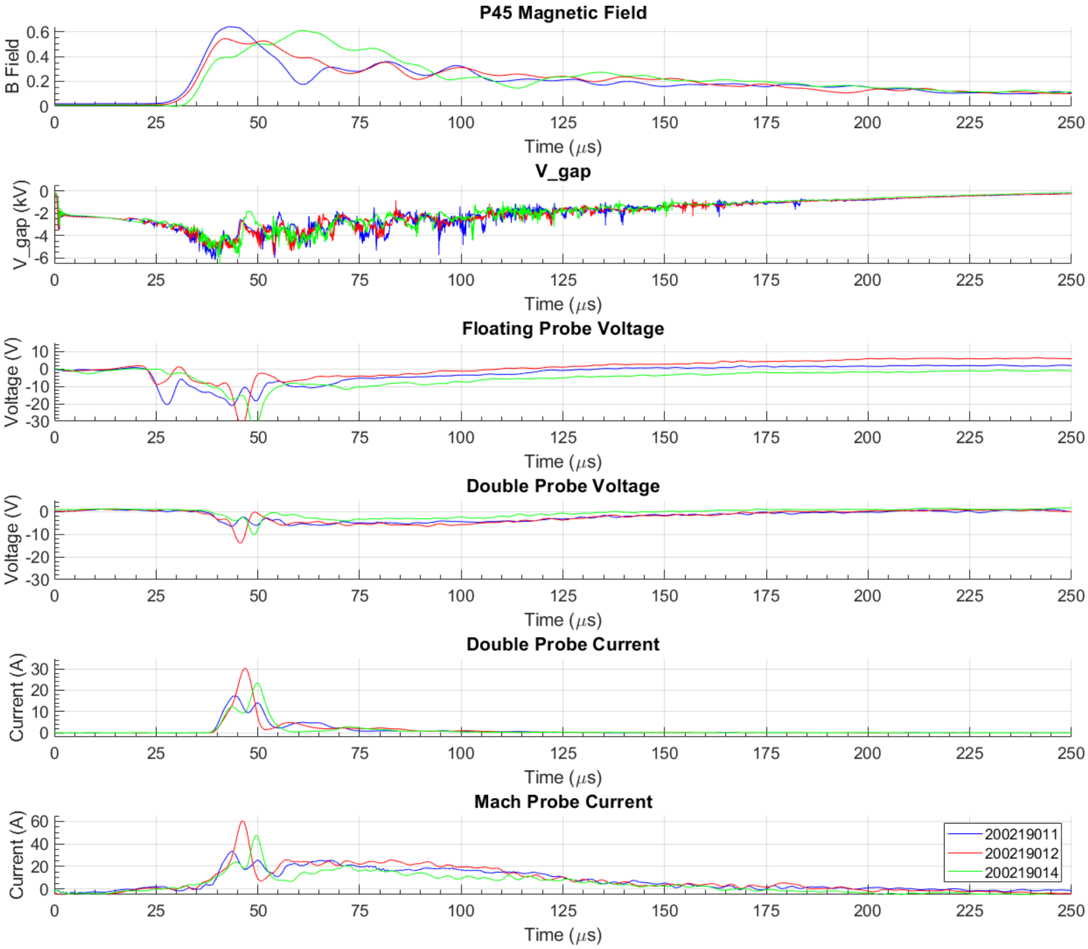

Figure B.5: Quadruple Langmuir probe data with probe positioned at R = 32 mm, for shots on 19 February as part of a radial scan of plasma profile measurements. This position is at the inner edge of the end wall spoke gap. No arcing signals are included in this figure.

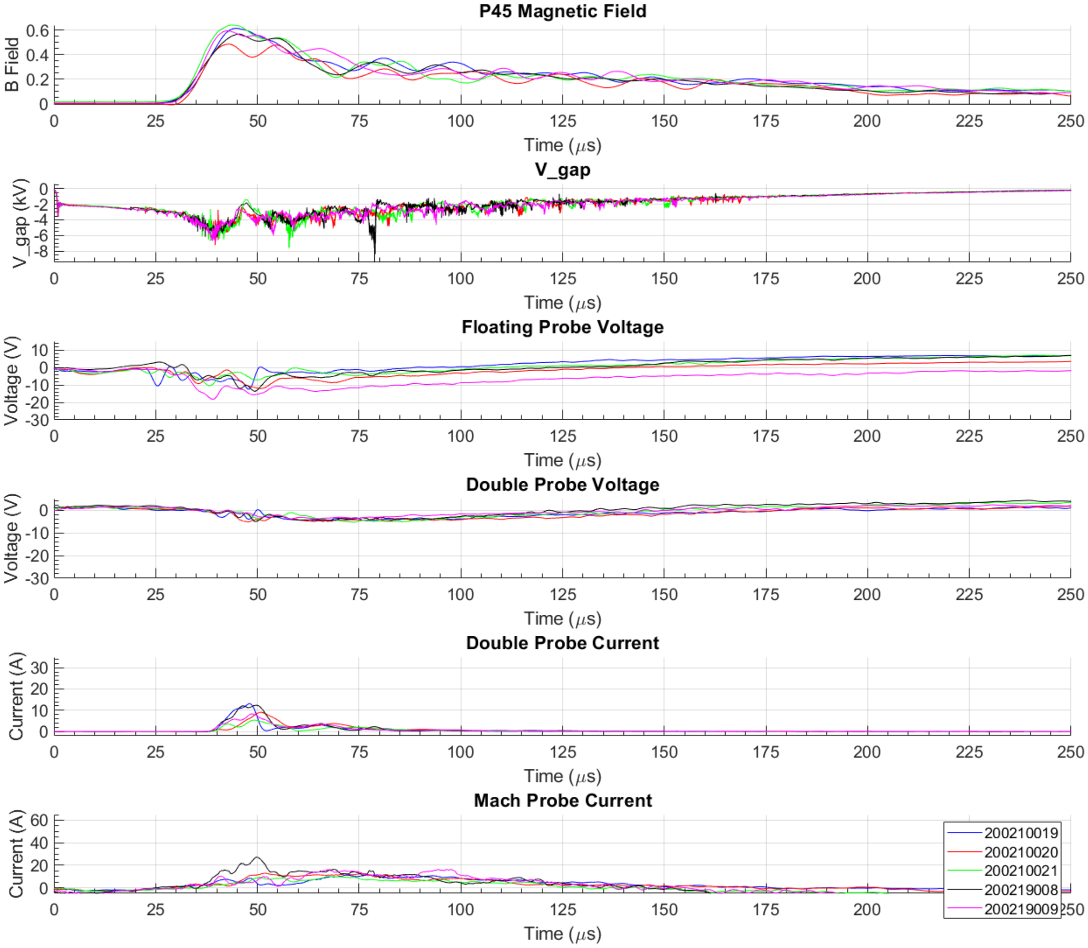

Figure B.6: Quadruple Langmuir probe data with probe positioned at R = 65 mm, for shots on 10 & 19 February as part of a radial scan of plasma profile measurements. This position is in the center of the end wall spoke gap. No arcing signals are included in this figure.

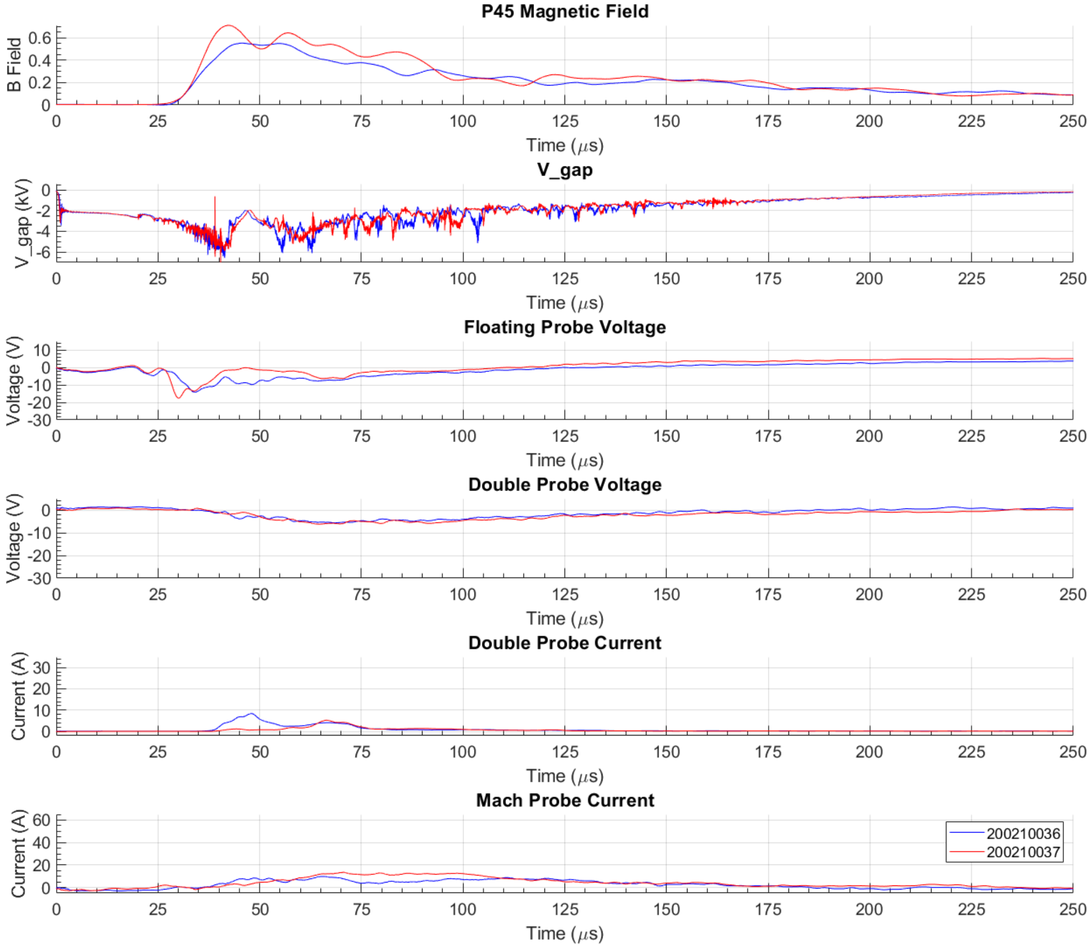

Figure B.7: Quadruple Langmuir probe data with probe positioned at R = 89 mm, for shots on 19 February as part of a radial scan of plasma profile measurements. This position is at the outer edge of the end wall spoke gap. No arcing signals are included in this figure.

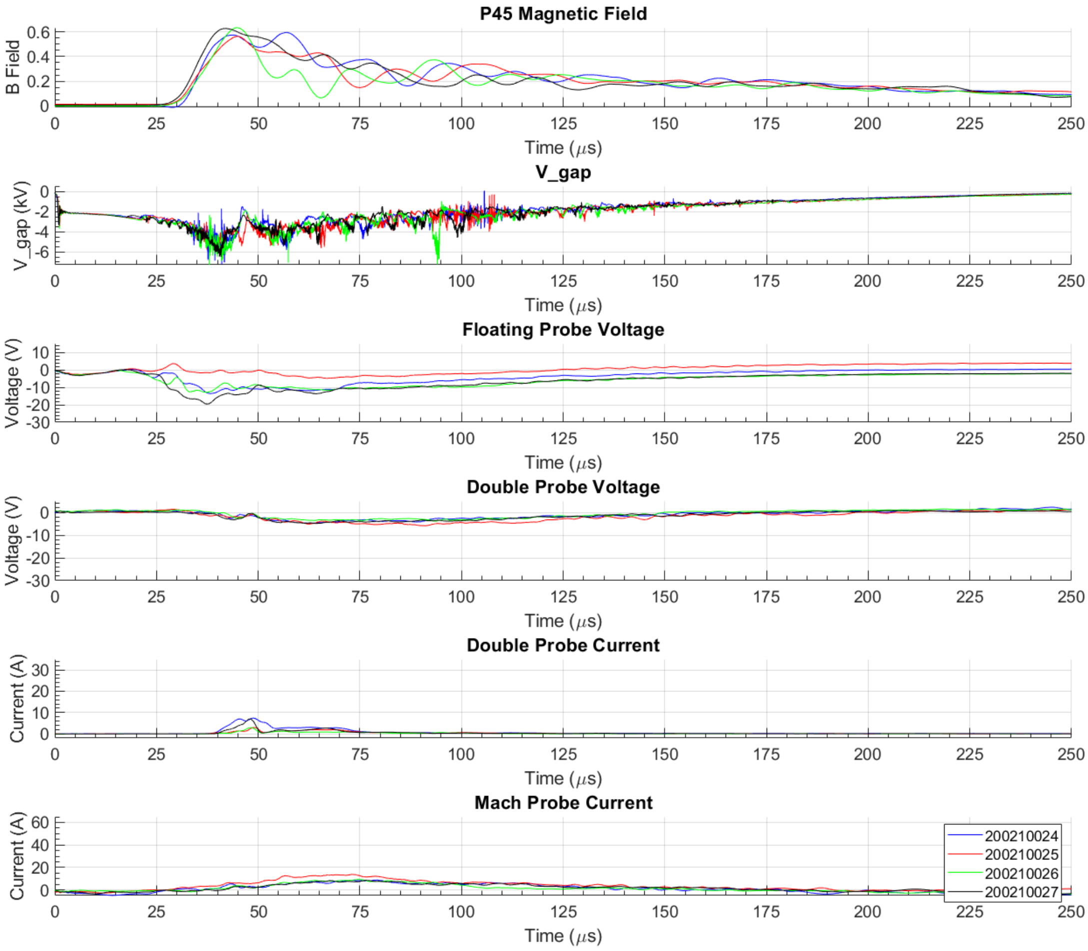

Figure B.8: Quadruple Langmuir probe data with probe positioned at R = 131 mm, for shots on 19 February as part of a radial scan of plasma profile measurements. This position is at the outer edge of the end wall. No arcing signals are included in this figure.

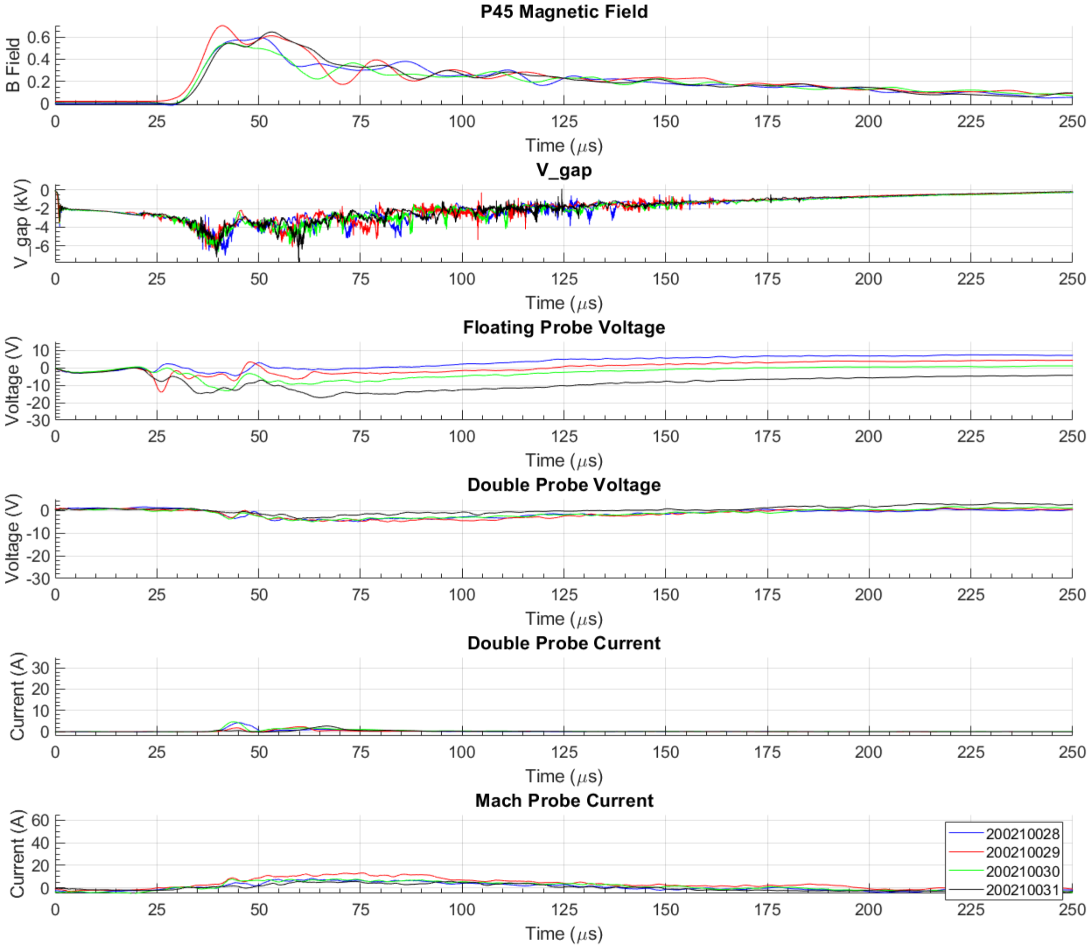

Figure B.9: Quadruple Langmuir probe data with probe positioned at R = 147 mm, for shots on 19 February as part of a radial scan of plasma profile measurements. This position is at the outer edge of the vacuum chamber. No arcing signals are included in this figure.

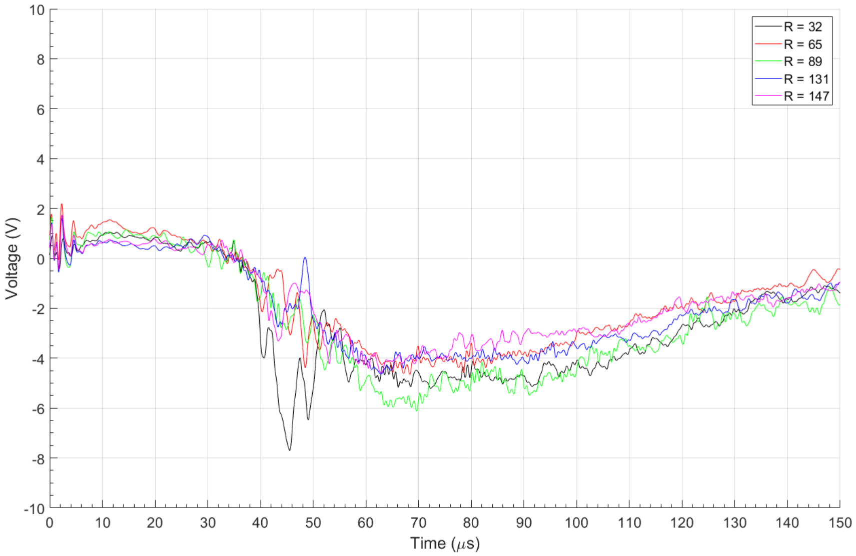

Figure B.10: Radial profile in double probe voltage as measured by the biased double probe tips of the Langmuir probe. This is a direct voltage measurement and has significant EMI noise which has been damped in this figure through triple smoothing.

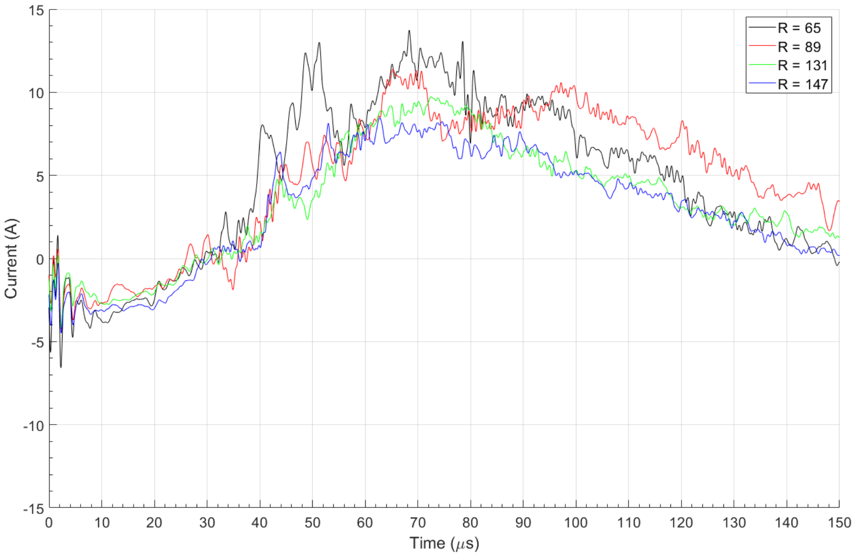

Figure B.11: Radial profile in Mach probe current as measured by taking the Mach probe voltage on the Langmuir probe and diving by a 0.5 Ω resistor. Because it is initially measured from a voltage, it has significant EMI noise like the other voltage measurements, which has been damped in this figure through triple smoothing.

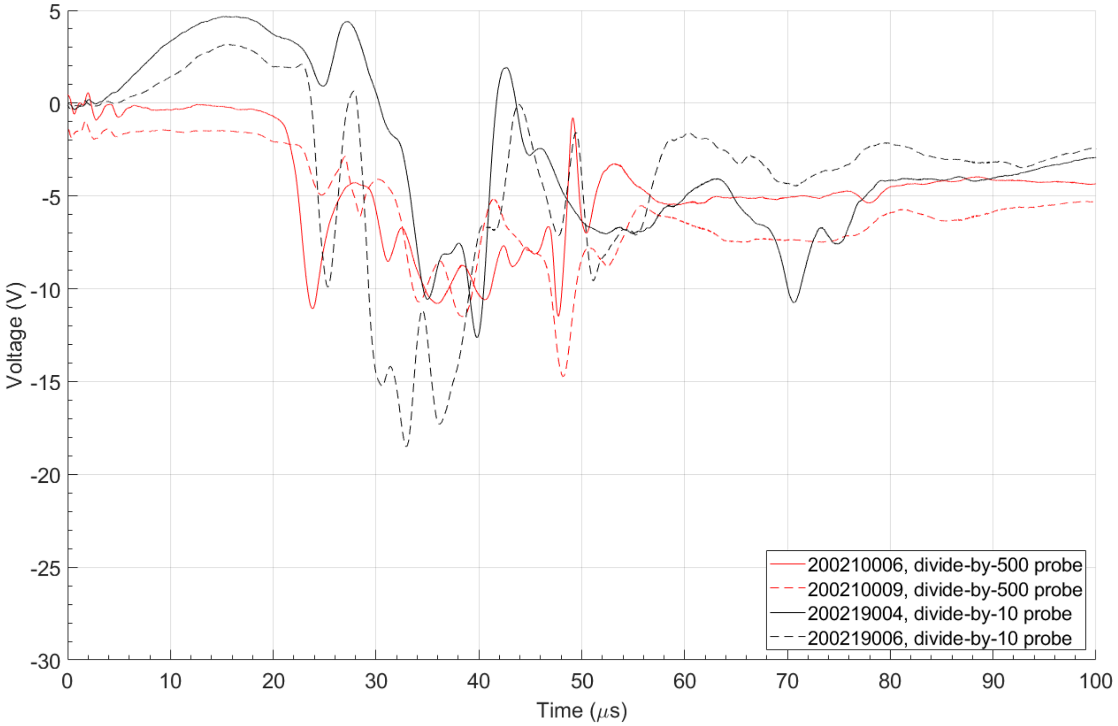

Figure B.12: Floating voltage traces with a divide-by-500 probe with active electronics and a divide-by-10 passive probe. Although there are subtle differences, such as the initial ramp between 0 and 10 μs not present in the probe with active electronics, generally these traces look very similar, showing that the active electronics in the divide-by-500 probe don't make that much of a difference when it comes to floating voltage measurements.

Appendix C

SUPPLEMENTAL FIGURES TO DISCUSSION

Table C.1: Discharge charges as recorded by the Pearson current monitor on the double probe circuit

Shot Number	**Charge Expended on Discharge (Coulombs)**
191125006	0.0035901
191125007	0.0032623
191125008	0.0035679
191125009	0.0034127
191125010	0.0034943
200114007	0.0032367
200114008	0.0034191
200114017	0.0035209
200114022	0.0037108
200114025	0.0035421
200210018	0.0035669
200210032	0.0035894
200210033	0.0037255
200210034	0.0038251
200210035	0.0035527

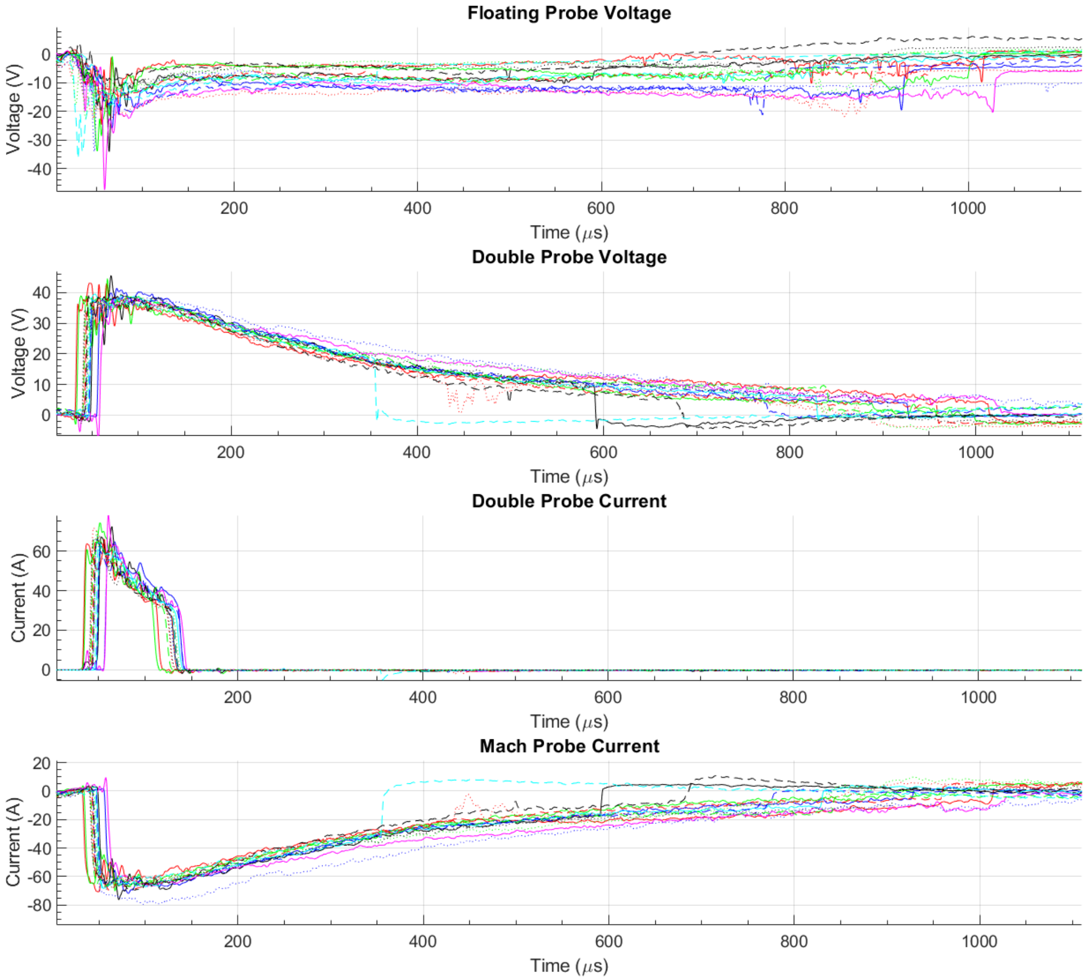

Figure C.1: Long-period decay of discharge traces. Although the double probe current consistently cuts off as the Pearson current monitor reaches its maximum current time product, voltage traces decay and cut off at times varying between 350 μs to the length of the data record at 2300 μs.

Table C.2: Discharge charges as calculated by the current across the 0.5 Ω resistor in the Mach probe circuit

Shot Number	**Charge Expended on Discharge (Coulombs)**
191125006	0.0257
191125007	0.0276
191125008	0.0150
191125009	0.0264
191125010	0.0389
200114007	0.0211
200114008	0.0310
200114017	0.0263
200114022	0.0347
200114025	0.0052
200210018	0.0170
200210032	0.0294
200210033	0.0268
200210034	0.0220
200210035	0.0201

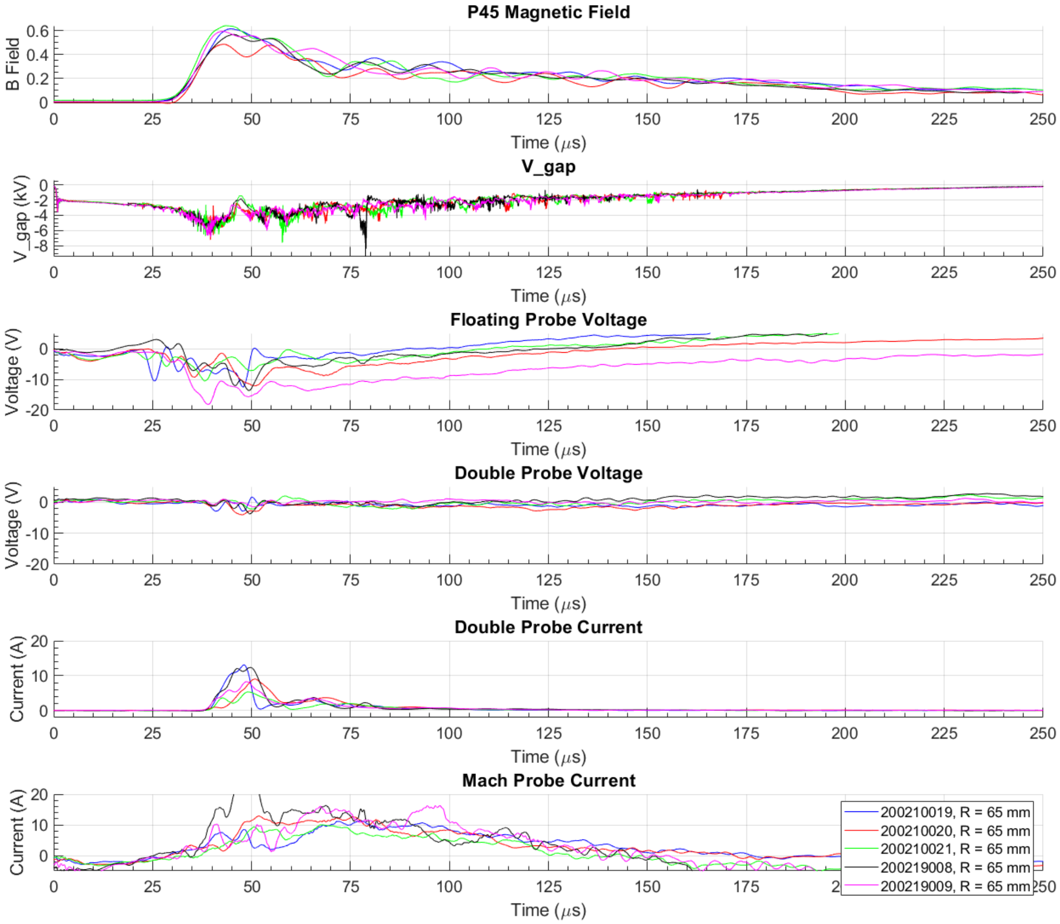

Figure C.2: Overlapping data for shots at R = 65 mm betwen shot numbers 200210019 and 200219009. This data shows that shots 200210019 and 200219008 are outliers, with double probe currents near 13 A whereas the rest of the shots have currents less than 9 A.

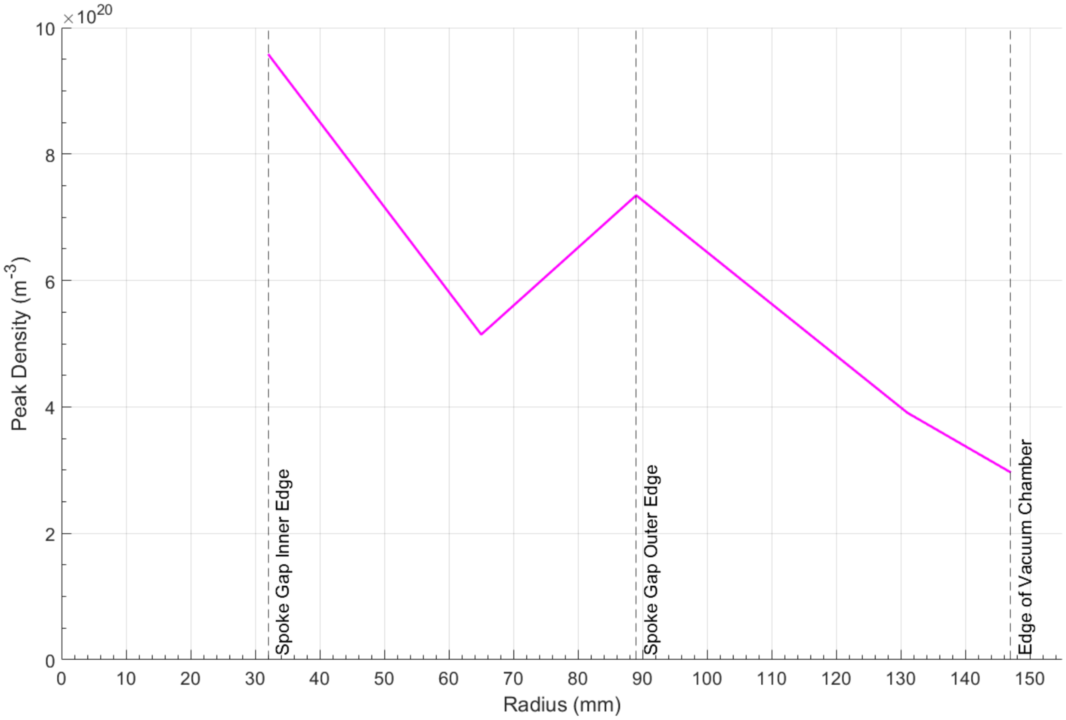

Figure C.3: Radial profile of peak electron density with outliers removed for a pulse at a given Langmuir probe position, ranging from the inner edge of the spoke gap to the outside of the vacuum chamber. Because the high outliers were removed at R = 65 mm, this density profile looks more like a cubic function than a linear function.

Appendix D

MATLAB CODE

This appendix contains some of the primary MATLAB used to calculate plasma parameters. For the sake of brevity, only the code essential to calculations is included here; code for miscellaneous attachments like plotting is left out. This code was written to run on MATLAB version 2018b.

D.1 L_Probe_Local.m: Reading and Filtering Quadruple Probe Data

```
%%%%%%%%%%%%%%%%%%%%%%%%%%%%%%%%%%%%%%%%%%%%%%%%%%%%%%%%%%%%
%
% The script "L_Probe_local" plots the pinch current & gap voltage & the
% magnetic field at P45 for a shot, along with the floating voltage, double
% probe voltage, double probe current for a Langmuir probe inserted into
% FuZE plasma. It also calculates and plots the electron temperature and
% density from data from the Langmuir probe. This uses locally saved data
% rather than mdsplus data directly as "L_probe" does.
%
% Author: Collin Parsons  UW MSAA Student/2020  cjpars@uw.edu
%
% Inputs:
%   savedshotdata.mat - matrix of saved shot data
%
% Outputs (Plots):
%   phi_float   - floating voltage of Langmuir probe
%   v_double    - voltage on Langmuir double probe
%   I_double    - current from Langmuir double probe
%   b_p45       - magnetic field at P45
%   I_p         - pinch current
%   T_e         - electron temperature
%   n_e         - electron number density
%   M           - Mach number
%
% Coupling:
```

```
%   L_probe_data_import.m - retrieves Langmuir probe data of the designated
%                           shots to local memory
%   plasma_T_n.m    - Finds electron density and temperature given data
%                     from langmuir triple probe
%   plasma_Mach_super.m - finds plasma flow velocity from Mach probe
%   L_probe_datasaver.m - saves Langmuir probe data to files. Must be run
%                         for the shots in question at least once before
%                         running this script.
%
% References:
%   None
%
%%%%%%%%%%%%%%%%%%%%%%%%%%%%%%%%%%%%%%%%%%%%%%%%%%%%%%%%%%%%%

clear all
close all

% Close existing wait bars
if exist(’fwait’,’var’)
    delete(fwait)
end
if exist(’nwait’,’var’)
    delete(nwait)
end
if exist(’mwait’,’var’)
    delete(mwait)
end

%% Begin loop structure

% Set shot number
shotnumbers = [200210019,200210020,200210021,200219008,200219009];
        % Radial Profiles:
        % R = 32:  [200219011,200219012,200219014]
        % R = 65:  [200210019,200210020,200210021,200219008,200219009]
        % R = 89:  [200210036,200210037]
        % R = 131: [200210024:200210027]
        % R = 147: [200210028:200210031]
        % Arcing shots:
        % [191125006:191125010,200114007,200114008,200114017,200114022,
        %  200114025,200210018,200210032:200210035]
        % Comparing noise:
```

```
        %[200210013:200210015,200210019:200210021]
        % All shots at R = 65
        %[200114016,200114018:200114021,200114023:200114024,
        % 200114026:200114028,200210019,200210020,200210021,
        % 200219008,200219009]
    % This can be a shot number or a 1-d matrix of shot numbers\
    % Ranges with data:
        %{
        191009001:191009016 First radius profile.
        191015001:191015006 Six shots by Akil, 100% He.
        191018001:191018008     [No valid data]
        191028001:191028004     [No valid data]
        191101001:191101011     [No valid data]
        191104001:191104026     [Ignitron bank, didn't check this data]
        191106001:191106011     [No valid data]
        191108001:191108018     [Ignitron bank, didn't check this data]
        191115001:191115006     [Ignitron bank, no valid data]
        191125001:191125010 Spectroscopy, shots 008-010 have light
        200109001:200109009 Fused silica window installed, 4 shots
        200114005:200114028 100% He shots w/ spectroscopy.
        200210001:200210037 100% He shots w/ spectroscopy. Radial profiles.
                                 First shots w/ direct-to-scope.
        200219001:200219022 100% He shots w/ spectroscopy. Direct-to-scope,
                                 finished radial profile, varied Vd3.
        200225001:200225010 Deuterium, ignitron bank. Pearson probe on Mach
                            probe circuit to test reliability.
        Total shots: 202
        %}
    % Ranges with only triple probe data:
        %{
        190820001:190820015 Data w/ noise. Only value may be for timing.
        190821001:190821012 Data w/ noise. Only value may be for timing.
        190903001:190903022 Data w/ noise. Gas valves at -200 us.
        %}

% Set triple probe only flag if no mach probe data exists for these shots
tripleprobe_only = 0;
if shotnumbers(1) < 190924000
    tripleprobe_only = 1;
end

% Define constants
```

```
m_ion = 6.7e-27; % kg
e0 = 8.85419 * 10^-12;
K = 1.38065 * 10^-23; % J/K
K_eV = 8.617333* 10^-5; % eV/K
e_ele = 1.602 * 10^-19;
m_ele = 9.109 * 10^-31;

% Define plot boundaries
plotset.x_min = 0; % microseconds
plotset.x_max = 250; % microseconds
plotset.x_ticks = 25; % put ticks every {} microseconds
plotset.style = 0; % Style 1 makes windows size for arcing. Style 0 sets the windows to
    known data size. Style 2 sets windows to fit.

% Variable check
if exist('shotnumbers','var')
else
    disp('Error: ''shotnumbers'' variable does not exist.')
    return
end

%% Import data

% Load data
[savedshotdata] = L_probe_local_import(shotnumbers);

% Start wait bar
fwait = waitbar(0,'Importing shots...','Name','L_Probe','CreateCancelBtn','setappdata(gcbf
    ,''canceling'',1)');
setappdata(fwait,'canceling',0);

for ii = 1:max(size(shotnumbers))

% Initialize variables
shotnum = shotnumbers(ii);
fieldname = ['shot_' num2str(shotnum)];

% Import probe values
probe.r(1,ii) = savedshotdata.(fieldname).probe_r; %mm
%probe.r(1,ii) = 147;
probe.dial(1,ii) = savedshotdata.(fieldname).probe_dial; %mm

```

```
% Import P45 magnetic field data
b_p45.raw(:,ii) = savedshotdata.(fieldname).b_p45;
b_p45.time(:,ii) = savedshotdata.(fieldname).b_p45_time;

% Import gap voltage data
v_gap.raw(:,ii) = savedshotdata.(fieldname).v_gap;
v_gap.time(:,ii) = savedshotdata.(fieldname).v_gap_time;

% Import pinch current data (circuit current)
I_p.raw(:,ii) = savedshotdata.(fieldname).I_p;
I_p.time(:,ii) = savedshotdata.(fieldname).I_p_time;

% Import floating voltage data
phi_float.raw(:,ii) = savedshotdata.(fieldname).phi_float;
phi_float.time(:,ii) = savedshotdata.(fieldname).phi_float_time;

% Import double probe voltage data
v_double.raw(:,ii) = savedshotdata.(fieldname).v_double;
v_double.time(:,ii) = savedshotdata.(fieldname).v_double_time;

% Import double probe current data
I_double.raw(:,ii) = savedshotdata.(fieldname).I_double;
I_double.time(:,ii) = savedshotdata.(fieldname).I_double_time;

% Import Mach probe current data
if tripleprobe_only == 0
    I_Mach.raw(:,ii) = -1*savedshotdata.(fieldname).I_Mach;
    I_Mach.time(:,ii) = savedshotdata.(fieldname).I_Mach_time;
end

% Set bias voltage
if shotnum == 200219015 || shotnum == 200219016 || shotnum == 200219017 || shotnum ==
    200219018
    Vd3_setting(ii) = 100; %V, bias voltage on double probe
elseif shotnum == 200219019 || shotnum == 200219020 || shotnum == 200219021 || shotnum ==
    200219022
    Vd3_setting(ii) = 300; %V, bias voltage on double probe
else
    Vd3_setting(ii) = 200; %V, bias voltage on double probe
end

% Update wait bar
```

```
waitbar(ii/max(size(shotnumbers)),fwait,'Importing shots...');
if getappdata(fwait,'canceling')
    break
end

end

% Check for clicked Cancel button
if getappdata(fwait,'canceling')
    delete(fwait)
    disp('Operation cancelled early.')
    return
end

delete(fwait)

%% Subtract noise and correct for background oscillations

% Subtract noise from floating voltage data
load('phi_float_5kvnoise.mat')
phi_float.avg5kvnoise = avgnoise;
clear avgnoise
for ii = 1:max(size(shotnumbers))
    phi_float.corr(:,ii) = phi_float.raw(:,ii) - phi_float.avg5kvnoise;
end

% Subtract background oscillation from double probe voltage data
for ii = 1:max(size(shotnumbers))
    % Find average just before gas valves fire (-350 to -330 us)
    [~,indexm350] = min(abs(v_double.time(:,1)+350e-6));
    [~,indexm330] = min(abs(v_double.time(:,1)+330e-6));
    v_double.bcgpre(ii) = mean(v_double.raw(indexm350:indexm330,ii));
    % Find average just at end of data record (2200 to 2250 us)
    [~,indexp2200] = min(abs(v_double.time(:,1)-2200e-6));
    [~,indexp2250] = min(abs(v_double.time(:,1)-2250e-6));
    v_double.bcgpost(ii) = mean(v_double.raw(indexp2200:indexp2250,ii));
    % Find values at time zero
    [~,indexm30] = min(abs(v_double.time(:,1)+30e-6)); %Index at -30 us
    [~,indexm10] = min(abs(v_double.time(:,1)+10e-6)); %Index at -10 us
    v_double.bcgzero(ii) = mean(v_double.raw(indexm30:indexm10,ii));
    % Interpolate linear function between these points
    v_double.bcg_m(ii) = (v_double.bcgpost(ii)-v_double.bcgpre(ii))/(2530e-6);
```

```
    v_double.bcg_b(ii) = -v_double.bcgzero(ii);
    v_double.bcg_line(:,ii) = v_double.bcg_m(ii)*v_double.time(:,ii)+v_double.bcg_b(ii);
    % Correct values with linear interpolation
    v_double.corr(:,ii) = v_double.raw(:,ii) + v_double.bcg_line(:,ii); % Subtract line values
    v_double.corr(:,ii) = v_double.raw(:,ii) + v_double.bcg_b(ii); % Just subtract the values to make them all zero at zero

    % Load in background noise
    load('v_double_bcgnoise.mat');
    v_double.corr(:,ii) = v_double.corr(:,ii) - v_double_bcgnoise;

    clear indexm350 indexm330 indexp2200 indexp2250 indexm30 indexm10
end

if tripleprobe_only == 0
for ii = 1:max(size(shotnumbers))
    % Find average just before gas valves fire (-350 to -330 us)
    [~,indexm350] = min(abs(I_Mach.time(:,1)+350e-6));
    [~,indexm330] = min(abs(I_Mach.time(:,1)+330e-6));
    I_Mach.bcgpre(ii) = mean(I_Mach.raw(indexm350:indexm330,ii));
    % Find average just at end of data record (2200 to 2250 us)
    [~,indexp2200] = min(abs(I_Mach.time(:,1)-2200e-6));
    [~,indexp2250] = min(abs(I_Mach.time(:,1)-2250e-6));
    I_Mach.bcgpost(ii) = mean(I_Mach.raw(indexp2200:indexp2250,ii));
    % Find values at time zero
    [~,indexm30] = min(abs(I_Mach.time(:,1)+30e-6)); %Index at -30 us
    [~,indexm10] = min(abs(I_Mach.time(:,1)+10e-6)); %Index at -10 us
    I_Mach.bcgzero(ii) = mean(I_Mach.raw(indexm30:indexm10,ii));
    % Interpolate linear function between these points
    I_Mach.bcg_m(ii) = (I_Mach.bcgpost(ii)-I_Mach.bcgpre(ii))/(2530e-6);
    I_Mach.bcg_b(ii) = -I_Mach.bcgzero(ii);
    I_Mach.bcg_line(:,ii) = I_Mach.bcg_m(ii)*I_Mach.time(:,ii)+I_Mach.bcg_b(ii);
    % Correct values with linear interpolation
    I_Mach.corr(:,ii) = I_Mach.raw(:,ii) + I_Mach.bcg_line(:,ii); % Subtract line values
    I_Mach.corr(:,ii) = I_Mach.raw(:,ii) + I_Mach.bcg_b(ii); % Just subtract the values to make them all zero at zero

    clear indexm350 indexm330 indexp2200 indexp2250 indexm30 indexm10
end
end

```

```matlab
% Choose to use raw or corrected values
usecorr = 1; %1 if corrected, 0 if raw
    if usecorr == 1
       phi_float.raw = phi_float.raw; % Use the raw value for floating voltage
       v_double.raw = v_double.corr; % Use the double probe voltage from which background noise has been subtracted
       if tripleprobe_only == 0
            I_Mach.raw = I_Mach.corr; % Use the Mach probe current corrected to read zero at time zero
       end
    end

%% Filter data

% Start wait bar
nwait = waitbar(0,'Filtering Data...','Name','L_Probe','CreateCancelBtn','setappdata(gcbf,''canceling'',1)');
setappdata(nwait,'canceling',0);

for nn = 1:max(size(shotnumbers))

    % Smooth P45 magnetic field data twice
    b_p45.smooth1(:,nn) = smoothdata(b_p45.raw(:,nn),'movmean',213);
    b_p45.smooth2(:,nn) = smoothdata(b_p45.smooth1(:,nn),'movmean',359);

    % Smooth pinch current data twice
    I_p.smooth1(:,nn) = smoothdata(I_p.raw(:,nn),'movmean',113);
    I_p.smooth2(:,nn) = smoothdata(I_p.smooth1(:,nn),'movmean',151);

    % Smooth gap voltage data twice
    v_gap.smooth1(:,nn) = smoothdata(v_gap.raw(:,nn),'movmean',61);
    v_gap.smooth2(:,nn) = smoothdata(v_gap.smooth1(:,nn),'movmean',113);

    % Smooth floating voltage data twice
    phi_float.smooth1(:,nn) = smoothdata(phi_float.raw(:,nn),'movmean',359);
    phi_float.smooth2(:,nn) = smoothdata(phi_float.smooth1(:,nn),'movmean',619);

    % Smooth double probe data twice
    v_double.smooth1(:,nn) = smoothdata(v_double.raw(:,nn),'movmean',359);
    v_double.smooth2(:,nn) = smoothdata(v_double.smooth1(:,nn),'movmean',619);
    I_double.smooth1(:,nn) = smoothdata(I_double.raw(:,nn),'movmean',359);
    I_double.smooth2(:,nn) = smoothdata(I_double.smooth1(:,nn),'movmean',619);
```

```

    % Smooth Mach probe data twice
    if tripleprobe_only == 0
        I_Mach.smooth1(:,nn) = smoothdata(I_Mach.raw(:,nn),'movmean',359);
        I_Mach.smooth2(:,nn) = smoothdata(I_Mach.smooth1(:,nn),'movmean',619);
    end

    % Update wait bar
    waitbar(nn/max(size(shotnumbers)),nwait,'Filtering Data...');
    if getappdata(nwait,'canceling')
        break
    end

end

% Check for clicked Cancel button
if getappdata(nwait,'canceling')
    delete(nwait)
    disp('Operation cancelled early.')
    return
end

delete(nwait)

%% Calculate temperature and density

% Start wait bar
mwait = waitbar(0,'Calculating Temperature and Density...','Name','L_Probe','
    CreateCancelBtn','setappdata(gcbf,''canceling'',1)');
setappdata(mwait,'canceling',0);

% Find maximum value for Vd2 difference voltage and populate array
Vd2.max_array = zeros(size(v_double.time));
Vd2.diff10_array = zeros(size(v_double.time));
for ii = 1:max(size(shotnumbers))
    [Vd2.max_array(:,ii),Vd2.diff10_array(:,ii)] = Te_regime(Vd3_setting(ii));
end

for mm = 1:max(size(shotnumbers))

    % Initialize temperature and density and velocity arrays for shot
    shot.Te_numer = zeros(size(v_double.time(:,mm),1),1);
```

```
shot.Te_linear = zeros(size(v_double.time(:,mm),1),1);
shot.n_e_corr = zeros(size(v_double.time(:,mm),1),1);
shot.numerical_flag = zeros(size(v_double.time(:,mm),1),1); % this array tells us which values of T_e and n_e are numerically convergent
shot.n_e = zeros(size(v_double.time(:,mm),1),1);
shot.M_i = zeros(size(I_double.time(:,mm),1),1);
shot.v_flow = zeros(size(I_double.time(:,mm),1),1);

% Calculate Vd2 difference voltage for shot
shot.Vd2 = v_double.smooth2(:,mm) - phi_float.smooth2(:,mm);

% Calculate temperature and density for each time point
for k = 1:size(v_double.time(:,mm),1)
    [shot.Te_numer(k),shot.Te_linear(k),shot.numerical_flag(k),shot.n_e(k)] = plasma_T_n(shot.Vd2(k),Vd3_setting(mm),I_double.smooth2(k,mm),m_ion,Vd2.max_array(1));
end

% Calculate flow velocity for each time point
if tripleprobe_only == 0
    for jj = 1:size(I_Mach.time(:,mm),1)
        [shot.M_i(jj),shot.v_flow(jj),shot.v_sound(jj)] = plasma_Mach_super(I_double.smooth2(jj,mm),I_Mach.smooth2(jj,mm),m_ion,shot.Te_numer(jj));
    end
end

% Fill total temperature arrays with shot data
T_e.numer(:,mm) = shot.Te_numer;
T_e.linear(:,mm) = shot.Te_linear;
T_e.numer_flags(:,mm) = shot.numerical_flag;

% Fill density array with shot data
n_e.calc(:,mm) = shot.n_e;

% Fill Vd2 difference voltage array with shot data
Vd2.calc(:,mm) = shot.Vd2;

% Fill velocity arrays with shot data
if tripleprobe_only == 0
    M_i.calc(:,mm) = shot.M_i;
    v_flow.calc(:,mm) = shot.v_flow;
    v_sound.calc(:,mm) = shot.v_sound;
```

```
    end

    % Update wait bar
    waitbar(mm/max(size(shotnumbers)),mwait,'Calculating Temperature and Density...');
    if getappdata(mwait,'canceling')
        break
    end

end

% Check for clicked Cancel button
if getappdata(mwait,'canceling')
    delete(mwait)
    disp('Operation cancelled early.')
    return
end

delete(mwait)

%% Calculate data statistics

% Smooth calculated data twice each
for nn = 1:max(size(shotnumbers))
    T_e.smooth1(:,nn) = smoothdata(T_e.numer(:,nn),'movmean',359);
    T_e.smooth2(:,nn) = smoothdata(T_e.smooth1(:,nn),'movmean',619);
    n_e.smooth1(:,nn) = smoothdata(n_e.calc(:,nn),'movmean',359);
    n_e.smooth2(:,nn) = smoothdata(n_e.smooth1(:,nn),'movmean',619);
    if tripleprobe_only == 0
    M_i.smooth1(:,nn) = smoothdata(M_i.calc(:,nn),'movmean',359);
    M_i.smooth2(:,nn) = smoothdata(M_i.smooth1(:,nn),'movmean',619);
    v_flow.smooth1(:,nn) = smoothdata(v_flow.calc(:,nn),'movmean',359);
    v_flow.smooth2(:,nn) = smoothdata(v_flow.smooth1(:,nn),'movmean',619);
    end
end

% Find data averages
phi_float.avg = mean(phi_float.raw,2);
v_double.avg = mean(v_double.raw,2);
I_double.avg = mean(I_double.raw,2);
if tripleprobe_only == 0
    I_Mach.avg = mean(I_Mach.raw,2);
end
```

```
T_e.numer_avg = mean(T_e.numer,2);
T_e.linear_avg = mean(T_e.linear,2);
n_e.avg = mean(n_e.calc,2);
n_e.smooth2avg = mean(n_e.smooth2,2);
Vd2.avg = mean(Vd2.calc,2);
if tripleprobe_only == 0
    M_i.avg = mean(M_i.calc,2);
    v_flow.avg = mean(v_flow.calc,2);
    v_sound.avg = mean(v_sound.calc,2);
end

% Find data standard deviations
phi_float.stdev = std(phi_float.raw,0,2);
v_double.stdev = std(v_double.raw,0,2);
I_double.stdev = std(I_double.raw,0,2);
T_e.numer_stdev = std(T_e.numer,0,2);
T_e.linear_stdev = std(T_e.linear,0,2);
n_e.stdev = std(n_e.calc,0,2);
n_e.smooth2stdev = std(n_e.smooth2,0,2);
Vd2.stdev = std(Vd2.calc,0,2);
if tripleprobe_only == 0
    M_i.stdev = std(M_i.calc,0,2);
    v_flow.stdev = std(v_flow.calc,0,2);
    v_sound.stdev = std(v_sound.calc,0,2);
end

% Smooth statistical data twice
phi_float.avg_smooth1 = smoothdata(phi_float.avg,'movmean',61);
phi_float.avg_smooth2 = smoothdata(phi_float.avg_smooth1,'movmean',113);
v_double.avg_smooth1 = smoothdata(v_double.avg,'movmean',61);
v_double.avg_smooth2 = smoothdata(v_double.avg_smooth1,'movmean',113);
I_double.avg_smooth1 = smoothdata(I_double.avg,'movmean',61);
I_double.avg_smooth2 = smoothdata(I_double.avg_smooth1,'movmean',113);
if tripleprobe_only == 0
    I_Mach.avg_smooth1 = smoothdata(I_Mach.avg,'movmean',61);
    I_Mach.avg_smooth2 = smoothdata(I_Mach.avg_smooth1,'movmean',113);
end
T_e.avg_smooth1 = smoothdata(T_e.numer_avg,'movmean',61);
T_e.avg_smooth2 = smoothdata(T_e.avg_smooth1,'movmean',113);
n_e.avg_smooth1 = smoothdata(n_e.avg,'movmean',61);
n_e.avg_smooth2 = smoothdata(n_e.avg_smooth1,'movmean',113);
if tripleprobe_only == 0
```

```
    M_i.avg_smooth1 = smoothdata(M_i.avg,'movmean',61);
    M_i.avg_smooth2 = smoothdata(M_i.avg_smooth1,'movmean',113);
    v_flow.avg_smooth1 = smoothdata(v_flow.avg,'movmean',61);
    v_flow.avg_smooth2 = smoothdata(v_flow.avg_smooth1,'movmean',113);
end

% Define upper and lower curves for standard deviations on T_e and n_e
T_e.std_error = T_e.numer_stdev / sqrt(max(size(shotnumbers)));
T_e.stdev_upper = T_e.avg_smooth2+T_e.numer_stdev;
T_e.stdev_lower = T_e.avg_smooth2-T_e.numer_stdev;

n_e.std_error = n_e.smooth2stdev / sqrt(max(shotnumbers));
n_e.stdev_upper = n_e.avg_smooth2+n_e.smooth2stdev;
n_e.stdev_lower = n_e.avg_smooth2-n_e.smooth2stdev;

% Define upper and lower curves for standard deviations on M_i and v_flow
if tripleprobe_only == 0
    M_i.stdev_upper = M_i.avg_smooth2+M_i.stdev;
    M_i.stdev_lower = M_i.avg_smooth2-M_i.stdev;

    v_flow.stdev_upper = v_flow.avg_smooth2+v_flow.stdev;
    v_flow.stdev_lower = v_flow.avg_smooth2-v_flow.stdev;
end


%% Data processing
% Calculate integral of double probe current
for kk = 1:max(size(shotnumbers))
    % Trim data to just the section where double probe current is present
    if max(I_double.smooth2(:,kk)) > 1
        I_double.startwindow(kk) = I_double.time(find(I_double.smooth2(:,kk) > 1,1,'first'
            ));

        startwindowdata = I_double.smooth2(find(I_double.smooth2(:,kk) > 1,1,'first')+250:
            max(size(I_double.smooth2(:,kk))));
            % The 250 forces the endwindow to be at least 1 microsecond after the
                startwindow
        I_double.endwindow(kk) = I_double.time(find(startwindowdata < 1,1,'first')+find(
            I_double.smooth2(:,kk) > 1,1,'first'));
        fullwindowdata = I_double.smooth2(find(I_double.smooth2(:,kk) > 1,1,'first'):find(
            startwindowdata < 1,1,'first')+find(I_double.smooth2(:,kk) > 1,1,'first'));
```

```
        fullwindowtime = I_double.time(find(I_double.smooth2(:,kk) > 1,1,'first'):find(
            startwindowdata < 1,1,'first')+find(I_double.smooth2(:,kk) > 1,1,'first'));
    else
        I_double.startwindow(kk) = NaN;
        I_double.endwindow(kk) = NaN;
        fullwindowtime = I_double.time(:,kk);
        fullwindowdata = I_double.smooth2(:,kk);
    end
    % Calculate integral of double probe current
    I_double.integral(kk) = trapz(fullwindowtime,fullwindowdata);

    clear startwindowdata fullwindowdata fullwindowtime
end

% Calculate integral of Mach probe current
for kk = 1:max(size(shotnumbers))
    I_Mach.integral(kk) = -trapz(I_Mach.time(:,kk),I_Mach.smooth2(:,kk));
end
```

D.2 plasma_T_n.m: Calculating Temperatures and Densities

```matlab
function [T_e_numer,T_e_linear,numerical_flag,n_e] = plasma_T_n(Vd2,Vd3,I_doub,m_ion,maxVd2)
%%%%%%%%%%%%%%%%%%%%%%%%%%%%%%%%%%%%%%%%%%%%%%%%%%%%%%%%%%%%
%
% The script "plasma_T_n" finds the electron temperature and density of a
% given plasma as measured by a triple langmuir probe.
%
% Author: Collin Parsons  UW MSAA Student/2020  cjpars@uw.edu
%
% Inputs:
%   I_doub = current flowing from double probe tip (A)
%   Vd2 = difference between floating voltage and double probe voltage (V)
%   Vd3 = bias voltage on double probe
%   m_ion = ion mass (kg)
%   maxVd2 = maximum value for Vd2 to get numerical convergence
%
% Outputs:
%   T_e = electron temperature (K)
%   numerical_flag = 1 if T_e value is from numerical convergence, 0 if
%       numerical didn’t converge
%   n_e = electron number density (m^-3)
%
% Coupling:
%   None
%
% References:
%  Calculations here are found in:
%   - "Time-resolved measurement of plasma parameters by means of triple
%   probe" by A. Qayyum, et. al.
%   - "Electric probes for plasmas: The link between theory and instrument"
%   by V. I. Demidov, et. al.
%   - "Determination of Plasma Flow Velocity by Mach Probe and Triple
%   Probe" by Y. S. Choi, et. al.
%   - http://golem.fjfi.cvut.cz/wiki/Diagnostics/ParticleFlux/
%       TripleProbe/Campaigns/1012MarcoM/files/TLP%20GOLEM.pdf
%
%%%%%%%%%%%%%%%%%%%%%%%%%%%%%%%%%%%%%%%%%%%%%%%%%%%%%%%%%%%%%

% Calculate linear electron temperature

```

```
    % Define variables
    K = 1.380649 * 10^-23; % J/K
    K_eV = 8.617e-5; % eV/K
    e_ele = 1.602 * 10^-19; % C
    ep0 = 8.854e-12; %Permittivity of free space
    T_e = Vd2*e_ele/(log(2)*K);
        % Note - this method is an approximation that assumes bias of double
        % probe is very large compared to the electron temperature (i.e.
        % e*Bias >> KT) so that the double probe collects the full ion
        % saturation current.
        T_e_linear = max(T_e,0);
    numerical_flag = 0;

% Calculate numerical electron temperature
Vd2_numer = min(maxVd2,Vd2); % If this line is active, the "if" statement below will always be true
if maxVd2 >= Vd2_numer

    numerical_flag = 1;
    % Force Vd2 to be positive for numerical calculation
    if Vd2_numer < 0.001
        Vd2_numer = 0.001;
    end

    % Set starting value as linear value
    T_e_numer = T_e;
    margin = 100; % 100 eV margin to start loop

    % Iterate until value is within 0.1 eV of previous
    while margin > 0.1
        % Calculate next step of T_e
        T_e = e_ele * Vd2_numer / (K*(log(2) - log(1+exp(-e_ele*Vd3 / (K*T_e_numer)))));
        % Reset margin
        margin = abs(T_e - T_e_numer)*K_eV;
        % Reset intermediate T_e
        T_e_numer = T_e;
    end
end

% Set minimum temperature
T_e_numer = max(0,T_e_numer);

```

```
% Decide which temperature to use for density calculations
%T_e = T_e_linear;
T_e = T_e_numer;

% Calculate electron density (Qayyum)
    % Define probe parameters
    r_probe = 0.025 * 2.54*0.01;                % Probe radius (m)
    l_probe = 0.066 * 2.54*0.01;                % Probe length (m)
    A = (pi*r_probe^2 + l_probe*pi*2*r_probe);  % Ion collection area

    % Calculate density
    n_e = I_doub / (exp(-1/2)*A*e_ele*sqrt(K*T_e/m_ion)) * exp(-e_ele*Vd2/(K*T_e)) / (1 - exp(-e_ele*Vd2/(K*T_e))); % From Qayyum paper

    % Set floor of n_e
    n_e = max(n_e,0);


end
```

D.3 plasma_Mach_super.m: Calculating Mach Number with Probe Data

```matlab
function [M_i,v_flow,v_s] = plasma_Mach_super(I_d,I_M,m_ion,T_e)
%%%%%%%%%%%%%%%%%%%%%%%%%%%%%%%%%%%%%%%%%%%%%%%%%%%%%%%%%%%%
%
% The function "plasma_Mach_super" finds the flow velocity of a
% plasma based on measurements from a quadruple probe for unmagnetized
% plasmas. Flow can be supersonic or subsonic.
%
% Author: Collin Parsons  UW MSAA Student/2020  cjpars@uw.edu
%
% Inputs:
%   I_d = current flowing from double probe tip (A) [Ion Saturation
%   Current Upstream]
%   I_M = current flowing from Mach probe tip (A) [Ion Saturation
%   Current Downstream]
%   m_ion = ion mass (kg)
%   T_e = electron temperature (K)
%
% Outputs:
%   v_flow = ion flow velocity (m/s)
%   M_i    = ion Mach number
%   v_is   = sound speed (m/s)
%
% Coupling:
%   None
%
% References:
%  Calculations here are found in:
%   - "Mach Probe Measurements in Unmagnetized Plasmas with Subsonic and
%   Supersonic Flow" by Ando, et. al.
%
%%%%%%%%%%%%%%%%%%%%%%%%%%%%%%%%%%%%%%%%%%%%%%%%%%%%%%%%%%%%%

% Calculate linear electron temperature

    % Define variables
    K_eV = 8.617e-5; % eV/K
    K = 1.3806e-23; % J/K
    T_i = T_e; % Ion temperature and electron temperature assumed the same for FuZE

```

```
% Set Mach probe constant (as calibrated by spectroscopy)
    K_constant = 1.5;

% Calculate sound speed
    % Hard code T_e for testing
    %T_e = 15 / K_eV; %15 eV

    % Calculate sound speed
    v_s = sqrt(K *(T_e)/m_ion);

% Calculate plasma Mach number and flow velocity
    % Set floor on I_double and I_Mach so that we don’t get imaginary
    % numbers. Current should not realistically go below zero anyways.

    if I_d < 0.01     % Floor is set to 10 mA current
        I_d = 0.01;
    end
    if I_M < 0.01
        I_M = 0.01;
    end

    M_i = 1/K_constant * log(I_d/I_M);


% Calculate mach number
    v_flow = M_i * v_s;


end
```

D.4 spectro_He.m: Finding Velocity and Temperature of a He-II Line

```
%%%%%%%%%%%%%%%%%%%%%%%%%%%%%%%%%%%%%%%%%%%%%%%%%%%%%%%%%%%%
%
% The script "spectro_He.m" analyzes data from a spectrometer and outputs
% the data to a structure.
%
% Author: Collin Parsons  UW MSAA Student/2020  cjpars@uw.edu
%
% Inputs:
%   shotnum             - shot number for data (e.g. 191125009)
%   'chord_range.mat'   - saved matrix of mix and max pixel values for
%                         individual spectroscopy chords
%   'spectro_calvalues.mat'  - saved structure of values for spectroscopy
%                              calibration
%
% Coupling:
%   ICCD_binning.m   - bins spectroscopy chord data separately
%       SpeReader.m     - reads in spectroscopy data from K: drive file
%       SpeImport.m     - cleanly formats SpeReader data
%   spectro_calfun.m - calibrates spectroscopy data using values from
%                      stationary lamp
%
% References:
%   None
%
%%%%%%%%%%%%%%%%%%%%%%%%%%%%%%%%%%%%%%%%%%%%%%%%%%%%%%%%%%%%%

%% Define parameters and input
shotnumbers = [200210018,200210020:200210021,...
    200210024:200210025,200210027:200210035,200210037];
    % Full sweep:[200210018,200210020:200210021,...
    % 200210024:200210025,200210027:200210035,200210037];
m_he =  6.64e-27; %kg
c = 2.998e8; %kg

% Define values for outside loop
avgvelocities = zeros(size(shotnumbers));
avgtemperatures = zeros(size(shotnumbers));

% Start wait bar
fwait = waitbar(0,'Calculating Velocities...','Name','Spectro_master','CreateCancelBtn','
```

```
    setappdata(gcbf,''canceling'',1)');
setappdata(fwait,'canceling',0);

for zz = 1:max(size(shotnumbers))
% Clear variables
close all
clear background calfile chordnum data gauss1offset gauss2offset nn peaks plot_velavg plot_veldata prevchordnum trimdata
commandwindow

% Define shot number
shotnum = shotnumbers(zz);
    %Cadmium lamp shots : 191114 (001-003 at 228 nm)
    %First spectroscopy shots: 191125 (008-009 have data)
    %Fused silica shots: 200109 (006-009)
    %Helium shots: 200114 (005-028)
    %First set of 35 deg scope FuZE data 191125 (008-009 only with light)

%% Process data from K: drive file

% Read in data
[data.ints_raw,data.wls_raw,data.numchords,data.gatedelay,data.gatewidth,data.gain] = ICCD_binning(shotnum,0);
data.gatedelay = (data.gatedelay/1000)-2000;

% Normalize data by gate width and gain
data.ints_raw = data.ints_raw/(data.gain * data.gatewidth/1000);

% Error check
if isnan(data.wls_raw)
    disp('Error: No data read in by ICCD_binning. Check your shot number, or connection to the K: drive...')
    return
end

% Calibrate data using the y=mx+b values found with spectro_calibration.m
calfile = 'spectro_calvalues_200117002.mat';
    % 2400 Grating, 468 nm center: spectro_calvalues_200117002.mat
    % 300  grating, 460 nm center: spectro_calvalues_200117003.mat
[data.wls_cal] = spectro_calfun(data.wls_raw,data.numchords,calfile);

% Remove most background light from data
```

```
    % Find minimum intensity of light
    background.minint = 10000;
    for nn = 1:data.numchords
        datamin = min(data.ints_raw(nn,:));
        background.minint = min(datamin,background.minint);
    end
    clear datamin
    % Subtract noise
    data.ints_adj(:,:) = data.ints_raw(:,:)-background.minint;

% Plot calibrated lines over each other
figure(’Name’,[’Calibrated Chord Intensity, Shot ’,num2str(shotnum)],’NumberTitle’,’off’);
sgtitle([’Calibrated Chord Intensities, Shot ’,num2str(shotnum)]);
hold on
for nn = 1:data.numchords
    %figure(’Name’,[’Chord Intensity, Shot ’,num2str(shotnum),’, Chord ’,num2str(nn)],’NumberTitle’,’off’,’units’,’normalized’,’outerposition’,[0 0 1 1]);
    plot(data.wls_cal(nn,:),data.ints_raw(nn,:),’b’);
        plotxmin = 467; plotxmax = 470;
        grid on;
        xlabel(’Wavelength (nm)’); ylabel(’Intensity’);
        xticks(plotxmin:0.5:plotxmax);
        axis([plotxmin plotxmax min(data.ints_raw,[],’all’)*0.95 max(data.ints_raw,[],’all’)*1.1]);
end
hold off
clear plotxmin plotxmax

% Sanity check: output peak values
%{
    for nn = 1:20
        fieldname = [’c’ num2str(nn)];
        [temppeakdata.(fieldname)(nn,:), temppeaklocs.(fieldname)(nn,:)] = findpeaks(data.ints_adj(nn,:),’MinPeakProminence’,std(data.ints_adj(nn,:))*2);
        temppeakwavs.(fieldname)(nn,:) = data.wls_cal(temppeaklocs.(fieldname)(nn,:));
    end
%}

%% Find wavelengths of notable peaks (direct peaks from data)
for nn = 1:data.numchords
    chordnum = [’c’ num2str(nn)];

```

```
    % Find peaks from the built in MATLAB peak finder
    [peaks.(chordnum).MLints, peaks.(chordnum).MLlocs] = findpeaks(data.ints_raw(nn,:),'
        MinPeakProminence',std(data.ints_raw(nn,:)*0.5));
    peaks.(chordnum).MLwls = data.wls_cal(peaks.(chordnum).MLlocs);

end

%% Isolate main He doublet at 468.5 nm

% Define window size for trimmed data
trimdata.minwl = 467;    trimdata.maxwl = 469;

% Trim data to window
for nn = 1:data.numchords
    % Initialize variables
    chordnum = ['c' num2str(nn)];
    trimdata.(chordnum).window = zeros(1,2);

    % Find index of first value over minwl
    [wl,index] = min(data.wls_cal(nn,:));
    index = index-1;
    while wl < trimdata.minwl
        index = index+1;
        wl = data.wls_cal(nn,index);
    end
    minwindow = index;

    % Find index of first value below maxwl
    [wl,index] = max(data.wls_cal(nn,:));
    index = index+1;
    while wl > trimdata.maxwl
        index = index-1;
        wl = data.wls_cal(nn,index);
    end
    maxwindow = index;

    % Define window for trimmed chord data
    trimdata.(chordnum).window = minwindow:maxwindow;

    % Trim data to window
    trimdata.(chordnum).wls  = data.wls_cal(nn,trimdata.(chordnum).window);
    trimdata.(chordnum).ints = data.ints_raw(nn,trimdata.(chordnum).window);
```

```

    % Find peak in trimmed window
    trimdata.(chordnum).maxint = max(trimdata.(chordnum).ints);
end
clear wl index maxwindow minwindow

%% Fit a double gaussian to each chord

% Find gaussian fits and plot individual peaks with their gaussian fits
figure('Name',['Individual Chords Gaussian Fit, Shot ',num2str(shotnum)],'NumberTitle','off','Position',[0 -300 1500 1300]);
sgtitle(['Individual Chords Gaussian Fit, Shot ',num2str(shotnum)],'FontSize',24);
for nn = 1:data.numchords
    % Initialize variables
    chordnum = ['c' num2str(nn)];
    plotxmin = 468; plotxmax = 469;

    % Find fit
    gauss2offset = fittype('A*exp(-((WL-468.57041-dWL)/OM)^2) + (12/30)*A*exp(-((WL-468.58041-dWL)/OM)^2) + C','dependent','INT','independent','WL','coefficients',{'A','OM','dWL','C'}); % Helium doublet at 468
    gauss1offset = fittype('A*exp(-((WL-468.57041-dWL)/OM)^2) + C','dependent','INT','independent','WL','coefficients',{'A','OM','dWL','C'}); % Helium doublet at 468
        if nn == 1
            startpoints = [trimdata.(chordnum).maxint , 0.05 , -0.01 , background.minint]; % Start point for fit for [A, OM, dWL, C]
        else
            prevchordnum = ['c' num2str(nn-1)];
            startpoints = [peaks.(prevchordnum).gaussfit.A , peaks.(prevchordnum).gaussfit.OM , peaks.(prevchordnum).gaussfit.dWL , peaks.(prevchordnum).gaussfit.C ]; % Start point for fit for [A, OM, dWL, C]
        end
        lowerlimits = [std(trimdata.(chordnum).ints) , 0.0001 , -1 , 0]; % Lower bound for parameters [A, OM, dWL, C]
        upperlimits = [inf , inf , 1 , 1000]; % Upper bound for parameters [A, OM, dWL, C]
    peaks.(chordnum).gaussfit = fit(trimdata.(chordnum).wls',trimdata.(chordnum).ints',gauss2offset,'StartPoint',startpoints,'Lower',lowerlimits,'Upper',upperlimits);

    % Plot fits alongside individual peaks
    subplot(4,5,nn)
    peaks.(chordnum).gaussplot = plot(peaks.(chordnum).gaussfit,trimdata.(chordnum).wls,trimdata.(chordnum).ints,'k');
```

```
        set(gca,'FontSize',14)
        title(['Chord ' num2str(nn)]);
        xlabel('Wavelength (nm)'); ylabel('Intensity');
        legend('off')
        set(peaks.(chordnum).gaussplot(2),'Color','r')
        set(peaks.(chordnum).gaussplot(2),'LineStyle','--')
        xticks(plotxmin:0.5:plotxmax);
        axis([plotxmin plotxmax min(data.ints_raw,[],'all')*0.95 max(data.ints_raw,[],'all')*1.1]);
        grid on


    % Output confidence levels
    peaks.(chordnum).gaussconf = confint(peaks.(chordnum).gaussfit);
    peaks.(chordnum).gaussAconf = (peaks.(chordnum).gaussconf(2,1)-peaks.(chordnum).gaussfit.A)/peaks.(chordnum).gaussfit.A*100;
    peaks.(chordnum).dWLconf = peaks.(chordnum).gaussconf(2,3)-peaks.(chordnum).gaussfit.dWL;

    % Determine if gauss fit is significant
    if peaks.(chordnum).gaussfit.A > 2*std(trimdata.(chordnum).ints) && peaks.(chordnum).gaussAconf < 20
        peaks.(chordnum).gaussfitflag = 1;
    else
        peaks.(chordnum).gaussfitflag = 0;
    end
end
clear startpoints lowerlimits upperlimits plotxmin plotxmax A95

% Output gaussian fit data to peaks structure
for nn = 1:data.numchords
    % Initialize variables
    chordnum = ['c' num2str(nn)];
    % Input data
    peaks.(chordnum).temp = (peaks.(chordnum).gaussfit.OM*10^-9)^2 * m_he*c^2 / ((486.57e-9)^2 * 8*log(2));
        peaks.(chordnum).temp = peaks.(chordnum).temp * (8.617e-5)/(1.38e-23); %Convert from J to eV
    peaks.(chordnum).dWL  = peaks.(chordnum).gaussfit.dWL;
    peaks.(chordnum).background = peaks.(chordnum).gaussfit.C;
end

```

```
%% Calculate velocity

% Calculate velocities
c = 299792458; %m/s
disp(’Velocities of light from each chord:’)
peaks.vel_array = zeros(1,20);
for nn = 1:data.numchords
    % Initialize variables
    chordnum = [’c’ num2str(nn)];

    % Calculate velocity of light
    peaks.(chordnum).vel_scopeaxis = -peaks.(chordnum).dWL/468.57041 * c/1000;
    peaks.(chordnum).vel_z = peaks.(chordnum).vel_scopeaxis/cos(35*pi/180);

    % Calculate confidence of velocity
    peaks.(chordnum).vel_scopeaxis_conf = peaks.(chordnum).dWLconf/468.57041 * c/1000;
    peaks.(chordnum).vel_z_conf = peaks.(chordnum).vel_scopeaxis_conf/cos(35*pi/180);

    % If gauss fit was small, say velocity was zero
    if peaks.(chordnum).gaussfitflag == 0
       peaks.(chordnum).vel_z_final = 0;
    else
        peaks.(chordnum).vel_z_final = peaks.(chordnum).vel_z;
    end

    % Output velocity values to an array
    disp([chordnum ’: ’ num2str(peaks.(chordnum).vel_z_final) ’ km/s’]);
    peaks.vel_array(1,nn) = peaks.(chordnum).vel_z_final;
    peaks.vel_array(2,nn) = peaks.(chordnum).vel_z_conf;
    peaks.temp_array(1,nn) = peaks.(chordnum).temp;


end

% Plot velocities
fig_velocity = figure(’Name’,[’Chord Velocities, Shot ’,num2str(shotnum)],’NumberTitle’,’off’,’Position’,[90 130 1500 900]);
%plot(1:20,peaks.vel_array(1,:),’Color’,[200 88 0]*(1/255),’LineWidth’,1.5);
plot_veldata = shadedErrorBar(1:20,peaks.vel_array(1,:),peaks.vel_array(2,:),’lineProps’,{’Color’,[200/255 88/255 0/255],’LineWidth’,2});
hold on
plot_velavg = plot(1:20,zeros(1,20)+mean(peaks.vel_array(1,:)),’b--’,’LineWidth’,2);
```

```
hold off
    set(gca,’FontSize’,18)
    %title([’Axial Velocity (Shot ’ num2str(shotnum) ’, ’ num2str(data.gatedelay) ’ \mus)’],’FontSize’,30)
    xlabel(’Chord Number’,’FontSize’,26); ylabel(’Axial Velocity (km/s)’,’FontSize’,26);
    yticks(0:10:1000); xticks(1:20);
    axis([1 20 0 100]);
    grid on
    legend(plot_velavg,[’Average = ’,num2str(mean(peaks.vel_array(1,:)))],’FontSize’,22)

% Plot temperatures
fig_temp = figure(’Name’,[’Chord Temperatures, Shot ’,num2str(shotnum)],’NumberTitle’,’off’,’Position’,[90 130 1500 900]);
%plot(1:20,peaks.vel_array(1,:),’Color’,[200 88 0]*(1/255),’LineWidth’,1.5);
plot_tempdata = plot(1:20,peaks.temp_array(1,:),’r’,’LineWidth’,2);
hold on
plot_tempavg = plot(1:20,zeros(1,20)+mean(peaks.temp_array(1,:)),’k--’,’LineWidth’,2);
hold off
    set(gca,’FontSize’,18)
    %title([’Axial Velocity (Shot ’ num2str(shotnum) ’, ’ num2str(data.gatedelay) ’ \mus)’],’FontSize’,30)
    xlabel(’Chord Number’,’FontSize’,26); ylabel(’Temperature (eV)’,’FontSize’,26);
    yticks(0:1:100); xticks(1:20);
    axis([1 20 0 15]);
    grid on
    legend(plot_tempavg,[’Average = ’,num2str(mean(peaks.temp_array(1,:)))],’FontSize’,22)


% Store values to be kept outside the loop
avgvelocities(zz) = mean(peaks.vel_array(1,:));
avgtemperatures(zz) = mean(peaks.temp_array(1,:));

% Update wait bar
waitbar(zz/max(size(shotnumbers)),fwait,’Calculating Velocities...’);
if getappdata(fwait,’canceling’)
    break
end

pause(0.5)

end

```

```
% Check for clicked Cancel button
if getappdata(fwait,'canceling')
    delete(fwait)
    disp('Operation cancelled early.')
    return
end

%close all
delete(fwait)
```